

2017

Accurate and robust spectral testing with relaxed instrumentation requirements

Yuming Zhuang
Iowa State University

Follow this and additional works at: <https://lib.dr.iastate.edu/etd>

 Part of the [Electrical and Electronics Commons](#)

Recommended Citation

Zhuang, Yuming, "Accurate and robust spectral testing with relaxed instrumentation requirements" (2017). *Graduate Theses and Dissertations*. 16249.

<https://lib.dr.iastate.edu/etd/16249>

This Dissertation is brought to you for free and open access by the Iowa State University Capstones, Theses and Dissertations at Iowa State University Digital Repository. It has been accepted for inclusion in Graduate Theses and Dissertations by an authorized administrator of Iowa State University Digital Repository. For more information, please contact digirep@iastate.edu.

Accurate and robust spectral testing with relaxed instrumentation requirements

by

Yuming Zhuang

A dissertation submitted to the graduate faculty
in partial fulfillment of the requirements for the degree of

DOCTOR OF PHILOSOPHY

Major: Electrical and Computer Engineering

Program of Study Committee:
Degang Chen, Major Professor
Randall Geiger
Nathan Neihart
Meng Lu
Yong Guan

The student author, whose presentation of the scholarship herein was approved by the program of study committee, is solely responsible for the content of this dissertation. The Graduate College will ensure this dissertation is globally accessible and will not permit alterations after a degree is conferred.

Iowa State University

Ames, Iowa

2017

Copyright © Yuming Zhuang, 2017. All rights reserved.

DEDICATION

I dedicate my dissertation work to my family and many friends who have supported me throughout my PhD study abroad.

TABLE OF CONTENTS

	Page
ACKNOWLEDGMENTS	vi
ABSTRACT.....	vii
CHAPTER 1. INTRODUCTION	1
1.1 Background on Spectral Testing	1
1.2 IEEE Standards and Conventional Spectral Testing.....	3
1.3 Conventional Spectral Testing Challenges	5
References	7
CHAPTER 2. ALGORITHMS FOR ACCURATE SPECTRAL ANALYSIS IN THE PRESENCE OF ARBITRARY NON-COHERENCY AND LARGE DISTORTION	9
2.1 Introduction.....	9
2.2 Problem Statement	13
2.3 Algorithms for Resolving Non-coherency with Large Distortion	16
2.4 Simulation Results	31
2.5 Measurement Results	35
2.6 Conclusion	38
References.....	39
CHAPTER 3. ACCURATE SPECTRAL TESTING WITH ARBITRARY NON- COHERENCY IN SAMPLING AND SIMULTANEOUS DRIFTS IN AMPLITUDE AND FREQUENCY	43
3.1 Introduction.....	44
3.2 Standard Test and Drift Issue.....	45
3.3 Proposed Algorithm	49
3.4 Simulation Results	62
3.5 Measurement Results	68
3.6 Conclusion	72
References.....	73
CHAPTER 4. HIGH-PURITY SINE WAVE GENERATION USING NONLINEAR DAC WITH PRE-DISTORTION BASED ON LOW-COST ACCURATE DAC- ADC CO-TESTING.....	78
4.1 Introduction.....	79
4.2 Challenges of the Standard Test	82
4.3 Proposed Method	85
4.4 Simulation Results	92
4.5 Measurement Results	96

4.6 Conclusion	102
References.....	103
CHAPTER 5. LOW COST ULTRA-PURE SINE WAVE GENERATION WITH SELF-CALIBRATION.....	
5.1 Introduction.....	106
5.2 Proposed Method	109
5.3 Simulation Results	121
5.4 Measurement Results	122
5.5 Conclusion	128
References.....	128
CHAPTER 6. ACCURATE SPECTRAL TESTING WITH NON-COHERENT SAMPLING FOR MULTI-TONE TEST	
6.1 Introduction.....	131
6.2 Non-Coherent Sampling for Multi-Tone Test	134
6.3 Proposed Method	136
6.4 Simulation Results	141
6.5 Measurement Results	145
6.6 Conclusion	147
References.....	147
CHAPTER 7. ACCURATE SPECTRAL TESTING WITH IMPURE TEST STIMULUS FOR MULTI-TONE TEST.....	
7.1 Introduction.....	150
7.2 Impure Test Stimulus for Multi-Tone Test.....	151
7.3 Proposed Method	153
7.4 Simulation Results	155
7.5 Conclusion	161
References.....	166
CHAPTER 8. MULTI-TONE SINE WAVE GENERATION ACHIEVING THE THEORETICAL MINIMUM OF PEAK-TO-AVERAGE POWER RATIO	
8.1 Introduction.....	169
8.2 Multi-tone Sine Waves and PAPR.....	169
8.3 Proposed Strategy	172
8.4 Simulation Results	176
8.5 Conclusion	188
References.....	192
CHAPTER 9. ACCURATE LINEARITY TESTING USING LOW PURITY STIMULUS ROBUST AGAINST FLICKER NOISE.....	
9.1 Introduction.....	197
9.2 Flicker Noise Effect on SEIR	198
9.3 Proposed Methods.....	199
9.4 Simulation Results	201
References.....	211

9.5 Conclusion	218
References.....	219
CHAPTER 10 . SUMMARY	221

ACKNOWLEDGMENTS

First, I would like to take this opportunity to thank my major professor Dr. Degang Chen for his fundamental role in my doctoral work. Dr. Chen provided me with every bit of guidance, assistance and his expertise that I need during my PhD study. He would patiently sit down with me in his office whenever I have problems during my research, and provide valuable feedback, advice, and encouragement. It was a great learning experience to work with him as it not only forged my skills and expertise in mixed-signal design and testing, but also passed on to me many valuable life lessons that would benefit me throughout my future career.

I would like to thank my committee members: Dr. Randall Geiger, Dr. Nathan Neihart, Dr. Meng Lu and Dr. Yong Guan for their precious time and valuable feedback on this work.

In addition, I would like to thank my colleagues for their support and friendship during these five years in this research group. I would also like to thank many of my friends, the department faculty and staff for making my time at Iowa State University a wonderful experience.

Finally, I am deeply thankful to my family for their love, support and sacrifices. A special feeling of gratitude to my loving parents: Yun Zhuang and Ru Song, who have supported me throughout my PhD study abroad.

ABSTRACT

Spectral testing has been widely used to characterize the dynamic performances of the electrical signals and devices, such as Analog-to-Digital Converters (ADCs) for many decades. One of the difficulties faced is to accurately and cost-effectively test the continually higher performance devices. Standard test methods can be difficult to implement accurately and cost effectively, due to stringent requirements. To relax these necessary conditions and to reduce test costs, while achieving accurate spectral test results, several new algorithms are developed to perform accurate spectral and linearity test without requiring precise, expensive instruments.

In this dissertation, three classes of methods for overcoming the above difficulties are presented. The first class of methods targeted the accurate, single-tone spectral testing. The first method targets the non-coherent sampling issue on spectral testing, especially when the non-coherently sampled signal has large distortions. The second method resolves simultaneous amplitude and frequency drift with non-coherent sampling. The third method achieves accurate linearity results for DAC-ADC co-testing, and generates high-purity sine wave using the nonlinear DAC in the system via pre-distortion. The fourth method targets ultra-pure sine wave generation with two nonlinear DACs, two simple filters, and a nonlinear ADC. These proposed methods are validated by both simulation and measurement results, and have demonstrated their high accuracy and robustness against various test conditions.

The second class of methods deals with the accurate multi-tone spectral testing. The first method in this class resolves the non-coherent sampling issue in multi-tone spectral testing. The second method in this class introduces another proposed method to deal with multi-tone impure sources in spectral testing. The third method generates the multi-tone sine

wave with minimum peak-to-average power ratio, which can be implemented in many applications, such as spectral testing and signal analysis. Similarly, simulation and measurement results validate the functionality and robustness of these proposed methods.

Finally, the third class introduces two proposed methods to accurately test linearity characteristics of high-performance ADCs using low purity sinusoidal or ramp stimulus in the presence of flicker noise. Extensive simulation results have verified their effectiveness to reduce flicker noise influence and achieve accurate linearity results.

CHAPTER 1

INTRODUCTION

In this dissertation, several methods for accurate, robust spectral testing with relaxed instrumentation requirements are presented. They focus on resolving one or several stringent test conditions simultaneously in the conventional spectral testing regulated by IEEE standards. It is shown these methods relaxed many stringent test conditions seen from conventional spectral testing. They can obtain accurate spectral performance of the device or signal under test compared with the conventional test with much lower test costs and faster test time.

This chapter introduces spectroscopy and spectral analysis, the spectral testing of circuits and systems, followed by test signal for spectral testing. Then the IEEE standards for performing accurate spectral testing are introduced. Finally, the challenges involved in the conventional spectral testing are discussed.

1.1 Background on Spectral Testing

Spectral analysis, or spectrum analysis, refers to the analysis with respect to a spectrum of frequencies and its related properties such as frequencies, energies, strength of different frequency components, eigenvectors, etc [1]. It is one of the most widely used methods for data analysis in many areas such as atmospheric science, geophysics, oceanography, astronomy, engineering, etc [2]. In some specific areas, spectral analysis may refer to many terms, such as spectroscopy in chemistry and physics, which is the method of analyzing properties of matter from their electromagnetic interactions [3]. In statistics and signal processing, spectral analysis refers to an algorithm that estimates the strength of

different frequency components of a time domain signal, which is often periodical signals [4]. In engineering, especially electrical engineering, spectral analysis can also be used to evaluate certain performances of circuits and systems in frequency domain [5-6]. Since the spectral analysis is done in the digital domain, the output signals after circuits and systems are often digitized by Analog-to-Digital Converters (ADCs). In spectral testing, a single-tone sine wave or multi-tone sine waves are used as test stimulus to test the devices under test (DUTs) and the DUTs' outputs are digitized for data processing. Many devices, such as Digital-to-Analog Converters (DACs), amplifiers, and ADCs are tested in this manner. The focus of this dissertation is on spectral testing of ADCs and its signal generation. The proposed methods can be extended to the spectral testing of all other types of devices.

Since the last few decades, with rapid advancements in semiconductor processing technology, the performance of data converters has increased dramatically. Nevertheless, the increase in performance inevitably increases the difficulties in testing these devices accurately and cost effectively. Moreover, the test signals associated with these devices need to have even better performances, which again increases the test cost and test difficulties. Therefore, there is a strong need to seek alternative solutions to conventional testing methods by using low-end instruments to obtain accurate test results.

In the conventional testing of the ADC, there are two major categories—static and dynamic testing [7-10]. This dissertation focuses on dynamic testing, or spectral testing. Currently, most of the ADCs are sampling ADCs, which have internal sample-and-hold functions. In addition to traditional DC specifications like offset, gain, Integral Nonlinearity (INL), and Differential Nonlinearity (DNL). Generally, ADCs are specified with respect to AC performance, such as Signal-to-Noise Ratio (SNR), Total Harmonic Distortion (THD),

Spurious Free Dynamic Range (SFDR), etc. These specifications are tested through dynamic or spectral testing.

1.2 IEEE Standards and Conventional Spectral Testing

There are several different IEEE Standards [8-10] that describe the method, which data converters should be tested to ensure accurate results are obtained. The IEEE Standards include several main recommendations to guarantee the spectral results of the ADC are characterized accurately:

1. Spectral purity of input signal should be 3~4 bits purer than the ADC under test.
2. The signal should be sampled coherently.
3. The test environment should be stationary and the test stimulus should possess stable signals to the devices under test.
4. The input signal range should be only slightly lower than the ADC input range.
5. The total number of sampled points should be sufficiently high.
6. The sampling clock should have relatively low level of jitter.

The first three recommendations are the targets throughout this dissertation. Another commonly practiced method is to make the data length a power of 2 to make the Fast Fourier Transform (FFT) more efficient.

Eq. (1.1) demonstrates the discrete representation of an impure sine wave that would be achieved after a sine wave passes through the ADC. There are three components: the fundamental, the harmonics, and an added white noise component $w[n]$.

$$x[n] = A_1 \cos(2\pi \frac{f_i}{f_s} n + \phi) + \sum_{h=2}^H A_h \cos(2\pi \frac{hf_i}{f_s} n + \phi_h) + w[n], \quad (1.1)$$

where f_i and f_s are the signal frequency and sampling frequency, respectively. A_1 and ϕ are the fundamental amplitude and initial phase, respectively. A_h and ϕ_h are the h^{th} harmonic amplitude and initial phase, respectively. $n=0,1,2\dots m-1$, and m is the total number of sampled data.

Upon obtaining the data record, the FFT algorithm can be applied to calculate the spectral results. The Discrete Fourier Transform (DFT) is calculated using the FFT algorithm and described in Eq. (1.2).

$$X[k] = \sum_{n=0}^{m-1} x[n] e^{-\frac{2\pi i}{m} nk}. \quad (1.2)$$

Good spectral results will occur, if the coherent sampling condition can be met. This is described in Eq. (1.3), where J is an integer and represents the number of cycles for the sinusoid sampled and m is the total data record length.

$$f_i = J \frac{f_s}{m}. \quad (1.3)$$

When coherent sampling is met, the FFT algorithm's output makes it possible to easily recover the phase and amplitude of the fundamental and harmonic components. These can be derived from the respective bins of the FFT output.

$$X[J] = \frac{A_1}{2} e^{j\phi_1}, X[J \cdot h] = \frac{A_h}{2} e^{j\phi_h}. \quad (1.4)$$

Once the amplitudes are determined, it is possible to calculate some of the common dynamic characteristics of the ADC [8-10].

$$THD = \frac{\sum_{h=2}^H A_h^2}{A_1^2}, \quad (1.5)$$

$$SFDR = \frac{A_1^2}{2 \cdot \max(X_k^2)}, \text{ excluding } k=J, \quad (1.6)$$

$$SNR = \frac{A_1^2}{P_{Noise}}, \quad (1.7)$$

where P_{Noise} is the total noise power. Figure 1.1 is an example of an output spectrum where the ADC was tested accurately, according to the criteria previously mentioned.

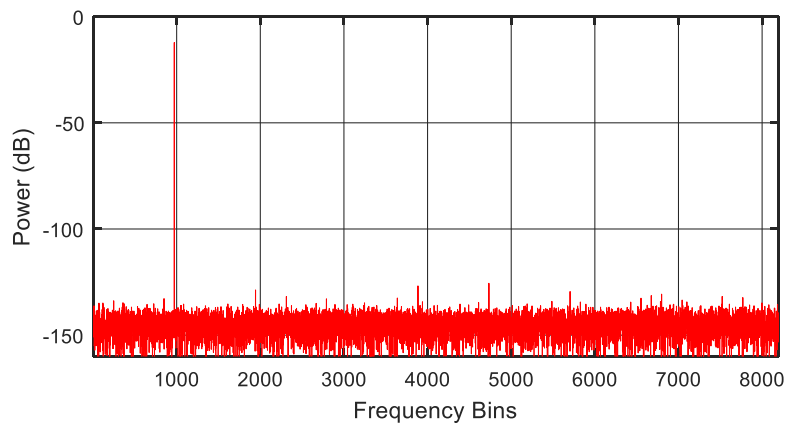


Figure 1.1 Output spectrum of an ADC

1.3 Conventional Spectral Testing Challenges

The previous section provides several recommendations to ensure accurate spectral testing results from conventional testing. These test conditions have become extremely difficult to achieve with the continued increase of the ADC performance.

The first condition is the input signal used to test the ADC needs to be at 3~4 bits higher level of linear purity than the ADC under test. This means about an extra 20dB higher purity, so an input signal with a THD of about 115dB would be required to test a 16-bit ADC with a THD of 95dB. This is generally difficult to achieve, as either the source at this

performance is unavailable or it is costly to bring in equipment from outside the system to generate an accurate test. Therefore, either an extra design effort must be developed to create a signal generator for test or a signal from off chip must be used to provide the test signal needed. Neither of these choices are attractive options, since they both increase the test cost.

The second condition is coherent sampling. Coherent sampling is a stringent condition to ensure the output spectrum provides accurate results. The criteria are that: there will be exactly an integer number of complete cycles of the sine wave as described by Eq. (1.3). If not, a “skirting” effect will be visible. When this occurs, the amplitude for the given signal frequency is no longer stored in just one bin, so the equations given to calculate the previous amplitude before will no longer be valid.

The third condition is to maintain a stationary test environment to ensure the accurate test results. This includes: the test stimulus, power supply, clock signal and other sources of the devices under test to maintain the stable signal condition. Otherwise, drift in the signal amplitude or frequency could corrupt the test results. The drift could be due to: changes in the test environment temperature, power supply variation, humidity and so on. Such condition has become more and more difficult to maintain, especially for high-precision or on-chip BIST testing, that even a slight drift could corrupt the entire spectrum, as the spectrum leakage will show up and covers the true noise and harmonics information.

The fourth condition is to control the ADC input signal amplitude to avoid clipping, while maximizing the signal power. This has become a challenge, especially for on-chip signal generators, where precise control over the signal amplitude is extremely difficult. If the signal is clipped, the ADC only samples the clipped data, whose output spectrum will have a plethora of distortions and lead to erroneous spectral results.

The next challenges occur in the last condition—the sampling clock should have a relatively low level of jitter. This requires a high-quality clock generator, which inevitably increases the design effort and test costs. Moreover, such a low level of clock jitter is almost impossible for on-chip clock generators. If this condition is not met, the clock jitter adds to the sampled signal and corrupts the output spectrum, such as increasing the noise level, producing spurs, and creating spectrum leakages.

In this dissertation, several methods are proposed, to relax several of these challenges one at a time and simultaneously.

References

- [1] R.M. Warner, *Spectral Analysis of Time-series Data*, the Guilford Press, New York, USA, 1998.
- [2] P. Stoica, *Introduction to Spectral Analysis*, Prentice Hall, USA, 1997.
- [3] J.M. Chalmers and P.R. Griffiths, *Handbook of Vibrational Spectroscopy*, Wiley, New York, USA, 2002.
- [4] P. Stoica, R.L. Moses, *Spectral Analysis of Signals*, Prentice Hall, USA, 2005.
- [5] J.N. Rayner, *An introduction to spectral analysis*, Pion, London, UK, 1971.
- [6] M. Burns and G.W.Roberts, *An Introduction to Mixed-Signal IC Test and Measurement*, Oxford Univerisity Press, New York, USA, 2012.
- [7] J. Doernberg, H.-S. Lee, and D.A. Hodges, "Full-Speed Testing of A/D Converters," *IEEE J. Solid State Circuits*, SC-19, pp. 820-827, Dec.1984.
- [8] IEEE Standard for Terminology and Test Methods for Analg-to-Digital Converters, *IEEE Std.1241*, 2010.

- [9] IEEE Standard for Terminology and Test Methods of Digital-to-Analog Converter Devices, *IEEE Std.1658*, 2011.
- [10] IEEE Standard for Digitizing Waveform Recorders, *IEEE Std.1057*, 2007.

CHAPTER 2

ALGORITHMS FOR ACCURATE SPECTRAL ANALYSIS IN THE PRESENCE OF ARBITRARY NON-COHERENCY AND LARGE DISTORTION

In spectral analysis, achieving coherent sampling, especially when signals have large distortion, has been a challenge for many years. This chapter introduces three algorithms to resolve this issue. In comparison to previous algorithms, and two widely used methods in industry: windowing and four parameter sine wave fit, these new algorithms are capable of obtaining accurate spectral results of the signal, while achieving high accuracy and computational efficiency. The novel contribution of this chapter is not only the proposal of three new algorithms, but also the analysis of their advantages and limitations in detail, providing their trade-offs and different fields of applications. Extensive simulations and measurements were performed to validate these algorithms. Combined with the high accuracy, computational efficiency, and robustness of these algorithms against signal purity, they are readily available to be implemented for bench or on-chip testing. In addition, it is suitable for data converter spectral testing when non-coherent sampling is present and spectrally pure test signal source is not available.

This chapter is mainly based on the published paper in *IEEE Trans. Instrum. Meas.* [1]. Partially results prior to that appeared in several conferences [2,3] and *IEEE Trans. on Circ. and Syst. II* [4].

2.1 Introduction

Analog and mixed-signal circuits are viewed as a bottleneck for the market acceptance of Systems-on-Chip (SoC) [5]. Meanwhile, analog, mixed-signal, Radio

Frequency (RF), Integrated Circuit (IC) test, and measurement have grown into a highly specialized field of electrical engineering [6,7]. In general, these tests all require signal analysis, which can be categorized into DC, time domain, and frequency domain analysis. Spectral analysis, which utilizes frequency domain data, is the most commonly used approach in signal processing. The digital signal processing employs sampling of signals, which can be classified in one of two different principles, coherent sampling and non-coherent sampling [5, 8-9]. Coherent sampling offers higher advantages in the mixed signal testing, but it is challenging to achieve. In addition, to perform accurate spectral testing, the IEEE Standard for Terminology and Test Methods for Analog-to-Digital Converters [10], the IEEE Standard for Terminology and Test Methods of Digital-to-Analog Converter (DAC) Devices [11], and the IEEE Standard for Digitizing Waveform Recorders [12] suggest coherent sampling.

Driven by the need for lower test cost, Built-In-Self-Test (BIST) circuits have become more and more popular and achieving coherent sampling is becoming more and more challenging. More often, the signal under test does not possess enough purity, which means a large distortion is inherited along with the fundamental signal. On-chip oscillators, such as Ring oscillator, Colpitts oscillators, Wien Bridge oscillators, and Hartley oscillators don't possess high signal purity [13]. The output signal purities of the high speed, low resolution DACs are also low. In that case, when signal is non-coherently sampled, not only fundamental bin, large power harmonic bins will also have severe spectral leakages, which makes actual spectral information of the signal harder to obtain.

Windowing and four parameter sine wave fitting have been two of the most widely implemented methods in the industry to resolve non-coherent sampling [14-16]. Windowing

is used in harmonic analysis to reduce the undesirable effects related to spectral leakage [14]. Applying countermeasures such as a careful selection of a windowing function to a non-coherent signal can reduce the effects of spectral leakage, but not completely remove it [5]. The selection of windows depends on the resolution of the Analog-to-Digital Converter (ADC) that is used. Also, to most efficiently reduce spectral leakage, it is important to select appropriate windows, which limits its practical usage. Since the ability of a window to remove spectrum leakage mainly depends on the power of the secondary lobes of the window spectrum, when multiplying actual data with corresponding window coefficients in time domain, it is equivalent to the convolution in frequency domain. This convolution requires that the power of secondary lobes of window should be lower than the noise floor of the ADC or digitizer and the window should exhibit low-amplitude side lobes far from the central main lobe and the transition to the low side lobes should be rapid [14]. However, as the resolution of the ADC increases, the noise floor of the ADCs is decreasing, for an ideal 18-bit ADC with 220 samples, the noise floor is about -168 dB level, which requires windows to have even lower peak side lobe levels. In addition, when the peak side lobe level is reduced, the main lobe's -3 dB bandwidth will be increased. Without careful consideration of appropriate types of windows, it is difficult to achieve accurate spectral results with severe non-coherent sampling.

Another widely used method: four parameter sine wave fitting has accurate estimation on the spectrum parameters such as THD, SNR, Effective Number of Bit (ENOB), etc. [17-18]. The limitation lies in its computational inefficiency, especially in the case when a non-harmonic component determines SFDR, a full spectrum test is required to obtain accurate spectral results [19]. In [20], another method was introduced: a multi-sine fitting

algorithm that can accurately estimate the fundamental and harmonics of the input signal. However, if the largest spur is not harmonics, the result of SFDR is incorrect. Recently an acceleration of the ADC test with sine wave fitting method is proposed in [21], this method utilized only a small fraction of the frequency domain sine wave data instead of using every time domain sample. It can provide faster estimation of the four parameters of the sine wave with no significant loss in the precision. However, the input requires high purity with only Gaussian noise.

In the literature, ways to resolve non-coherent sampling have been proposed. Interpolating DFT (IpDFT) methods [22-26] was introduced to eliminate non-coherent sampling requirement, but the results can be inaccurate if a non-harmonic spur is dominating the harmonics. In [27], 2-D FFT method was proposed, but the computational efficiency is low, which has the time complexity of $O(M^2 \log_2 M)$. Filter bank methods were proposed in [28]-[29], the price to be paid for such solutions is either additional circuitry area or the fact that Fast Fourier Transform (FFT) cannot be directly utilized. The 2-FFT method [30], closed form method [31], and Fundamental identification and Replacement (FIRE) method [32] were proposed where the non-coherency is removed by identifying non-coherent fundamental using time & frequency domain data and Newton's iterations with accurate results and efficient computation. The FIRE method has wide applications in high-resolution ADC testing. However, no estimations are done for harmonics, if the input signal contains large harmonics, whose power is comparable to the fundamental, their leakage power would overlap with the fundamental in the spectrum and the FIRE method would give erroneous result. In [2-3], the two-step algorithm was introduced to remove fundamental and harmonics leakages; therefore, accurately estimating signal's spectral characteristics when the signal has

large distortions. Both simulation and measurement results have demonstrated the accuracy and robustness of these proposed algorithms. However, the detailed analysis regarding its limitation and trade-offs were yet to be addressed. In this chapter, three algorithms are addressed in detail to resolve the issue of non-coherency when the signal possesses large distortions. The novel contribution of this chapter is that with the three algorithms discussed, it explores the advantages and limitations of these algorithms, providing their fields of applications. Furthermore, it validated the proposed algorithm with extensive simulation and measurement results for both functionality and robustness.

The rest of the chapter is organized in the following sections: Section II discusses the spectral testing and non-coherent sampling, Section III introduces the proposed algorithms, Section IV provides the comparison of different algorithms and extensive functionality and robustness simulations, Section V presents the measurement result, and Section VI concludes the chapter.

2.2 Problem Statement

Since sinusoidal signal is the main interest, the input signal is modeled as a cosine wave, with distortions represented by harmonics. The time domain expression is given by:

$$x(t) = A \cos(2\pi f_i t + \phi) + \sum_{h=2}^H A_h \sin(2\pi h f_i t + \phi_h) + w(t), \quad (2.1)$$

where A is the amplitude of the fundamental, f_i is the input signal frequency, ϕ is the initial phase, A_h and ϕ_h are the amplitude and initial phase of the signal's h^{th} harmonics ($2 \leq h \leq H$). H is the total number of harmonics considered in the input signal and w is the noise in the signal. It is assumed that higher order harmonics are small enough to be ignored.

The analog interpretation of the digital output from ADC/digitizer is given by:

$$x[n] = A \cos\left(2\pi \frac{J}{M} n + \phi\right) + \sum_{h=2}^H A_h \sin\left(2\pi h \frac{J}{M} n + \phi_h\right) + w[n], \quad (2.2)$$

where $n = 0, 1, \dots, M-1$, $w[n]$ is the noise in the ADC output.

By taking Discrete Fourier Transform (DFT), the spectral parameters can be obtained.

The DFT of $x[n]$ is given by:

$$X_k = \frac{1}{M} \sum_{n=0}^{M-1} x[n] e^{-j \frac{2\pi k n}{M}}, \quad (2.3)$$

where $k = 0, 1, \dots, M-1$.

To achieve coherent sampling condition, the input signal frequency, sampling frequency f_s , total sampled points M and number of sampled period J , must satisfy the following condition:

$$\frac{J}{M} = \frac{f_i}{f_s} \Rightarrow f_i = \frac{J}{M} f_s, \quad (2.4)$$

where J is an integer, J and M should be co-prime. M is usually chosen to be a power of 2 for faster FFT processing.

When coherent sampling is achieved, both amplitude and phase information of the signal's fundamental harmonics can be obtained accurately. When $k=J$, X_k is the fundamental bin in the spectrum, when $k = h \cdot J$, X_k is the h^{th} harmonic bin in the spectrum.

They are given by:

$$X_J = \frac{A}{2} e^{j\phi}, X_{hJ} = \frac{A_h}{2} e^{j\phi_h}. \quad (2.5)$$

If the coherent sampling condition is not met, then J is not an integer. If taking direct DFT of such signal, skirting effect around the fundamental bin, known as the spectral

leakage, can be seen from Figure 1.1. J is divided into two parts: $J = J_{\text{int}} + \delta$, where the integer part is J_{int} and fraction part is δ , the range of δ is from -0.5 to 0.5.

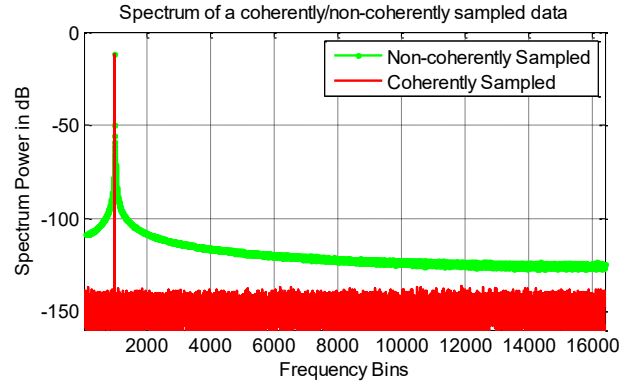


Figure 2.1 Spectrum of a coherently (red)/non-coherently (green) sampled pure signal

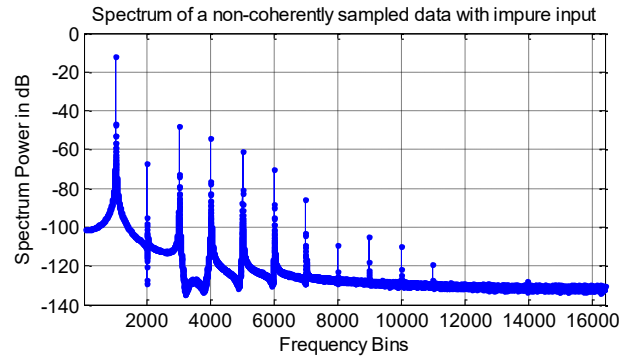


Figure 2.2. Spectrum of a non-coherently sampled signal with large distortions

The input signal purity is defined as the sum of the input harmonics power

$\sum_{k=2}^H (HD_k^2)$ over its fundamental power A^2 :

$$THD_{\text{input}} = 10 \times \log_{10} \left(\frac{\sum_{k=2}^H (HD_k^2)}{A^2} \right), \quad (2.6)$$

When δ is in 10^{-1} level, the leakage in the fundamental due to non-coherency is severe, whose power leakage is usually shown as skirting 40~50dB below the fundamental

tone. For the input signal that has high purity, since the harmonics power is much smaller than the fundamental power, the leakage of the harmonics due to non-coherency is below the noise floor. However, when the input signal has large distortions, the harmonics leakages power can no longer be ignored and they are comparable to the fundamental. Severe spectrum leakages can be found in both fundamentals and harmonics as shown in Figure 2.2. If no corrections are done to non-coherent harmonics, the power of harmonics cannot be accurately estimated, the spectral results, such as SNR and THD, could be erroneous. Therefore, the new algorithms need to consider harmonics leakages as well.

2.3 Algorithms for Resolving Non-coherency with Large Distortion

In this section, three algorithms are introduced to resolve the issue of non-coherency with large distortion to noise ratios. In addition, their advantages and limitations are discussed in detail.

Since the signal under test has large distortions, which is different from the case when FIRE method is used [32], the new algorithms need to separately estimate non-coherent fundamental and harmonics via iteration. Thus, reducing the overlapping leakage power influence on the estimation and making both fundamental and harmonics identifications more robust and accurate. The general steps of proposed algorithms are shown in Figure 2.3. During the initial estimation, the harmonics leakages are no longer negligible, rather, they are above the noise floor and will leak into the fundamental bin and other harmonic bins (Figure 2.3(1)), which causes inaccurate estimation of the fundamental initially (Figure 2.3(2)). After the initial estimation of the fundamental, it is removed from original output, along with most of the leakages. However, the removal is not complete, the residual leakages will still affect

the initial estimation of the harmonics, as shown in Figure 2.3(3). After the removal of initial estimated harmonics, most of the leakages from harmonics are removed (Figure 2.3(4)), the rest has much less influence on fundamental estimation than previously. Thus, the re-estimation of the fundamental will be more accurate, FIRE, four parameter sine fit, and even closed form formula can be used for re-estimation of the fundamental (Figure 2.3(5)). With the more accurate estimated fundamental removed, the residual leakages are below the noise level (Figure 2.3(6)), harmonics can be more accurately estimated without the influence of the fundamental leakages (Figure 2.3(7)). Finally, the accurate estimation of both fundamental and harmonics are obtained as shown in Figure 2.3(8) and spectrum leakages are removed.

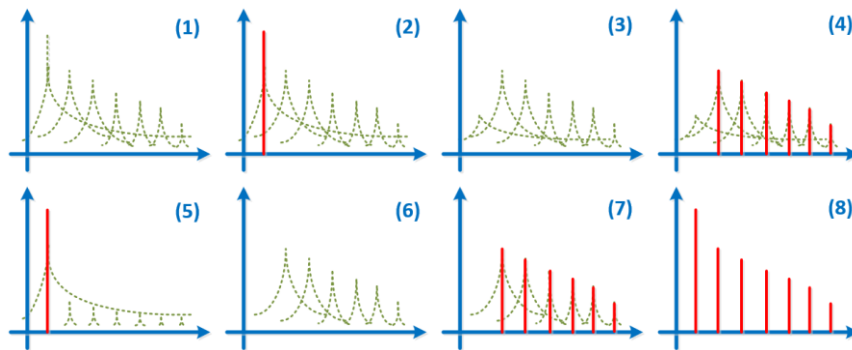


Figure 2.3. Spectrum of each step in generalized proposed algorithms

Before going to the detailed steps of the proposed algorithms, the flowchart of these algorithms is shown in Figure 2.4 to 2.6.

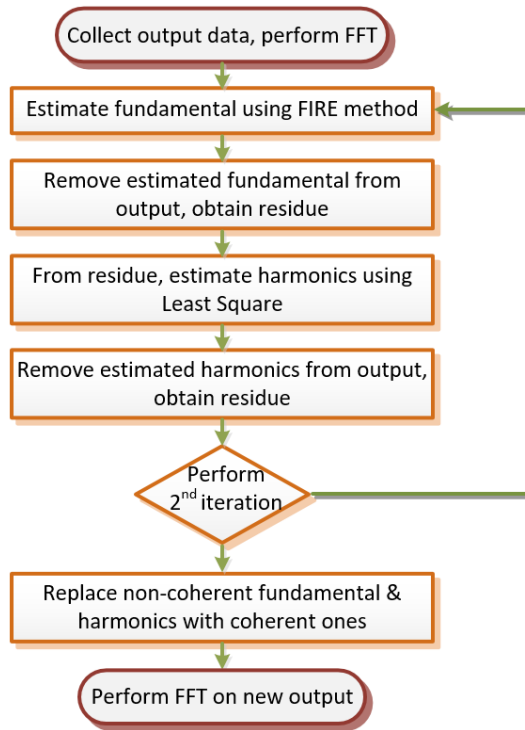


Figure 2.4. Flowchart of the algorithm 1

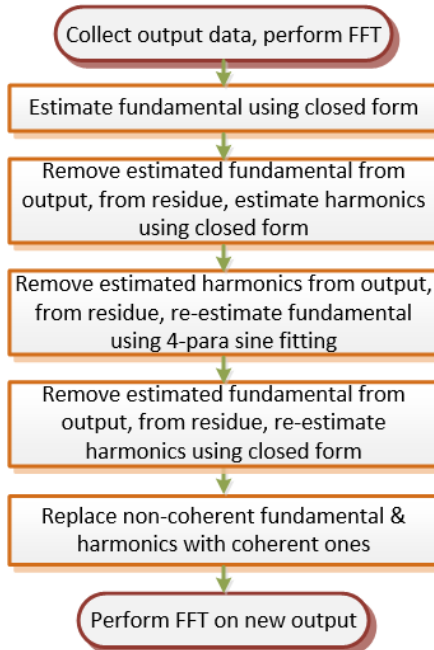


Figure 2.5. Flowchart of the algorithm 2

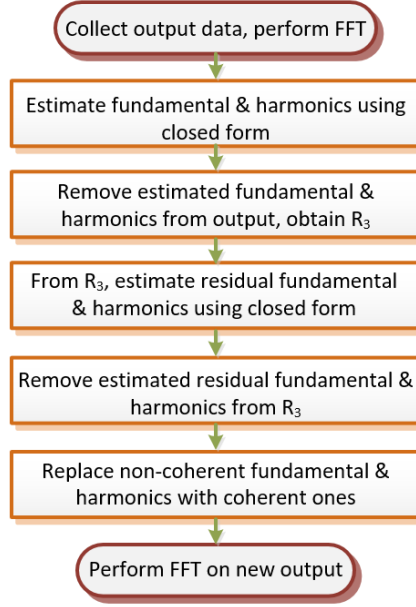


Figure 2.6. Flowchart of the algorithm 3

A. Algorithm 1

The algorithm 1 first introduced the idea of estimating non-coherent fundamental and harmonics separately via iterations. The Fundamental is estimated using FIRE method [13], and harmonics are estimated using the standard least square method. It is shown that two iterations are sufficient to obtain accurate estimation on both fundamental and harmonics.

The first step involves identifying and removing the non-coherent fundamental using FIRE method. The fundamental parameters: amplitude A , phase ϕ , and number of sampled periods J can be estimated by using both time domain and frequency domain data. The detailed descriptions can be found in [32].

The initial estimated fundamental is given by:

$$x_{Fund_i}[n] = A \sin\left(\frac{2\pi(J_{int} + \hat{\delta})}{M}n + \hat{\phi}\right) + V_{os}. \quad (2.7)$$

After the initial estimation of the non-coherent fundamental, it is subtracted from the original signal, with the residue containing harmonics information. The residue is given by:

$$R[n] = x[n] - x_{Fund_i}[n]. \quad (2.8)$$

Once the major leakage source is mostly removed, though the estimation error exists in the residue, the initial harmonics estimation can be obtained by least square. Since the harmonics components are a linear combination in terms of their unknown amplitude; therefore, least square is used to solve for each harmonic's amplitude from the residue.

$$r = \begin{bmatrix} R[0] \\ R[1] \\ \vdots \\ R[M-1] \end{bmatrix} \quad s_o = [a_1 \ b_1 \ \dots \ \mathcal{DC}]^T, \quad (2.9)$$

where r is the vector of residue, s_o is the parameters needs to be estimated. The least square solution is given by:

$$\hat{s}_o = (D_o^T D_o)^{-1} (D_o^T r), \quad (2.10)$$

where

$$D_o = \begin{pmatrix} c_{11} & d_{11} & \dots & \dots & \dots & 1 \\ c_{21} & d_{21} & \dots & \dots & \dots & 1 \\ \vdots & \vdots & \ddots & \vdots & \vdots & \vdots \\ c_{M1} & d_{M1} & \dots & \dots & \dots & 1 \end{pmatrix}, \quad (2.11)$$

$$c_{nh} = \cos(2\pi \frac{h \times (J_{int} + \hat{\delta})}{M} (n-1)), \quad n = 1, 2, \dots, M, \quad (2.12)$$

$$d_{nh} = \sin(2\pi \frac{h \times (J_{int} + \hat{\delta})}{M} (n-1)), \quad h = 1, 2, \dots, H. \quad (2.13)$$

Therefore, the initial estimated harmonics from original data is given by:

$$x_{Harm_i}[n] = \sum_{h=2}^H \left[\hat{a}_h \cos(2\pi h \frac{(J_{int} + \hat{\delta})}{M} n) + \hat{b}_h \sin(2\pi h \frac{(J_{int} + \hat{\delta})}{M} n) \right]. \quad (2.14)$$

Once the initial estimation on the fundamental and the harmonics are done, one can be subtracted from the original signal to obtain more accurate results of the other. The new residue is given by:

$$R_2[n] = x[n] - x_{Harm_i}[n]. \quad (2.15)$$

Similar to the previous step, FIRE method and least square were used to re-estimate the fundamental and harmonics to obtain more accurate estimations. Once the initial estimated harmonics are removed, fundamental can be more accurately estimated in $R_2[n]$. The same FIRE method is used to estimate the fundamental. The detailed steps are not repeatedly shown here. The re-estimated fundamental is given by:

$$x_{Fund}[n] = \hat{A}_F \sin\left(\frac{2\pi(J_{int} + \hat{\delta}_F)}{M} n + \hat{\phi}_F\right) + V_{osF}. \quad (2.16)$$

Similarly, the estimated fundamental is subtracted from the original output and using new residue and least square, without the influence of fundamental leakage, more accurate estimation of harmonics can be obtained, the steps are the same as in Eq. (2.8)-(2.14). The more accurate estimated harmonics are given by:

$$x_{Harm}[n] = \sum_{h=2}^H \left[\hat{a}_{hF} \cos(2\pi h \frac{(J_{int} + \hat{\delta}_F)}{M} n) + \hat{b}_{hF} \sin(2\pi h \frac{(J_{int} + \hat{\delta}_F)}{M} n) \right]. \quad (2.17)$$

Finally, the coherently sampled fundamental and harmonics are constructed to replace the non-coherently sampled ones.

$$x_{Fund_C}[n] = \hat{A}_F \sin\left(\frac{2\pi J_{int}}{M} n + \hat{\phi}_F\right) + V_{osF}. \quad (2.18)$$

$$x_{Harm_C}[n] = \sum_{h=2}^H \left[\hat{a}_{hF} \cos(2\pi h \frac{J_{int}}{M} n) + \hat{b}_{hF} \sin(2\pi h \frac{J_{int}}{M} n) \right]. \quad (2.19)$$

The new constructed output, which is coherently sampled, is therefore given by:

$$x_{new}[n] = x[n] - x_{Fund}[n] - x_{Harm}[n] + x_{Fund_C}[n] + x_{Harm_C}[n]. \quad (2.20)$$

Performing FFT on $x_{new}[n]$, accurate spectral performance of the signal can be obtained.

B. Algorithm 2

Algorithm 2 uses a similar idea, to estimate the non-coherent fundamental and harmonics separately. For algorithm 1, since FIRE and least square are used twice, the efficiency is a concern. Therefore, in algorithm 2, the fundamental can be estimated by a closed form combined with a four parameter sine fit. The closed form formula [31] is used as the initial estimation of the fundamental. The fractional part of J, fundamental amplitude, and phase are given by:

$$\hat{\delta} = -\frac{M}{2\pi} \text{imag} \left(\ln \left(\frac{\frac{X_{J_{int}}}{X_{J_{int+1}}} - \frac{X_{J_{int}}}{X_{J_{int-1}}}}{\frac{X_{J_{int}}}{X_{J_{int+1}}} - \frac{X_{J_{int}}}{X_{J_{int-1}}} + e^{j\frac{2\pi}{M}} - e^{-j\frac{2\pi}{M}}} \right) \right), \quad (2.21)$$

$$\hat{A} = 2M \left| X_{J_{int}} \right| \left| \frac{1 - e^{j\frac{2\pi}{M}\hat{\delta}}}{1 - e^{j2\pi\hat{\delta}}} \right|, \quad (2.22)$$

$$\hat{\phi} = -\text{imag} \left(\ln \left(\frac{2M \cdot X_{J_{int}}}{\hat{A}} \frac{1 - e^{j\frac{2\pi}{M}\hat{\delta}}}{1 - e^{j2\pi\hat{\delta}}} \right) \right). \quad (2.23)$$

The initial estimated fundamental is given by:

$$x_{Fund_1}[n] = A \sin\left(\frac{2\pi(J_{int} + \hat{\delta})}{M} n + \hat{\phi}\right). \quad (2.24)$$

The initial estimated fundamental is then subtracted from original output data. The residue is given by:

$$R[n] = x[n] - x_{Fund_1}[n]. \quad (2.25)$$

Similarly, from $R[n]$, the closed form formula is used on each harmonic bin to estimate the amplitude and phase. Since the sampled period J is estimated, each harmonic bin is: $J_h = \text{round}(h \cdot (J_{int} + \hat{\delta}))$. The fractional part of J_h is given by: $\hat{\delta}_h = h \cdot (J_{int} + \hat{\delta}) - J_h$

$$\hat{A}_h = 2M |X_{J_h}| \left| \frac{1 - e^{j\frac{2\pi}{M}\hat{\delta}_h}}{1 - e^{j2\pi\hat{\delta}_h}} \right|, \quad (2.26)$$

$$\hat{\phi}_h = -\text{imag} \left(\ln \left(\frac{2M \cdot X_{J_h} \cdot \frac{1 - e^{j\frac{2\pi}{M}\hat{\delta}_h}}{1 - e^{j2\pi\hat{\delta}_h}}}{\hat{A}_h} \right) \right). \quad (2.27)$$

Therefore, the initial estimated harmonics are constructed by:

$$x_{Harm_1}[n] = \sum_{h=2}^H \left[\hat{A}_h \cos\left(2\pi h \frac{(J_{int} + \hat{\delta})}{M} n + \hat{\phi}_h\right) \right]. \quad (2.28)$$

Then, the initial estimated harmonics are subtracted from original output, so that most of the harmonics leakages are removed, leaving only the fundamental to estimate. The residue $R_2[n]$ is given by:

$$R_2[n] = x[n] - x_{harm_1}[n]. \quad (2.29)$$

From the residue, instead of using the FIRE method like in algorithm 1, four parameter sine fit is used to re-estimate the fundamental. Since the initial value for the sine fit is obtained from closed form formula Eq. (2.21)-(2.23), which is close to the true value,

the sine fit converges to minima only after several iterations. The re-estimated fundamental is then given by:

$$x_{Fund_2}[n] = \hat{A}_{SF} \sin\left(\frac{2\pi(J_{int} + \hat{\delta}_{SF})}{M} n + \hat{\phi}_{SF}\right), \quad (2.30)$$

where \hat{A}_{SF} , $\hat{\delta}_{SF}$, $\hat{\phi}_{SF}$ are estimated amplitude, fractional part of J , and initial phase obtained from sine fit, respectively.

Then the same steps from Eq. (2.26)-(2.27) are used again to re-estimate the harmonics. With the more accurate estimated fundamental removed, the leakage influence to other harmonics bins are reduced to a minimum and more accurate estimation of harmonics can be obtained. The re-estimated harmonics are given by:

$$x_{Harm_2}[n] = \sum_{h=2}^H \hat{A}_{h2} \cos\left(2\pi h \frac{(J_{int} + \hat{\delta}_{SF})}{M} n + \hat{\phi}_{h2}\right), \quad (2.31)$$

where A_{h2} and ϕ_{h2} are h^{th} harmonics amplitude and phase.

Using the re-estimated information, the coherent fundamental and harmonics are obtained:

$$x_{Fund_C2}[n] = \hat{A}_{SF} \sin\left(\frac{2\pi J_{int}}{M} n + \hat{\phi}_{SF}\right), \quad (2.32)$$

$$x_{Harm_C2}[n] = \sum_{h=2}^H \hat{A}_{h2} \cos\left(2\pi h \frac{J_{int}}{M} n + \hat{\phi}_{h2}\right). \quad (2.33)$$

Finally, by subtracting the non-coherent fundamental and harmonics and replacing with coherent fundamental and harmonics, the new output without non-coherent sampling is given by:

$$x_{new_2}[n] = x[n] - x_{Fund_2}[n] - x_{Harm_2}[n] + x_{Fund_C2}[n] + x_{Harm_C2}[n]. \quad (2.34)$$

Performing FFT on $x_{new_2}[n]$, accurate spectral performance of the signal can be obtained.

C. Algorithm 3

To reduce the computational time and further improve efficiency, FIRE and four parameter sine fit are no longer suitable; rather, the closed form formula can be used more often to obtain an accurate estimation. In addition, both the fundamental and harmonics can be estimated by the closed form formula. From Eq.(2.21)-(2.23), and (2.26)-(2.27), the initial estimation of the fundamental and harmonics can be obtained. They are then subtracted from the original output to obtain the residue:

$$R_3[n] = x[n] - x_{Fund_1}[n] - x_{Harm_1}[n]. \quad (2.35)$$

Since the fundamental and harmonics estimated by the closed form formula may not be accurate enough, the closed form formula is used again on residue $R_3[n]$ to estimate the residual fundamental and harmonics, given by:

$$x_{Fund_r}[n] = A_r \sin\left(\frac{2\pi(J_{int} + \hat{\delta}_r)}{M} n + \hat{\phi}_r\right), \quad (2.36)$$

$$x_{Harm_r}[n] = \sum_{h=2}^H \hat{A}_{hr} \cos\left(2\pi h \frac{(J_{int} + \hat{\delta}_r)}{M} n + \hat{\phi}_{hr}\right). \quad (2.37)$$

The two estimated fundamentals (x_{Fund_1} and x_{Fund_r}) can be constructed in the frequency domain. The initial estimated fundamental and residual fundamental in the frequency domain representation are given by:

$$X_{Fi} = \frac{\hat{A}}{2} \cos(\hat{\phi}) + j \cdot \frac{\hat{A}}{2} \sin(\hat{\phi}), \quad (2.38)$$

$$X_{Fr} = \frac{\hat{A}_r}{2} \cos(\hat{\phi}_r) + j \cdot \frac{\hat{A}_r}{2} \sin(\hat{\phi}_r), \quad (2.39)$$

$$X_F = X_{Fi} + X_{Fr}. \quad (2.40)$$

where the amplitude and phase are given by: $\hat{A}_{F2} = \text{abs}(2X_F)$, $\hat{\phi}_{F2} = \text{phase}(X_F)$, respectively.

The two harmonics can be constructed in a similar way:

$$X_{hi} = \frac{\hat{A}_{h3}}{2} \cos(\hat{\phi}_{h3}) + j \cdot \frac{\hat{A}_{h3}}{2} \sin(\hat{\phi}_{h3}), \quad (2.41)$$

$$X_{hr} = \frac{\hat{A}_{hr}}{2} \cos(\hat{\phi}_{hr}) + j \cdot \frac{\hat{A}_{hr}}{2} \sin(\hat{\phi}_{hr}), \quad (2.42)$$

$$X_h = X_{hi} + X_{hr}, \quad (2.43)$$

where the h^{th} harmonic's amplitude and phase are given by: $\hat{A}_{hF} = \text{abs}(2X_h)$, $\hat{\phi}_{hF} = \text{phase}(X_h)$, respectively.

Finally, the coherently sampled fundamental and harmonics can be constructed by:

$$x_{Fund_C3}[n] = \hat{A}_{F2} \sin\left(\frac{2\pi J_{\text{int}}}{M} n + \hat{\phi}_{F2}\right), \quad (2.44)$$

$$x_{Harm_C3}[n] = \sum_{h=2}^H \hat{A}_{hF} \cos\left(2\pi h \frac{J_{\text{int}}}{M} n + \hat{\phi}_{hF}\right). \quad (2.45)$$

Similar to the previous two algorithms, the new output is obtained by replacing non-coherently sampled fundamental and harmonics with coherent ones.

$$x_{\text{new}_3}[n] = R_3[n] - x_{Fund_r}[n] - x_{Harm_r}[n] + x_{Fund_C3}[n] + x_{Harm_C3}[n]. \quad (2.46)$$

Performing FFT on $x_{\text{new}_3}[n]$, accurate spectral performance of the signal can be obtained.

D. Algorithm Analysis

In this section, the accuracy and time efficiency of each proposed algorithm are discussed in detail. In addition, such analysis is verified in both simulation and measurement results.

Based on the derivations in [32], and from Eq.(2.2)-(2.3), neglecting the effect of noise, X_k can be given by:

$$X_k = \frac{A}{2M} e^{j\phi} \frac{1 - e^{j2\pi(J-k)}}{1 - e^{j\frac{2\pi(J-k)}{M}}} + \frac{A}{2M} e^{-j\phi} \frac{1 - e^{-j2\pi(J+k)}}{1 - e^{-j\frac{2\pi(J+k)}{M}}} + \sum_{h=2}^H \left[\frac{A_h}{2M} e^{j\phi_h} \frac{1 - e^{j2\pi(hJ-k)}}{1 - e^{j\frac{2\pi(hJ-k)}{M}}} + \frac{A_h}{2M} e^{-j\phi_h} \frac{1 - e^{-j2\pi(hJ+k)}}{1 - e^{-j\frac{2\pi(hJ+k)}{M}}} \right]. \quad (2.47)$$

For algorithm 1, after using the FIRE method to remove the initial estimated fundamental, which is given by: $\frac{Ae^{j\phi}}{2M} \frac{1 - e^{j2\pi\delta}}{1 - e^{j\frac{2\pi\delta}{M}}} + \frac{Ae^{-j\phi}}{2M} \frac{1 - e^{-j2\pi(2J_{\text{int}}+\delta)}}{1 - e^{-j\frac{2\pi(2J_{\text{int}}+\delta)}{M}}}$, the estimation errors

introduced by the harmonics are:

$$X_{hJ_{\text{int}}} = \sum_{h=2}^H \left[\frac{A_h}{2M} e^{j\phi_h} \frac{1 - e^{j2\pi(h\delta)}}{1 - e^{j\frac{2\pi(h\delta)}{M}}} + \frac{A_h}{2M} e^{-j\phi_h} \frac{1 - e^{-j2\pi(h\delta)}}{1 - e^{-j\frac{2\pi(2hJ_{\text{int}}+h\delta)}}{M}} \right]. \quad (2.48)$$

The initial estimated harmonics are estimated by Least Square, the error standard deviation (std) caused by Least Square estimation [33] is $\sigma(e) = \frac{\sigma(w)}{\sqrt{M}}$, where $\sigma(w)$ is the white noise std in the signal. Since the signal noise std is usually in the order of Least Significant Bits (LSBs) of the ADC that samples the signal, which is small for high-resolution ADC. After the estimated harmonics are removed, the leakages from the residual

harmonics that leak into the fundamental bin have the leakage power of given approximately by $X_{J_{\text{int}},hJ_{\text{int}}}$:

$$X_{J_{\text{int}},hJ} = \sum_{h=2}^H \left[\frac{A_h}{2M} \frac{1 - e^{j2\pi(hJ - J_{\text{int}})}}{1 - e^{j\frac{2\pi(hJ - J_{\text{int}})}{M}}} + \frac{A_h}{2M} \frac{1 - e^{-j2\pi(hJ + J_{\text{int}})}}{1 - e^{-j\frac{2\pi(hJ + J_{\text{int}})}{M}}} \right]^2. \quad (2.49)$$

Since A_h is much smaller than A_h , which is noise power per bin, and is much smaller than the leakages from the harmonics which is near or below the noise level. Therefore, the fundamental can be more accurately estimated using the FIRE method without controlling for leakages from the harmonics. Similarly, after the accurate estimation of the fundamental, the removal is complete, whose accuracy is in the order of 10^{-7} [32] and the estimation of the harmonics will no longer be affected by the fundamental leakages.

For algorithm 2, four parameter sine fit has the property of high accuracy, which is suitable for fundamental estimation, and in the algorithm, the accuracy tolerance is set to be same order as newton iteration in the FIRE method. For the harmonics estimation, since closed form is used, after the fundamental is accurately estimated and removed, the residual harmonics or harmonics estimation errors on the spectrum is given by:

$$X_{hJ_{\text{int}}} = \sum_{h=2}^H \left[\frac{\Delta A_h}{2M} e^{j\phi_h} \frac{1 - e^{j2\pi(h\delta)}}{1 - e^{j\frac{2\pi(h\delta)}{M}}} + \frac{A_h}{2M} e^{-j\phi_h} \frac{1 - e^{-j2\pi(h\delta)}}{1 - e^{-j\frac{2\pi(2hJ_{\text{int}} + h\delta)}{M}}} \right], \quad (2.50)$$

where ΔA_h is the estimation error of h^{th} harmonic amplitude.

$\frac{\Delta A_h}{A_h}$ is in the order of 10^{-4} according to [31-32]. The second part of $X_{hJ_{\text{int}}}$ is ignored

when calculating the closed form formula due to its much smaller value compared with the first portion [32]. Although non-coherency varies as δ is arbitrary in each test, the small

quantity of ΔA_h and second part of $X_{hJ_{int}}$ make the overall estimation error of harmonics to be small enough, as they do not add more estimation errors than noise inherited in the signal. The quantitative verification is studied in section IV.B.

For algorithm 3, both the fundamental and harmonics are estimated twice using closed form formula. After the initial estimation, the residual fundamental is approximately:

$$X_k = \frac{A}{2M} e^{-j\phi} \frac{1 - e^{-j2\pi(\delta)}}{1 - e^{-j\frac{2\pi(2J_{int} + \delta)}{M}}} + \sum_{h=2}^H \left[\frac{A_h}{2M} e^{j\phi_h} \frac{1 - e^{j2\pi(h\delta)}}{1 - e^{j\frac{2\pi(h\delta)}{M}}} + \frac{A_h}{2M} e^{-j\phi_h} \frac{1 - e^{-j2\pi(h\delta)}}{1 - e^{-j\frac{2\pi(2hJ_{int} + h\delta)}{M}}} \right]. \quad (2.51)$$

After the residual estimation using closed form, such residual fundamental will be further reduced by the order of 10^{-4} [32], the residual fundamental after second estimation and removal is approximately:

$$X_{J_{int},2} = \frac{A}{2M} e^{-j\phi} \frac{1 - e^{-j2\pi(\delta)}}{1 - e^{-j\frac{2\pi(2J_{int} + \delta)}{M}}} + \sum_{h=2}^H \left[\frac{A_h}{2M} e^{j\phi_h} \frac{1 - e^{j2\pi(h\delta)}}{1 - e^{j\frac{2\pi(h\delta)}{M}}} + \frac{A_h}{2M} e^{-j\phi_h} \frac{1 - e^{-j2\pi(h\delta)}}{1 - e^{-j\frac{2\pi(2hJ_{int} + h\delta)}{M}}} \right]. \quad (2.52)$$

This is basically the error introduced in Eq.(2.40). If the fundamental and harmonics bins are far away from each other (hundreds of bins or more), the residual leakages from the harmonic bins will be near or below the noise level when they reach the fundamental bin locations (J_{int}). Although this value varies due to the variation of non-coherency (δ), simulations in section IV showed that the estimation using algorithm 3 is accurate enough and the removal of the leakages are complete.

If the fundamental and harmonics bins are close, the leakages from the harmonics bins to the fundamental bin increase. For example, when the fundamental bin and 2nd harmonic bin are next to each other, the 2nd harmonic bin will leak significant power into its nearby bin (the fundamental), which is given by:

$$X_{J_{\text{int}}, J_{\text{int}}+1} = \frac{A_2}{2M} e^{j\phi_2} \frac{1 - e^{j2\pi\delta}}{1 - e^{j\frac{2\pi(\delta+1)}{M}}} + \frac{A_2}{2M} e^{-j\phi_2} \frac{1 - e^{-j2\pi\delta}}{1 - e^{-j\frac{2\pi(2J_{\text{int}}+1+\delta)}{M}}}, \quad (2.53)$$

where A_2 and ϕ_2 are amplitude and phase of the 2nd harmonic. This value is almost the power of the 2nd harmonic bin itself, which contributes non-negligible power to the fundamental estimation. Likewise, the harmonics estimation will be corrupted by nearby fundamental leakages. This phenomenon is shown in Section IV.A.

This estimation error happens due to the nature of the closed form formula, although it has high efficiency, it relies on the frequency domain data, without any iterations involved like previous two methods (FIRE or four parameter sine fit involved), and it is susceptible to large overlapping leakages when bins are close to each other. However, the accuracy of algorithm 3 is on similar level compared with the previous two methods when bins are far away from each other. This is demonstrated in both simulation and measurement results.

Table 2.1. Comparison of computational time ($J_{\text{int}}=971$, $M=2^{14}$, 16-bit ADC)

Method	Time (ms)
FFT	32
FIRE	71
Proposed Algorithm 1	137
Proposed Algorithm 2	102
Proposed Algorithm 3	66

With respect to computational efficiency, algorithm 1 has the complexity of $O(4 \cdot M \log_2 M)$, where the most time-consuming part is the two FFTs in each iteration. Algorithm 2 has the complexity of $O(3 \cdot M \log_2 M)$, as the four parameter sine fit consumes similar time in simulation compared with FFT. For algorithm 3, since the closed form formula has better efficiency than FIRE or FFT, the complexity is $O(2 \cdot M \log_2 M)$, where the

time-consuming part is two FFTs. Table 2.1 summarizes the simulation time for different algorithms.

In general, after discussing the accuracy and efficiency trade-offs, all three algorithms have their own fields of application. Algorithms 1 and 2 are robust and accurate for large distortions, which can be used when high accuracy is required and efficiency is less of concern, especially when the data only sampled a few periods (J), where the fundamental and harmonic bins are close. Algorithm 3 is also accurate and more efficient when hundreds of periods (or more) are sampled and where the test requires efficiency, but it comes with the price of accuracy degradation on certain test cases when J is small.

2.4 Simulation Results

In this section, extensive simulations were conducted in MATLAB to evaluate the functionality and robustness of each algorithm.

A. Functionality

The functionality of various algorithms is examined for two different cases: when the fundamental and harmonic bins are far away from each other; and when they are close to each other. ADC is modeled in MATLAB as a 16-bit ideal digitizer, with the normalized full range of 0 to 1. Sinusoidal signal with a total data record length (M) of 2^{14} was generated as input of the digitizer, with randomly generated initial phase and input Gaussian noise corresponding to 0.5 LSB of the digitizer. 14 input harmonics were randomly generated with the given range (-60dB to -120dB), whose phases were also randomly generated. δ is arbitrarily generated from -0.5 to 0.5.

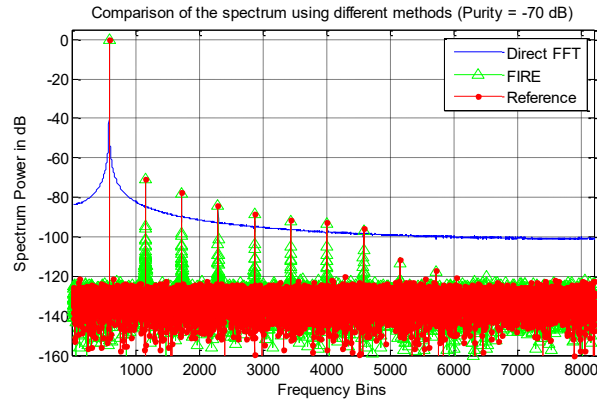


Figure 2.7. Spectrum of a signal with non-coherent sampling and large distortion

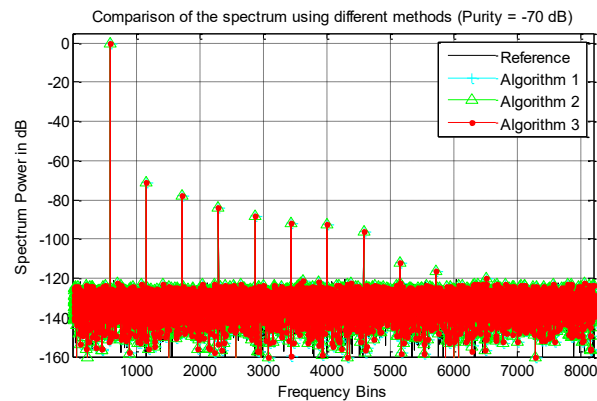


Figure 2.8. Spectrum of a signal with different algorithms

Figure 2.7 shows the spectrum when signal purity is only -70dB , and $J_{int}=571$, so that the fundamental and harmonic bins are far away from each other. The red spectrum serves as the reference, which is the same signal, but coherently sampled. The blue spectrum is the original non-coherently sampled signal, which has large leakage around the fundamental bin, and covers most of the noise and harmonics information. This results in erroneous spectral results such as SNR and THD. The green spectrum is after using the FIRE method and the fundamental leakage is mostly removed, but some harmonic bins still have large leakages around them, so the harmonics and noise power estimation is no longer accurate. This can also be seen from Table 2.2, as THD using FIRE method have about a 4dB difference

compared with the reference. On the contrary, in 2.8 all three algorithms are capable of removing spectral leakage on both fundamental and harmonics, the spectrum overlaps with reference well. In addition, from Table 2.2, the spectral parameters of the signal can be successfully recovered by using three algorithms.

When $J_{int}=57$, both algorithm 1 and algorithm 2 can recover the correct spectrum after non-coherent sampling; however, for algorithm 3 there are a few bins of leakages around the fundamental bin (Figure 2.9). This is due to the closed form estimation being more computational efficient but less accurate than FIRE method, especially when the fundamental bins are close to the harmonic bins. The overlapping leakage power will affect the closed form estimation accuracy. Since the leakages around the fundamental are only several bins, including these bins when calculating fundamental power will result in accurate SNR.

Table 2.2. Spectral parameters of the signal under test using different algorithms

Methods\Spectral Parameters	SNR (dB)	THD (dB)	SFDR (dB)
Reference	91.86	-69.79	71.89
FIRE	86.63	-65.81	71.65
Algorithm 1	92.01	-69.75	71.88
Algorithm 2	91.93	-69.64	71.94
Algorithm 3	91.89	-69.88	71.79

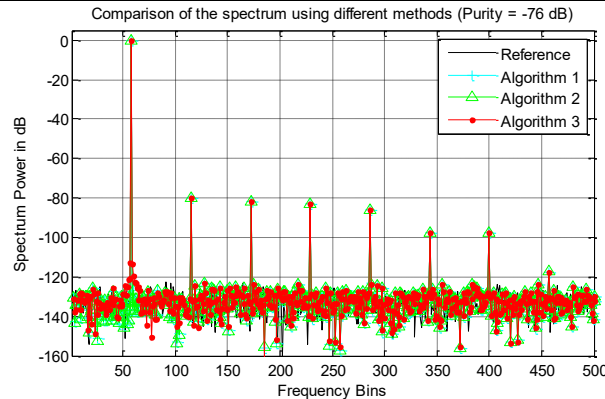


Figure 2.9. Spectrum of an impure signal with different algorithms when $J_{int}=57$

B. Robustness

In this section, the test of robustness of the three algorithms is setup similarly to the functionality test described previously, with a total 2^{14} number of samples on the input sinusoidal signal, randomly generated initial phase for the fundamental and harmonics and given range of harmonic amplitudes (-50dB to -120dB), is also arbitrarily generated from -0.5 to 0.5. The input signal purity defined by Eq. (2.6) is tested from -100dB to -50dB. In each test input signal purity, a total of 100 different simulations were performed with different δ , noise corresponding to 0.5LSB rms value. The harmonics power and noise power are evaluated for different algorithms. For the harmonics power estimation error, the estimated harmonics power \hat{P}_{Harm} is compared with the harmonics power P_{Harm} when the same signal is coherently sampled, shown in dB: $10 \times \log(P_{Harm} - \hat{P}_{Harm})$ and is similar to the one used in [2-3]. For reference, the error is compared with noise power in the same number of bins. For example, if a total of 10 harmonics are used to calculate THD, then the error should compare with 10 times the expected noise power per bin in dB, given by, $10 \log(10P_{Noise} / M)$. Since at each run the noise will be different, the variation is bounded by $\pm 4\sigma$ or $\pm 12dB$ where σ is the standard deviation of noise power. For the upper bound of 4σ , it is $10 \times \log(4^2 \cdot P_{Noise} / M) \approx 12 + 10 \times \log(P_{Noise} / M)$, which is about 12dB above the expected noise power per bin. If they are in the similar level ($\pm 12dB$) or if the estimation error is much smaller than the reference, the estimation is considered as accurate.

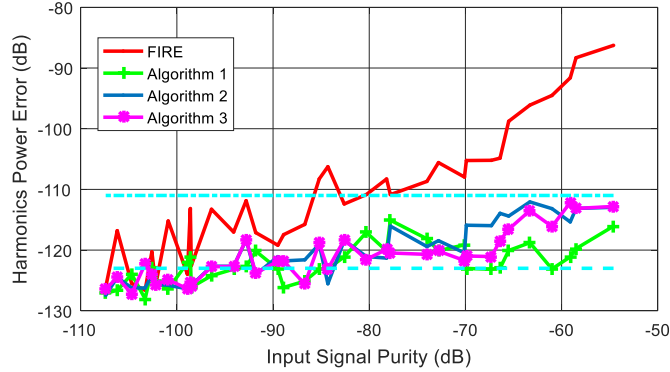


Figure 2.10. Harmonics power estimation error for different algorithms versus input signal purity ($J_{int}=101$)

Figure 2.10 shows the harmonics power estimation error for the algorithms versus the purity of the signal under test. Four solid lines correspond to the error power of different algorithms, which is the averaged value of 100 runs at each input signal purity level. The two dotted blue lines are the noise reference and its upper bound of 12dB, respectively. It can be seen that for the FIRE method (red), it is accurate when the input signal purity is high, which validated the assumption mentioned in [32] and in Section III, which states when the harmonics power is much smaller than the fundamental power, only removing the leakages from the fundamental will result in accurate spectral results. However, as the purity becomes worse, the harmonics power becomes larger and the FIRE method gradually shows estimation error, which is above the upper bound of the noise reference. For the three proposed algorithms, they demonstrate the similar accuracy, as the input signal purity varies, and the errors stay within the reference, showing the robustness against different levels of input signal purity.

2.5 Measurement Results

In addition to the extensive simulation results, the proposed algorithms are verified by measurement results, measured from different ADCs and different signals under test.

Firstly, an 18-bit ADC (ADS8881) was used to evaluate the accuracy of the proposed algorithms. Due to its high resolution and high performance, it is viewed as the ideal digitizer which will not introduce a large amount of noise and distortion to the signal under test. However, the signal under test is generated by a standard lab function generator (Agilent 33220A) without any filtering, which has a certain amount of distortion. In the lab, a total of 5 sets of data were sampled, each with different signal frequency and sampling frequency from ADS8881 and $M=2^{13}$. Figure 2.11 shows the spectrum of 1st set, with sampling frequency of 20kHz and signal frequency of roughly 1kHz. For the reference, the same input signal is generated, except that the input frequency is controlled carefully to achieve coherent sampling. It can be seen that the proposed algorithms are able to remove the leakages from both the fundamental and harmonics and their spectrums (red, black and blue) overlap with the reference well (green). Table 2.3 also confirms the accuracy of the proposed algorithms. Similar spectrum results were observed from other test sets, the spectrums are not repeatedly shown but their spectral performance are summarized in Table 2.3, which also demonstrates the accuracy of the proposed algorithms.

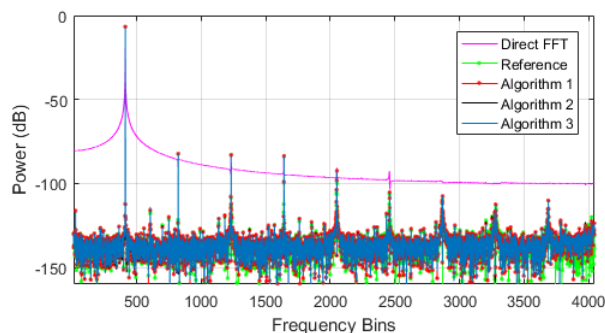


Figure 2.11. Spectrum of the sampled signal with different algorithms (ADS8881)

Table 2.3. Spectral Performance of 5 data sets using proposed methods (ADS8881)

Date Set	Methods	SNR(dB)	THD(dB)	SFDR(dB)
Test 1	Reference	81.93	-71.04	76.14
	Algorithm 1	81.85	-70.85	75.98
	Algorithm 2	81.67	-71.24	76.18
	Algorithm 3	82.01	-71.16	73.33
Test 2	Reference	80.42	-65.85	70.42
	Algorithm 1	80.25	-65.75	70.41
	Algorithm 2	80.21	-65.89	70.26
	Algorithm 3	80.16	-65.92	70.56
Test 3	Reference	82.45	-73.25	79.52
	Algorithm 1	82.14	-73.04	79.48
	Algorithm 2	82.36	-73.51	79.86
	Algorithm 3	82.52	-73.15	79.37
Test 4	Reference	79.51	-67.14	71.56
	Algorithm 1	79.34	-67.02	71.52
	Algorithm 2	79.53	-67.34	71.29
	Algorithm 3	79.29	-67.25	71.68
Test 5	Reference	83.17	-76.85	82.48
	Algorithm 1	83.01	-76.59	82.29
	Algorithm 2	83.24	-76.96	82.36
	Algorithm 3	83.19	-76.72	82.41

To further validate the proposed algorithm, another high-performance 18-bit ADC (ADS9110) is used as the digitizer. A similar test setup was used as stated previously. The sampling frequency is 500kHz in this case and the input is generated by Audio precision without any filtering, whose frequency is roughly 30kHz, 20kHz, and 10kHz, with arbitrary level of non-coherency. Similarly, the reference signal is coherently sampled by the same ADC. A total of 2^{20} samples were acquired by the ADC, and the spectrum of 30kHz input signal is shown in Figure 2.12. As it shows, the proposed algorithms successfully removed the leakages and were able to match the reference spectrum well. Table 2.4 summarize the test results from all 3 test sets. These demonstrate that the proposed algorithms are accurate

and are capable of recovering correct spectral performance with non-coherent sampling and various level of signal purities.

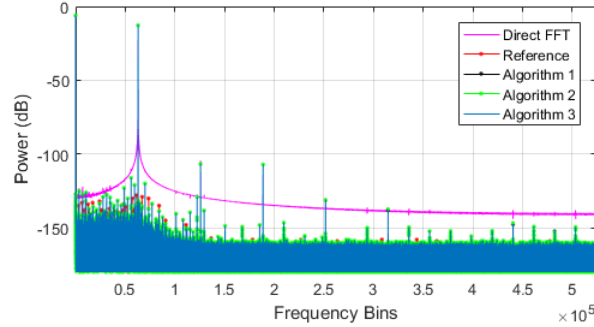


Figure 2.12. Spectrum of the sampled signal with different algorithms (ADS9110)

Table 2.4. Spectral Performance of 3 data sets using proposed methods (ADS9110)

Date Set	Methods	SNR(dB)	THD(dB)	SFDR(dB)
Test 1	Reference	91.93	-89.47	91.84
	Algorithm 1	91.85	-89.27	91.58
	Algorithm 2	91.69	-89.53	91.69
	Algorithm 3	91.74	-89.38	91.78
Test 2	Reference	90.65	-85.65	88.74
	Algorithm 1	90.58	-85.48	88.67
	Algorithm 2	90.48	-85.39	88.59
	Algorithm 3	90.68	-85.42	88.91
Test 3	Reference	91.25	-87.42	90.04
	Algorithm 1	91.05	-87.12	89.78
	Algorithm 2	91.38	-87.63	89.95
	Algorithm 3	91.41	-87.58	90.15

2.6 Conclusion

In this chapter, three algorithms are introduced that deal with non-coherent sampling when the signal under test has large distortions. Using the idea of separately estimating and removing non-coherent fundamental and harmonics, the issues with overlapping leakage power was reduced and accurate spectral results such as SNR, THD, and SFDR can be obtained. The novel contribution of this chapter is that it proposes two new algorithms, and

explores the advantages and limitations of these algorithms. Based on their trade-offs it provides their different fields of applications. In addition, both extensive simulation results and measurement results have validated the accuracy and robustness of the proposed algorithms. These algorithms are readily available for bench test, characterization test, and on-chip implementations. Furthermore, it can be implemented for high-resolution ADC spectral testing, to eliminate non-coherent sampling requirement when high-purity input signals are not available.

References

- [1] Y. Zhuang and D. Chen, "Algorithms for Accurate Spectral Analysis in the Presence of Arbitrary Noncoherency and Large Distortion," *IEEE Trans. Instrum. Meas.*, vol.66, no.10, pp. 2556-2565, Oct.2017.
- [2] Y. Zhuang and D. Chen, "Accurate spectral testing with non-coherent sampling for large distortion to noise ratios," in Proc. *IEEE 34th VLSI Test Symp. (VTS)*, Apr. 2016, pp. 1–6.
- [3] Y. Zhuang and D. Chen, "New strategies in removing non-coherency from signals with large distortion to noise ratios," in Proc. *IEEE Int. Symp. Circuits Syst.*, Sep. 2016, pp. 2901.
- [4] Y. Zhuang and D. Chen, "New Strategies in Removing Non-coherency from Signals with Large Distortion to Noise Ratios", *IEEE Trans. on Circ. and Syst. II: Express Brief*, vol. 63, no. 12, pp. 1136-1140, Dec.2016.
- [5] J. L. Huertas, *Test and Design-for-Testability in Mixed-Signal Integrated Circuits*. New York, NY, USA: Springer, 2004.

- [6] P. Stoica and R. Moses, *Spectral Analysis of Signals*. Englewood Cliffs, NJ, USA: Prentice-Hall, 2005.
- [7] M. Burns and G. W. Roberts, *An Introduction to Mixed-Signal IC Test and Measurement*. New York, NY, USA: Oxford Univ. Press, 2012.
- [8] P. Stoica and R. L. Moses, *Spectral Analysis of Signals*. Englewood Cliffs, NJ, USA: Prentice-Hall, 2011.
- [9] S. M. Alessio, *Digital Signal Processing and Spectral Analysis for Scientists: Concepts and Applications*. Switzerland: Springer, 2016.
- [10] IEEE Standard for Terminology and Test Methods for Analg-to-Digital Converters, *IEEE Std.1241*, 2010.
- [11] IEEE Standard for Terminology and Test Methods of Digital-to-Analog Converter Devices, *IEEE Std.1658*, 2011.
- [12] IEEE Standard for Digitizing Waveform Recorders, *IEEE Std.1057*, 2007.
- [13] B. Razavi, *RF Microelectronics*. Englewood Cliffs, NJ, USA: Prentice-Hall, 2012.
- [14] F. J. Harris, "On the use of windows for harmonic analysis with the discrete Fourier transform," *Proc. IEEE*, vol. 66, no. 1, pp. 51–83, Jan. 1978.
- [15] M. Bertocco, P. Carbone, E. Nunzi, and D. Petri, "Windows for ADC dynamic testing via frequency-domain analysis," *IEEE Trans. Instrum. Meas.*, vol. 50, no. 6, pp. 1571–1576, May 2000.
- [16] S. Raze, D. Dallet, and P. Marchegay, "Non coherent spectral analysis of ADC using FFT windows: An alternative approach," in *Proc. IEEE Workshop Intell. Data Acquisition Adv. Comput. Syst.*, Sep. 2005, pp. 474–478.

- [17] T. Z. Bilau, T. Megyeri, A. Sárhegyi, J. Márkus, and I. Kollár, “Four parameter fitting of sine wave testing result: Iteration and convergence,” *Comput. Standards Interfaces*, vol. 26, no. 1, pp. 51–56, 2004.
- [18] K. F. Chen, “Estimating parameters of a sine wave by separable nonlinear least squares fitting,” *IEEE Trans. Instrum. Meas.*, vol. 59, no. 12, pp. 3214–3217, Dec. 2010.
- [19] P. Handel, “Properties of the IEEE-STD-1057 four-parameter sine wave fit algorithm,” *IEEE Trans. Instrum. Meas.*, vol. 49, no. 6, pp. 1189–1193, Dec. 2000.
- [20] G. Simon, R. Pintelon, L. Sujbert, and J. Schoukens, “An efficient nonlinear least square multisine fitting algorithm,” *IEEE Trans. Instrum. Meas.*, vol. 51, no. 4, pp. 750–755, Aug. 2002.
- [21] V. Palfi and I. Kollar, “Acceleration of the ADC test with sine-wave fit,” *IEEE Trans. Instrum. Meas.*, vol. 62, no. 5, pp. 880–888, May 2013.
- [22] D. K. Mishra, “ADC testing using interpolated fast Fourier transform (IFFT) technique,” *Int. J. Electron.*, vol. 90, no. 7, pp. 459–469, 2003.
- [23] J. Schoukens, R. Pintelon, and H. Van Hamme, “The interpolated fast Fourier transform: A comparative study,” *IEEE Trans. Instrum. Meas.*, vol. 41, no. 2, pp. 226–232, Apr. 1992.
- [24] D. Belega and D. Dallet, “Multipoint interpolated DFT method for frequency estimation,” in *Proc. Int. Multi-Conf. Syst. Signals Devices*, Mar. 2009, pp. 1–6.
- [25] D. Belega, D. Dallet, and D. Petri, “Estimation of the effective number of bits of ADCs using the interpolated DFT method,” in *Proc. IEEE Instrum. Meas. Technol. Conf.*, May 2010, pp. 30–35.

- [26] D. Belega, D. Dallet, and D. Stoiciu, "Choice of the window used in the interpolated discrete Fourier transform method," *Revue Roumaine Sci. Techn. Serie Electrotechn. Energetique*, vol. 54, no. 4, pp. 365–374, 2009.
- [27] X. M. Gao, S. J. Ovaska, S. Shenghe, and Y. C. Jenq, "Analysis of second-order harmonic distortion of ADC using bispectrum," *IEEE Trans. Instrum. Meas.*, vol. 45, no. 1, pp. 50–55, Feb. 1996.
- [28] C. Rebai, D. Dallet, and P. Marchegay, "Noncoherent spectral analysis of ADC using filter Bank," *IEEE Trans. Instrum. Meas.*, vol. 53, no. 3, pp. 652–660, Jun. 2004.
- [29] A. R. Varkonyi-Koczy, G. Simon, L. Sujbert, and M. Fek, "A fast filter bank for adaptive Fourier analysis," *IEEE Trans. Instrum. Meas.*, vol. 47, no. 5, pp. 1124–1128, Oct. 1998.
- [30] S. Sudani, C. Degang, and G. Randy, "A 2-FFT method for on chip spectral testing without requiring coherency," in *Proc. IEEE Int. Instrum. Meas. Technol. Conf.*, Hangzhou, China, May 2011, pp. 1–6.
- [31] S. Sudani, M. Wu, and D. Chen, "A novel robust and accurate spectral testing method for non-coherent sampling," in *Proc. Int. Test Conf.*, Sep. 2011, pp. 1–10.
- [32] S. Sudani and D. Chen, "FIRE: A fundamental identification and replacement method for accurate spectral test without requiring coherency," *IEEE Trans. Instrum. Meas.*, vol. 62, no. 11, pp. 15–25, Nov. 2013.
- [33] A. Bergamin, G. Cavagnero, and G. Mana, "Accuracy assessment of a least-squares estimator for scanning X-ray interferometry," *Meas. Sci. Technol.*, vol. 2, no. 8, pp. 725–734, 1991.

CHAPTER 3

ACCURATE SPECTRAL TESTING WITH ARBITRARY NON-COHERENCY IN SAMPLING AND SIMULTANEOUS DRIFTS IN AMPLITUDE AND FREQUENCY

Accurate spectral testing plays a crucial role in modern high-precision ADCs' evaluation process. One of the challenges is to be able to test the continually higher resolution ADCs accurately and cost-effectively. Due to its stringent test requirement, the standard test method for ADCs can be difficult to implement with low cost. This chapter proposes an algorithm that relaxes the requirements of precise control over source amplitude and frequency and of the need to achieve coherent sampling. The algorithm divides the output data into segments and estimates the drifting fundamental via Newton iteration. By removing the estimated drift fundamental and replacing with a coherent, non-drift, fundamental in time domain, accurate spectral results can be achieved. Various simulation results have validated the accuracy of proposed algorithm. The proposed algorithm is capable of tolerating various test condition variations such as any-level of non-coherency, various input frequency range and different numbers of segmentations. In addition, several measurement results from different ADCs have verified the accuracy of the proposed algorithm, which is able to accurately obtain spectral performance of an 18-bit high-resolution ADC. Such an algorithm relaxes the standard test requirement such as precise control over source frequency and amplitude, which dramatically reduces the test setup complexity and cost.

This chapter is mainly based on the published paper in *IEEE Trans. Instrum. Meas.* [1]. Partially results appeared in *Journal of Electronic Testing: Theory and Applications* [2].

3.1 Introduction

Analog-to-Digital Converters (ADCs) provide the link between the analog domain and digital world of signal processing, computing, and other digital data collection or data processing systems [1]. It is one of the most crucial building blocks in modern signal processing [2]. In ADC dynamic testing, obtaining accurate spectral specifications of the ADCs such as Total Harmonic Distortion (THD), Spurious Free Dynamic Range (SFDR), and Signal to Noise Ratio (SNR), has become a challenging task, especially for high-resolution, high-precision ADCs [3-4]. These dynamic specifications of the ADC are vital for high-speed applications such as communication or audio systems. Such dynamic spectral testing is the focus of this chapter.

Currently, there is a strong need for Built-in-Self-Test (BIST) solutions, which enable engineers to test higher integrated circuitry in a more cost-effective way. For standard test methods, they must have high-precision, high-linearity stimulus generators. These high-performance signal generators require a substantial design effort and often need large areas. However, with a BIST solution, the test circuitry is designed in the same chip as the Device Under Test (DUT). Adding such a large area for the test circuitry alone inevitably compromises its primary goal of lower cost. Moreover, as the performance of the ADC continues to increase, it is pushing the test solutions to have even better performance, which is unavailable for on-chip implementation. In that case, there is longer precise control over input signal's frequency nor its amplitude. This test non-stationarity could result in erroneous spectral test results of the ADC under test. Therefore, there is a growing need to develop new test algorithms that can obtain accurate spectral test results without requiring precision instrumentations/test environment.

The rest of the chapter is arranged as follows: Section II introduces the standard spectral test of the ADC and their challenges, discussing the issue with amplitude drift, frequency drift, and non-coherent sampling. Section III introduces the proposed algorithm that is capable of obtaining accurate spectral performance with drift and non-coherent sampling, and investigates various error sources with detailed analysis. Section IV presents the simulation results in MATLAB, the proposed algorithm is verified by both functionality and robustness tests. Section V validates the proposed algorithm by measurement results, and Section VI elaborates on the conclusions of this research chapter.

3.2 Standard Test and Drift Issue

A. Standard Test

For ADC standard test, the IEEE standards [7-9] describe the ways to ensure accurate results are obtained. In the standards, there are five test conditions that are recommended:

1. The signal should be sampled coherently.
2. Spectral purity of input signal should be 3~4 bits purer than ADC under test.
3. The input signal range should be only slightly lower than the ADC input range.
4. The total number of sampled points should be sufficiently high.
5. The sampling clock should have relatively low levels of jitter.

Given an analog sinusoidal signal $V(t)$:

$$V(t) = A_1 \cos(2\pi f_i t + \phi). \quad (3.1)$$

The discrete representation of the ADC output, assuming the gain error and offset have been calibrated, is given by:

$$V_{out}[n] = A_1 \cos(2\pi \frac{f_i}{f_s} n + \phi) + \sum_{h=2}^H A_h \cos(2\pi \frac{hf_i}{f_s} n + \phi_h) + w[n], \quad (3.2)$$

where f_i and f_s are the signal frequency and sampling frequency, respectively. A_1 and ϕ are the fundamental amplitude and initial phase, respectively. A_h and ϕ_h are the h^{th} harmonic amplitude and initial phase, respectively. $w[n]$ is the noise. $n=0,1,2,\dots,M-1$, and M is the total sampled data record length.

Define the Discrete Fourier Transform (DFT) of total M output as:

$$X_k = \frac{1}{M} \sum_{n=0}^{M-1} x[n] e^{-j \frac{2\pi k n}{M}}, \text{ for } k = 0, 1, \dots, M-1, \quad (3.3)$$

where k represents the frequency bin's index.

If the coherent sampling condition is met, the integer number of cycles of the waveform in the data record J , the input and sampling frequency, and total number of sampled data M , satisfy the following relation:

$$f_i = J \frac{f_s}{M}. \quad (3.4)$$

Under the condition of coherent sampling, it is possible to recover correct amplitude and phase information of the fundamental and harmonics. They can be derived from the respective bins of the FFT output, given by:

$$X_J = \frac{A_1}{2} e^{j\phi}, \quad X_{J_h} = \frac{A_h}{2} e^{j\phi_h}. \quad (3.5)$$

B. Challenges of Amplitude/ Frequency Drift and Non-coherent Sampling

If coherent sampling is not achieved, J is not an integer and is given as $J = J_{\text{int}} + \delta$, where J_{int} is the integer part of J , and δ is the fractional part of J . This results in severe “skirting” effect in the frequency spectrum, known as spectral leakages. In the industry, two algorithms: windowing [10-14] and sine fitting [15-18] are currently widely used. The

advantages and limitations are described in detail in [20-21, 23-24]. In the literature, many algorithms are proposed to resolve non-coherent sampling issue. Interpolating DFT (IpDFT) algorithms [19], closed form formula [20], Fundamental Identification and Replacement (FIRE) algorithm [21], and the two-step algorithm [22-24] are all capable of handling non-coherent sampling issue given different fields of applications. However, all these algorithms are targeted to resolve non-coherent sampling issue alone, they cannot be used for the test condition where the input signal also suffers from amplitude and frequency drift.

Another issue is the drift in the signal generator, which causes the signal frequency and amplitude to drift over time. This non-stationary test environment could be due to changes in the test environment's temperature, humidity, power supply variation, electronic instrumentation aging, and other variables. It is challenging and expensive to maintain a stable test environment for high-resolution ADC testing, and it is even more challenging for on-chip BIST solutions. If there is drift in the input signal, spectrum leakages will show up at the ADC output spectrum, which cannot be removed by conventional algorithms that resolve non-coherent sampling.

Non-stationary signal has been analyzed and studied for many years. A considerable variety of approaches have been developed to analyze the non-stationary signal in both time and frequency domain, such as moving-window method [25-26], or digital equivalent of moving-windowing method [27]. However, the use of these methods does not lead to sufficient accuracy. In [28], authors used an adaptive linear prediction filter, which can provide instantaneous frequency of a signal, but information about the amplitude is completely lost. Another approach is to use Short-Time Fast Fourier Transform (STFFT), however, the disadvantage lies in its trade-off between time and frequency resolution [29]. In

[30-31], an algorithm that can compensate amplitude and frequency drift is proposed. By using Adaptive Fourier Analyzer (AFA) and sine fit algorithm, the algorithm can detect and compensate amplitude/frequency drift, which is recursive, accurate, and robust. However, the algorithm relies on the sine fit and iterations, which is less attractive due to its computational inefficiency. In [32], a new algorithm is proposed to resolve frequency drift issue in ADC spectral testing. It divides the output of the ADC into segments and averages them after initial phase correction. The simulation results verified the accuracy of the algorithm. This algorithm requires the frequency drift to be small so that it is almost constant in one segment. However, there is no control of how much drift the test environment could have. Moreover, when the test environment becomes unstable, not only signal frequency, but amplitude could suffer from the drifting issue.

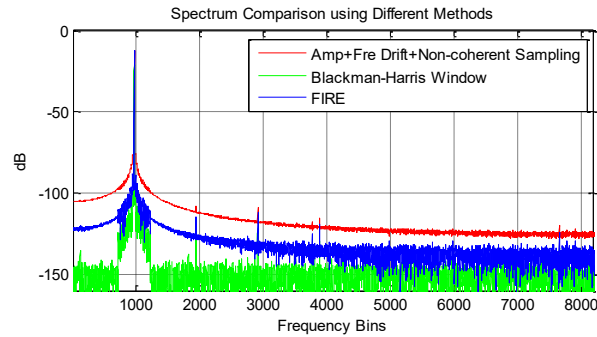


Figure 3.1. ADC Spectrum with amplitude/frequency drift and non-coherent sampling

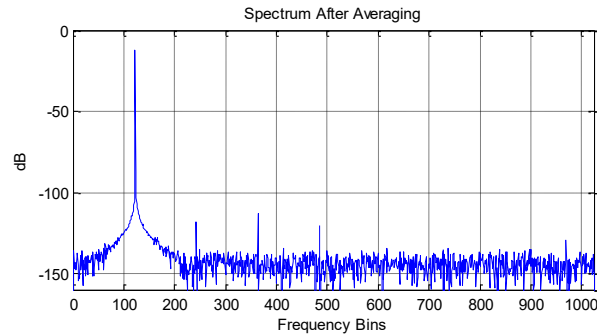


Figure 3.2. ADC Spectrum after using averaging algorithm in [32]

Figure 3.1 shows the spectrum (red) when ADC's input signal is non-coherently sampled and has amplitude/frequency drift. The blue spectrum is after using the FIRE algorithm where there are still leakages around the fundamental bin. The green spectrum is after using 4-term Blackman-Harris window, similarly the leakages due to drift are not completely removed. Figure 3.2 shows the spectrum of one segment using the algorithm in [32], with the same ADC under test. Similar results were observed as it cannot resolve the amplitude/frequency drift issue with non-coherent sampling.

As none of the algorithms described above have the way to effectively and efficiently deal with the situation of simultaneous amplitude/frequency drift and non-coherent sampling, there is a strong need to develop a low cost and efficient algorithm that resolves this issue. In this chapter, a new algorithm is proposed, which is capable of resolving amplitude/frequency drift and non-coherent sampling effectively and efficiently. The accuracy and robustness of the proposed algorithm is validated by both extensive simulation and measurement results.

3.3 Proposed Algorithm

A. Drift Segmentation

The drift is unpredictable, there is no exact form of the drift over time, and it will be different during each measurement. Due to its low frequency property, during a short time, the drift amount is small and can be treated as a linear varying function versus time (best fit line versus time). Within a short time, it is possible to obtain a good estimate of both amplitude and frequency drift. Thus, the data sequence is divided into segments. This is shown in Figure 3.3, as the blue curve is the normalized drift amplitude with maximum of

$\pm 1\%$ drift, where the scale is from 99% to 101% over the entire sampling period. The x-axis is normalized from 0 to 1, which is the time duration ratio t/t_{total} , where t is the time and t_{total} is the total sampling time. After the data sequence is segmented by the green dotted line, the drift contained in the data is also divided into segments. In each segment, a linear estimation of the drift can be obtained, which is shown in red.

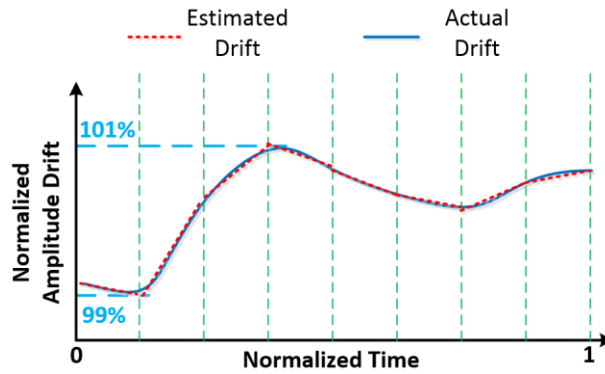


Figure 3.3. Drift segmentation.

B. Drift Modeling

Before developing the algorithm that can estimate the drifted fundamental and frequency, the drift needs to be modeled in accordance with the real test setup. The input signal without drift is given by:

$$V_{in}(t) = A_1 \cdot \cos(2\pi f_0 t + \phi) + w(t), \quad (3.6)$$

where A_1 is the constant amplitude, f_0 is the constant frequency, ϕ is the initial phase and $w(t)$ is the noise.

When the drift is significant or the accuracy requirement is high, such constant amplitude and frequency model is not sufficient. In the proposed algorithm, the drifted

amplitude and frequency are modeled by Eq.(3.7). When the amplitude is changing with time, it is given by:

$$A(t) = A_1 \cdot (1 + m(t)), \quad (3.7)$$

where $m(t)$ is the time varying component of the drifted amplitude.

Since any level of non-coherency is allowed, it is assumed that the sampling clock and the signal source are independent of each other, meaning that there is no need for synchronization between the two. In addition, although both clock and the source can drift, only the relative drift is critical, then we assume the clock is ideal and all the drift is due to the source.

Similarly, the input frequency can be modeled as:

$$f(t) = f_0 \cdot (1 + \varepsilon(t)), \quad (3.8)$$

where $\varepsilon(t)$ is the time varying component of the drifted frequency.

The drift input signal is then given by:

$$V_{in}(t) = A_1 \cdot (1 + m(t)) \cdot \cos(2\pi f_0 \cdot (1 + \varepsilon(t))t + \phi) + w(t), \quad (3.9)$$

where $w(t)$ is the noise inherited in the signal, which is treated as white noise. The sampled ADC output is given by:

$$V_{out}[n] \approx A_0 + A[n] \cdot \cos(2\pi \frac{f[n]}{f_s} n + \phi) + h.d + W[n], \quad (3.10)$$

where $A[n] = A_1 \cdot (1 + m[n])$, $f[n] = f_0(1 + \varepsilon[n])$, $h.d$ is high order harmonics of the ADC, A_0 is the DC offset and $W[n]$ is the sampled noise.

Since the expressions for $m[n]$ and $\varepsilon[n]$ are unknown, as mentioned earlier, by segmentation, the linear approximation of the drift amplitude/frequency becomes possible. Assuming total K segments, with equal segment length of L . In k^{th} segment ($1 \leq k \leq K$),

$m[n]$ has n ranging from $(k-1)L$ to kL . Within k^{th} segment, there is an unknown but best fit line. Then $m[n]$ can be represented by:

$$m[n] = m_k + S_k \cdot [n - (k-1) \cdot L] + \tilde{r} \quad , \quad (3.11)$$

where m_k and S_k are the offset and slope of k^{th} segment best fit line, and \tilde{r} is the difference between best fit line and actual drift.

By plugging Eq.(3.11) into the amplitude expression in Eq.(3.10), the sampled amplitude $A[n]$ can be written as:

$$A[n] = A_k + A_{S_k} \cdot n + A_n \quad , \quad (3.12)$$

where $A_k = A_1 \cdot m_k$, $A_{S_k} = A_1 \cdot S_k$, and $A_n = A_1 \cdot \tilde{r}$.

Similarly, the drifted frequency can be modeled as

$$f_0[n] = f_k + f_{S_k} \cdot n + f_n \quad . \quad (3.13)$$

For the random drift part: A_n and f_n , they can be treated as noise, in the following estimation they are neglected due to their small quantity, this part of estimation error is discussed in Section III.D. In addition, the drift on harmonics is small, whose leakage is below the noise floor and negligible compared to the fundamental drift. Therefore, the harmonics are considered to have no drift in the following derivations.

C. Signal Segmentation & Drift Estimation

After the drifted amplitude and frequency are modeled in k^{th} segment, the sampled ADC output at k^{th} segment is given by:

$$V_{out,k}[n] \approx A_0 + (A_k + A_{S_k} \cdot n) \cdot \cos\left(2\pi \frac{f_k + f_{S_k} \cdot n}{f_s} n + \phi_k\right) + h.d + W[n] \quad , \quad (3.14)$$

where the k^{th} segment drift fundamental is given by:

$$V_{fund,k}[n] = (A_k + A_{Sk} \cdot n) \cdot \cos(2\pi \frac{f_k + f_{Sk} \cdot n}{f_s} n + \phi_k). \quad (3.15)$$

From Eq.(3.15), there are 5 unknowns ($A_k, A_{Sk}, \phi_k, f_k, f_{Sk}$) that need to be estimated. Since these are not in the linear combination, direct Least Square cannot be used for the estimation of these unknowns. Instead, Newton iteration is used to estimate these parameters. The first step is to obtain initial estimation of these parameters. For input frequency f_0 , it can be obtained by four parameter sine fit [7-9], with closed form formula as the initial estimate [20]. The initial amplitude A_1 , phase ϕ_1 , and fractional part of sampled periods δ_1 are given by:

$$\delta_1 = \frac{M}{2\pi} \text{imag} \left(\ln \left(\frac{\frac{X_{J_{int}}}{X_{J_{int+1}}} - \frac{X_{J_{int}}}{X_{J_{int-1}}}}{\frac{X_{J_{int}}}{X_{J_{int+1}}} - \frac{X_{J_{int}}}{X_{J_{int-1}}} + e^{j\frac{2\pi}{M}} - e^{-j\frac{2\pi}{M}}} \right) \right), \quad (3.16)$$

$$A_1 = 2M \left| X_{J_{int}} \right| \left| \frac{1 - e^{j\frac{2\pi\delta_1}{M}}}{1 - e^{j2\pi\delta_1}} \right|, \quad (3.17)$$

$$\phi_1 = -\text{imag} \left(\ln \left(\frac{2MX_{J_{int}}}{A_0} \frac{1 - e^{j\frac{2\pi\delta_1}{M}}}{1 - e^{j2\pi\delta_1}} \right) \right). \quad (3.18)$$

Since the closed form formula is close to the true value, only a few iterations would be sufficient for sine fit to converge and obtain accurate estimation of f_0 .

The initial phase at k^{th} segment can then be given by:

$$\phi_k = 2\pi f_o(k-1)LT_s + \phi_1, \quad (3.19)$$

where $T_s = 1/f_s$.

For the linear drift component A_{Sk} and f_{Sk} , since they are small, their initial estimation values are given 0 and DC offset can be obtained from FFT spectrum bin X_0 . After all initial values of unknowns are obtained, Newton iteration is used, the value of y in $(i+1)^{\text{th}}$ iteration, y_{i+1} , is given by:

$$y_{i+1} = y_i - B_i \setminus F_i, \quad (3.20)$$

where “\” operator is the least squares operator, y_i is the vector containing the 5 estimated parameters in k^{th} iteration, F_i is shown in Eq.(3.22), which is the difference between estimated drift fundamental in Eq.(3.15) and actual output and B_i is the Jacobean matrix evaluated using values in y_i as shown in Eq.(3.21).

$$B_i = \begin{bmatrix} \frac{\partial V_{out,k1}}{\partial A_k} & \frac{\partial V_{out,k1}}{\partial A_{Sk}} & \frac{\partial V_{out,k1}}{\partial \phi_k} & \frac{\partial V_{out,k1}}{\partial f_k} & \frac{\partial V_{out,k1}}{\partial f_{Sk}} \\ \vdots & \vdots & \vdots & \vdots & \vdots \\ \frac{\partial V_{out,kL}}{\partial A_k} & \frac{\partial V_{out,kL}}{\partial A_{Sk}} & \frac{\partial V_{out,kL}}{\partial \phi_k} & \frac{\partial V_{out,kL}}{\partial f_k} & \frac{\partial V_{out,kL}}{\partial f_{Sk}} \end{bmatrix}_{y_i}, \quad (3.21)$$

$$y_i = \begin{bmatrix} A_k \\ A_{Sk} \\ \phi_k \\ f_k \\ f_{Sk} \end{bmatrix}_i, F_i = \begin{bmatrix} f_1 \\ \cdot \\ \cdot \\ \cdot \\ \cdot \\ f_L \end{bmatrix}_{y_i}. \quad (3.22)$$

After 5 to 10 iterations, the Newton iteration always converges to a global minimum as the initial points to start the iterations are very close (10^{-4} accuracy level) to the actual values. The accuracy in estimating these 5 unknowns is limited by the noise power per bin [21]. This accuracy will reflect how accurate the THD, SNR, and SFDR on the spectrum are estimated, which will be shown in detail in Section IV.B-D.

After each unknown parameter is accurately estimated, the k^{th} segment estimated fundamental can be given by:

$$\hat{V}_{fund,k}[n] = (\hat{A}_k + \hat{A}_{Sk} \cdot n) \cdot \cos(2\pi \frac{\hat{f}_k + \hat{f}_{Sk} \cdot n}{f_s} n + \hat{\phi}_k). \quad (3.23)$$

Since the proposed algorithm treats each segment identically, there is no need to distinguish different segments. The next step, after estimating all K segment's drift fundamentals, is to combine them consecutively in time domain to obtain the estimated drift fundamental:

$$V_{fund_Dr}[n] = [\hat{V}_{fund,1}, \dots]. \quad (3.24)$$

Now the estimated drift fundamental has the same length with original ADC output, it is subtracted from original output, removing the drift leakage, and the non-drift fundamental $V_{fund,nom}$ can be added to the residue. The new output is therefore given by:

$$V_{new}[n] = V_{out}[n] - V_{fund_Dr}[n] + V_{fund,nom}[n], \quad (3.25)$$

where $V_{fund,nom}[n] = \hat{A}_1 \cos(2\pi \frac{\hat{f}_0}{f_s} n + \hat{\phi}_1)$.

The final step involves coherency correction. With the drift estimated and removed, different non-coherent sampling algorithms can be used. Since harmonics of the ADC are much smaller compared with fundamental, they have leakages that are well below the noise floor [20-21], and there is no need to correct non-coherency for harmonics. Only the non-coherent fundamental needs correction. Therefore, the FIRE algorithm is used to remove non-coherency on the new output $V_{new}[n]$. The detailed steps for non-coherent fundamental identification and replacement are shown in [21] and are not repeated in this chapter. After

using FIRE algorithm, the final output $V_F[n]$ without the influence of non-coherency, amplitude and frequency drift is obtained.

Alternatively, after subtracting estimated drift fundamental from each segment, harmonics and noise can be accurately obtained from the residue in each segment. Moreover, by averaging the results from every segment, the averaged result is equivalent to estimating them as one sequence mentioned before. Figure 3.4 summarizes the flowchart of the proposed algorithm.

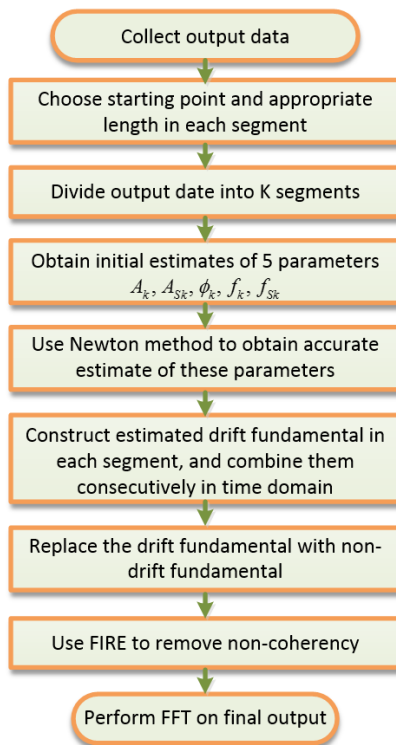


Figure 3.4. Flowchart of the proposed algorithm

D. Error Analysis

The goal is to provide insight of how the drift induced error behaves and how it affects the accuracy of the algorithm, so that proper segment length can be selected. The drift

induced error e_L is either A_n for amplitude drift, or f_n for frequency drift as defined in Section III.B.

The more segments that are divided, the more accurate model and estimation of the drift can be achieved. To illustrate this, one example of drift amplitude is shown in Figure 3.5, with the same scaling factor and time duration as Figure 3.3. If only one segment is used, which is shown in Figure 3.5a, the drift induced error is large. However, when multiple segments are divided (Figure 3.5b), the drift can be more accurately modeled and drift induced error becomes smaller.

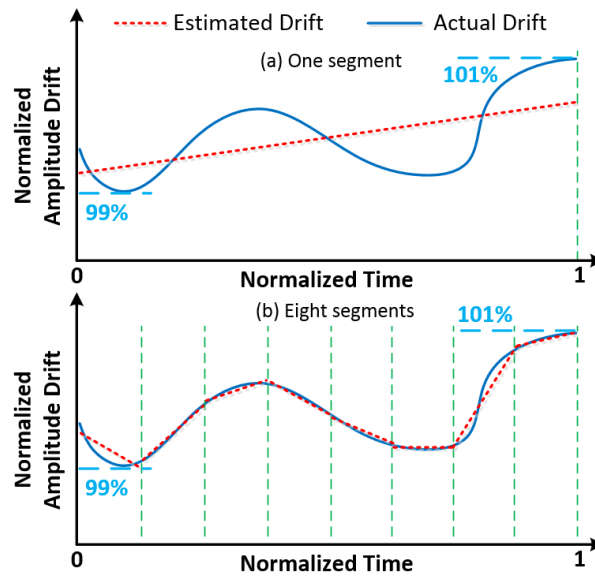


Figure 3.5. Drift segmentation and modeling with (a) one segment, and (b) eight segments

On the other hand, with more segments divided, each segment will have less samples. The estimation accuracy of the drift model, which is the best fit line, depends on the number of samples. If more samples are used in each segment for estimation, better estimation accuracy can be achieved [33-34]. However, for the whole output data (length of $M = K \cdot L$),

when analyzing the error for estimation, for example, the 2nd harmonic estimation, the error is still given by: Var_n^2/M , where Var_n^2 is the total noise variance, and part of the noise is Least Square induced error. This shows that the least square induced error should be independent of number of segment chosen.

Extensive simulations are conducted to investigate the drift induced error. Total K segments are generated, each segment length L . The drift is generated in MATLAB as follows:

1. Generate a normal distribution sequence $z[n]$
2. Take FFT of $z[n]$ to obtain Z_k .
3. Use ideal low pass filter to filter out high frequency component. The bandwidth of the ideal low pass filter can be 1/8 of sampling frequency or smaller.
4. Convert FFT data back to time domain data, and integral it to obtain $I[n]$.
5. Normalize the range of $I[n]$ to given range, for example, for amplitude drift, it can be 1% of ADC's full range.

The final generated drift is given by:

$$D[n] = D_l \cdot (1 + I[n]), \quad (3.26)$$

where D_l is the constant part of the drift, which is either A_o or f_o defined in Section III.B.

After that, it is divided into total K segments.

Before investigating the drift induced error, several terms are defined:

In one segment with length L , there are total L of sampled drift induced errors $e_L[n]$, and the mean of e_L is given by:

$$\bar{e}_L = \sum_{i=1}^L e_L(i) / L. \quad (3.27)$$

The standard deviation is given by:

$$\sigma_{eL} = \sqrt{\frac{1}{L-1} \sum_{i=1}^L (e_L(i) - \bar{e}_L)^2}. \quad (3.28)$$

For total K segments, the mean of all segments' \bar{e}_L is given by:

$$E(\bar{e}_L) = \sum_{i=1}^K \bar{e}_L(i) / K. \quad (3.29)$$

The mean of all segment's σ_{eL} is given by:

$$E(\sigma_{eL}) = \sum_{i=1}^K \sigma_{eL}(i) / K. \quad (3.30)$$

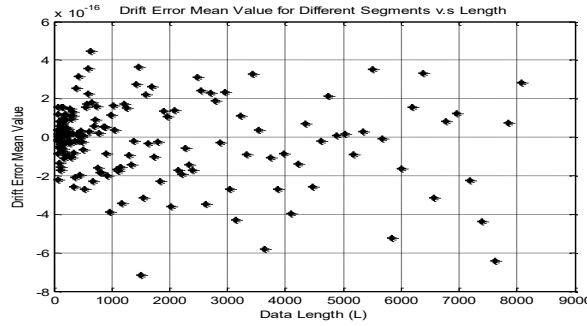


Figure 3.6. Mean of all segments averaged drift error vs data length

In MATLAB, total 1000 segments were generated, with each segment length L ranging from 64 to 8200, and the length increases 3% each time. The drift is normalized up to 1% of full scale, which is 1 in the simulation.

Figure 3.6 shows the statistical results of $E(\bar{e}_L)$. The mean value of all segments' mean is very close to 0, which is expected as the drift induced noise is averaged out and the mean value is close to 0.

Figure 3.7 shows the statistical results of $E(\sigma_{el})$, which is also rms value of drift induced error. The mean of all segments' standard deviation is proportional to \sqrt{L} . This is expected because the drift induced noise has 0 mean, the drift induced noise power is proportional to its variance, which is proportional to data length.

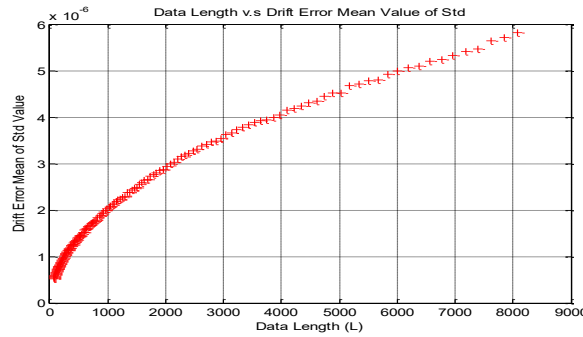


Figure 3.7. Mean of all segments std drift error vs data length

All these statistical results illustrate the property of drift induced noise, whose mean value is small, and the power is proportional to data length. These results provide insight of choosing appropriate segment length and it is validated by both extensive simulation and measurement results in the next two sections.

E. Segment Length Selection

There are certain requirements on the length selection in each segment, in addition, the appropriate segment length depends on the drift and noise inherited in the ADC output, which can be seen from the previous section. Firstly, the length needs to be small so that the drift is close to a linear function over time. The drift induced error is also discussed in previous section, which recommends small segment length, such as 80-200. Secondly, if the

length is small that the noise floor covers harmonic bins on spectrum, the correct spectral information of the ADC is lost. Thirdly, to calculate spectral parameters correctly, there are minimum number of bins on the spectrum needed. For example, usually for calculating the fundamental power on spectrum, the fundamental bin and two bins nearby are included. It is calculated similarly for harmonics as 3 bins are used and for DC, 1 bin is used. If 13 harmonics are included to calculate THD, then minimum number of bins used are 80. In the algorithm, the segment length can be chosen from 80 to 200. Finally, although we assume equal length previously for derivation convenience, the length in each segment is not required to be the same, the algorithm does not depend on equal length for each segment, which relaxes the length selection requirement.

Figure 3.8 illustrates the selection of length in each segment. At first, after discarding any unsettled initial points, the starting point p is selected near zero crossing, which has largest slope for sinusoidal signals and making it distinctive to select. Starting from p , the segment length L is selected between 80 and 200. Among them, 5 consecutive points ($q-4$ to q) are found that match the initial points (p to $p+4$) the best. The segment length L is then determined by $q-p+1$. Finally, output with data record length of M is divided into K

segments, with each segment length of L_k , and K is selected such that $\sum_{k=1}^K L_k \leq M$. The

remaining points $M - \sum_{k=1}^K L_k$ are included into the last segment for estimation. It may seem that

L_k can be anywhere between 80 and 200, but once L_l is selected, the rest of L_{ks} only differ from L_l by ± 1 . To evaluate the segment length selection, its performance into the proposed algorithm is presented in Section IV.B.

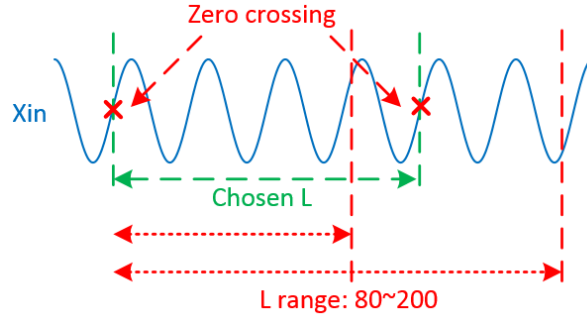


Figure 3.8. Length selection in each segment.

3.4 Simulation Results

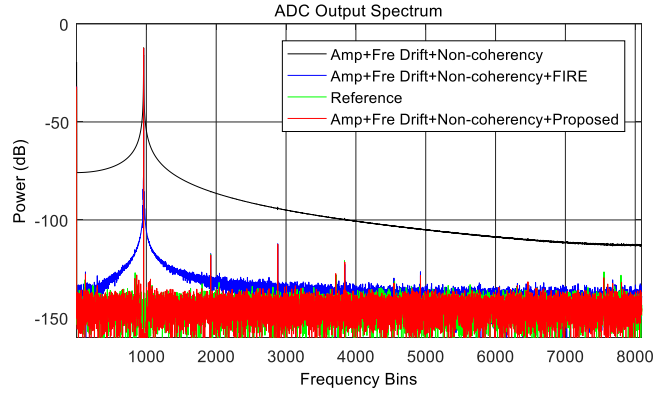
In this section, extensive simulation results are shown to verify the functionality and robustness of the proposed algorithm.

A. Functionality

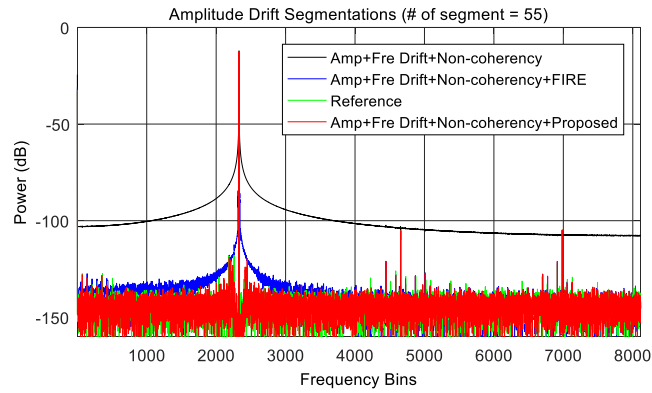
In MATLAB, the proposed algorithm is used to verify the spectral performance of a 16-bit nonlinear ADC, with INL of 1.8LSB. The input sinusoidal signal suffers from both amplitude drift, frequency drift and non-coherent sampling. Drift is modeled similarly in Section III.D. For amplitude drift, the maximum drift is up to 2% of the full range of the ADC under test. For frequency drift, the drift maximum drift is 100 ppm/s. For non-coherency, δ is randomly generated from -0.5 to 0.5, while J_{int} is 971. The ADC input referred noise is randomly generated with Gaussian distribution and 0.5LSB rms value. The true ADC's SNR, THD, and SFDR are obtained by sending a pure, non-drift sinusoidal signal with same level of noise (0.5LSB rms) to the ADC under test, which is coherently sampled (sampled periods of 971). It serves as the reference to evaluate the functionality of the proposed algorithm, with the expected ADC performance shown in Table 3.1: column 'Reference'. The proposed algorithm divided the drift data ($M=2^{14}$) into 112 segments.

Figure 3.9 shows the following four spectrums: black spectrum, obtained by direct FFT of raw ADC output, which suffers from amplitude and frequency drift and non-coherent sampling; blue spectrum obtained by FIRE algorithm only; green spectrum, obtained by a pure, non-drift input with coherent sampling, and red spectrum, obtained after using the proposed algorithm. For the black spectrum, large leakage around the fundamental bin can be seen, and it masks the harmonics underneath. In this case, correct noise and harmonics information cannot be obtained. For the blue spectrum, after only using the FIRE algorithm, the spectrum leakage due to non-coherency is removed, however, there is still leakage left, which is due to the amplitude drift and frequency drift that cannot be removed by the FIRE algorithm. Although harmonics that are far away from the fundamental bins are recovered, harmonics bins that are close to the fundamental bin and noise cannot be successfully recovered. After using the proposed algorithm, the leakages due to both non-coherent sampling and drift are removed and harmonics and noise information can be accurately recovered. The accurate estimation using proposed algorithm can also be seen from Table 3.1.

Another set of data is acquired, from a different 16-bit nonlinear ADC, with INL of 2.4LSB, the number of sampled periods is 2351, the segments used in the proposed algorithm then becomes 97. Similar results from other tests can be seen from Figure 3.10 and Table 3.2 which both direct the FFT and FIRE algorithm alone cannot obtain accurate ADC spectral performance, and the proposed algorithm is able to recover the correct spectrum as it matches well with the reference spectrum and its spectral performance.

Figure 3.9. ADC output spectrum using different algorithms ($J_{int}=971$)Table 3.1. Spectral Specifications of ADC Under Test ($J_{int}=971$)

Input Signal	THD(dB)	SFDR(dB)	SNR(dB)
Reference	-98.99	100.65	91.63
Direct FFT	-60.21	61.71	62.27
FIRE	-98.24	99.62	78.04
Proposed	-99.01	100.35	91.18

Figure 3.10. ADC output spectrum using different algorithms ($J_{int}=2351$)Table 3.2. Spectral Specifications of ADC Under Test ($J_{int}=2351$)

Input Signal	THD(dB)	SFDR(dB)	SNR(dB)
Reference	-89.62	92.73	91.09
Direct FFT	-58.07	58.06	56.58
FIRE	-89.06	92.06	72.23
Proposed	-89.69	92.59	90.91

B. Robustness: Segment Length

The first characteristic that is examined to validate the robustness of the proposed algorithm is the segment length. The following section investigates how different sources of errors affect the accuracy of the proposed algorithm as different segment lengths are chosen. The THD of the ADC under test is examined. The true total harmonics power hd is measured by using the standard way, whose input to the ADC has no amplitude nor frequency drift, and is coherently sampled. While the estimated total harmonics power hd_{est} is measured by using the proposed algorithm, with the drift and non-coherently sampled input. They are given by:

$$hd = \sum_{h=2}^{14} |2 \times X_{Ref_Jint\cdot h}|^2, \quad (3.31)$$

$$hd_{est} = \sum_{h=2}^{14} |2 \times X_{Pro_Jint\cdot h}|^2, \quad (3.32)$$

where X_{Ref} and X_{Pro} are the FFT of the ADC output data obtained by standard way, and by the proposed algorithm, respectively.

The difference between hd and hd_{est} is defined as estimation error in dB: $10\log(hd - hd_{est})$. The error is compared with noise power in these same number of bins, which serves as a reference. For example, if first 14 harmonics are used to calculate THD, then the error should compare with 14 times of the expected noise power per bin in dB, given by: $10\log(14 \times P_n / M)$, where P_n is the ADC's total noise power. Since at each run the noise will be different, the variation is bounded by $\pm 4\sigma$ or $\pm 12dB$ where σ is the standard deviation of the noise power. If they are in the similar level ($\pm 12dB$) or error is much smaller than

noise in these bins, the estimation is considered as accurate, otherwise it is considered as inaccurate. In MATLAB, different number of segment lengths, from 60 to 2000, are used to verify the proposed algorithm. A 16-bit nonlinear ADC is generated and is tested for various segment lengths. Other test setups are the same as previous section. The total harmonics power estimation error for different segment lengths is shown in Figure 3.11.

As it shows, accurate estimation of the total harmonics power is achieved across various segment lengths, although there is a slight increase in estimation errors (red triangle) due to a lower number of segments, they are still in the similar level ($\pm 12dB$) of the reference (blue flat line), which is the expected noise power in the same number of bins. This demonstrates that the proposed algorithm is capable of accurately estimating and removing leakages caused by the drift & non-coherent sampling, and can recover the correct harmonics information, which is robust against different segments lengths. Accurate harmonics estimation of the ADC can all be obtained by using different segments lengths.

C. Robustness: Number of Periods

Another parameter that needs to be examined is the number of the sampled periods. Again, THD of the ADC under test is examined and the same criteria is used for evaluating the estimation accuracy. The J_{int} is randomly generated from 101 to 4999, and odd numbers are selected. Similarly, given each J_{int} , δ is randomly generated from -0.5 to 0.5 and so does signal noise (rms of 0.5LSB), the number of segments is fixed at 128 and $M=2^{14}$. The total harmonics power estimation errors for different sampled periods are shown in Figure 3.12.

From Figure 3.12, as before, accurate estimations of the total harmonics power are achieved for all different number of the sampled periods, as the estimation errors (red triangle) are in the neighborhood of the reference (blue flat line). This reveals that the proposed algorithm is independent of input signal sampled periods, and it is robust against various input signal frequencies.

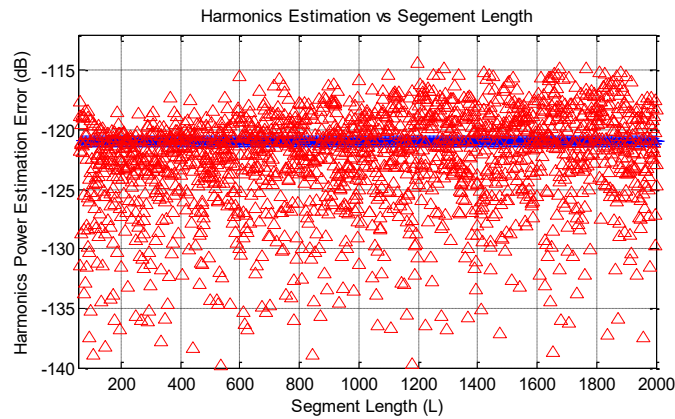


Figure 3.11. Harmonic power estimation error versus segment length

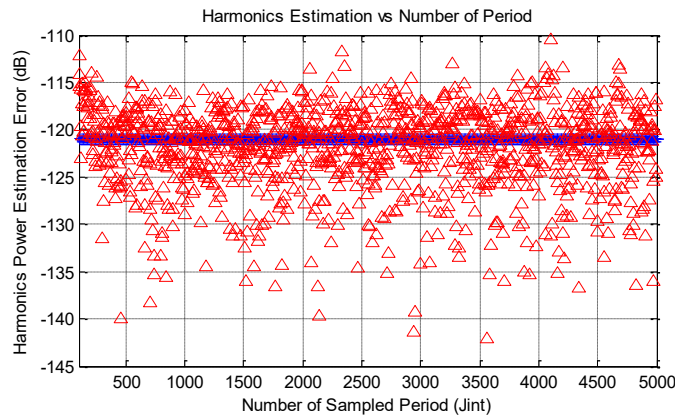


Figure 3.12. Harmonic power estimation error versus sampled periods

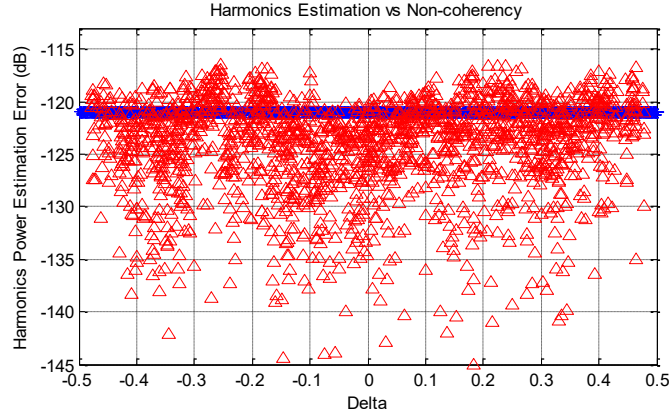


Figure 3.13. Harmonic power estimation error versus non-coherency level

D. Robustness: Non-coherency

One of the goals of this algorithm is to completely remove non-coherency. To investigate the robustness against non-coherency, a total 1000 runs were simulated in MATLAB, with randomly generated δ from -0.5 to 0.5 and signal noise (rms of 0.5LSB). J_{int} is fixed to 971 and number of segments is fixed to 128. The total harmonics power estimation errors are shown in Figure 3.13.

In Figure 3.13, the harmonic power estimation errors (red triangle) are near the reference (blue flat line) across all δs , meaning that any level of non-coherency can be taken care of by the proposed algorithm. This demonstrates that the proposed algorithm is robust against any level of non-coherent sampling.

3.5 Measurement Results

To further validate the proposed algorithm, several measurement results were obtained from different test instruments and different ADCs.

The first measurement data is obtained using MSP430 from Texas Instruments. The 10-bit ADC on board is used as the device under test. The input signal is generated by a regular lab function generator (Agilent 33220A function generator), which has a certain amount of drift at its output sine wave. The power supply is provided by Agilent E3548A DC power supply. To compare the result, the reference input signal to the ADC is generated by Audio Precision AP2700, which has high-purity sinusoidal output, precise reference voltages, and high-precision clock synthesizer to avoid amplitude and frequency drift, and it is coherently sampled by the ADC. The ADC spectral performance obtained using such signal serves as the accurate reference result. To observe the drift effect on the signal, a long test time is preferred and a total 2^{17} samples were taken to verify the proposed algorithm.

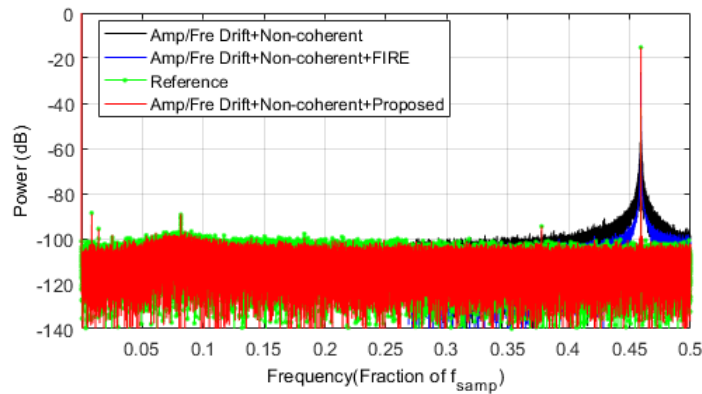


Figure 3.14. MSP ADC output spectrum using different algorithms

Table 3.3. Spectral Specifications of MSP ADC Under Test

Input Signal	THD(dB)	SFDR(dB)	SNR(dB)
Reference	-71.12	73.96	48.05
Direct FFT	-65.58	70.12	10.67
FIRE	-70.61	73.18	26.17
Proposed	-70.96	73.75	47.66

Figure 3.14 shows the ADC output spectrum using different algorithms. For direct FFT (black), due to the non-coherent sampling and amplitude/frequency drift, accurate spectral performance of the ADC cannot be obtained as there are certain amount of leakages around the fundamental bin. Using the FIRE algorithm alleviates the leakage problem as the blue spectrum shows less leakage, but the leakage due to amplitude and frequency drift is not removed. After using the proposed algorithm (red), leakages due to both non-coherent sampling and drift are removed, and it matches with the reference spectrum (green) well. Correct noise and distortion information of the ADC can be recovered. The spectral performance of the ADC using different algorithms are shown in Table 3.3, which also verifies the accuracy of proposed algorithm.

In addition, an 18-bit commercial ADC (ADS9110) was used to further validate the proposed algorithm. Two different input frequencies were tested: 2kHz and 4.17kHz sinusoidal signals, with 2.5V peak-to-peak value. The reference signal is also generated by Audio Precision. The test signal is generated by low precision signal generator with filtering, which has less stable reference voltages, so there was a small amount of drift in the signal, and it is non-coherently sampled by the ADC.

Upon testing the ADS9110, for the reference signal, the signal frequency has to be precisely controlled to 2.00081kHz and 4.16946kHz to achieve coherent sampling. In comparison, the test signal's frequency is roughly controlled around 2kHz and 4.17kHz, which requires much less effort to achieve. The DAS9110 spectrum at different input frequencies are shown in Figure 3.15 and Figure 3.16, respectively. Direct FFT (black) cannot obtain accurate spectrum performance of the ADC because of the leakages due to the non-coherent sampling and amplitude and frequency drift. After applying only the FIRE

algorithm, the leakages due to non-coherency are removed, but there are still some leakages around the fundamental bin that is caused by amplitude and frequency drift (blue). Also from Table 3.4 and 3.5, the FIRE algorithm can obtain estimate the THD and SFDR marginally well, but the SNR estimation is not accurate. For the proposed algorithm, as it can be seen from red spectrum that the leakages due to both non-coherency and drift are successfully removed, and it matches well with the green spectrum, which is the reference. Both results have demonstrated that the proposed algorithm can accurately test a high-performance ADC, with non-coherent sampling and amplitude and frequency drift at the input signal.

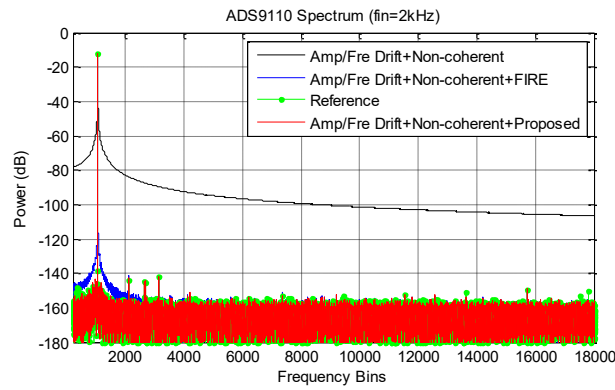


Figure 3.15. ADS9110 ($f_i=2\text{kHz}$) spectrum using different algorithms

Table 3.4. Spectral Specifications of ADS9110 ($f_i=2\text{kHz}$)

Input Signal	THD(dB)	SFDR(dB)	SNR(dB)
Reference	-120.28	127.37	97.97
Direct FFT	-79.54	83.15	62.63
FIRE	-119.86	126.65	86.47
Proposed	-120.05	127.11	97.63

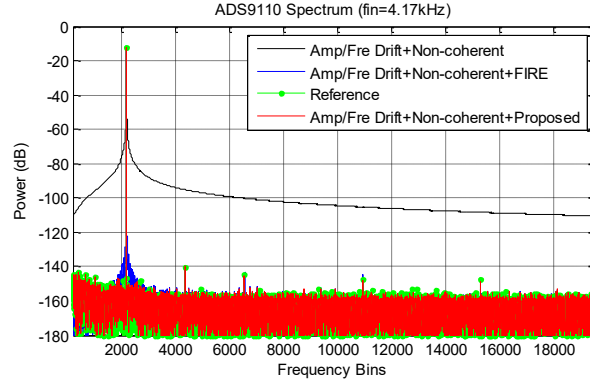


Figure 3.16. ADS9110 ($f_i=4.17\text{kHz}$) spectrum using different algorithms

Table 3.5. Spectral Specifications of ADS9110 ($f_i=4.17\text{kHz}$)

Input Signal	THD(dB)	SFDR(dB)	SNR(dB)
Reference	-118.94	126.31	96.87
Direct FFT	-80.89	82.28	67.46
FIRE	-116.56	125.09	88.79
Proposed	-118.78	126.42	96.55

3.6 Conclusion

A new algorithm that can achieve accurate spectral testing with simultaneous amplitude, frequency drift, and arbitrary non-coherency is proposed. The algorithm uses segmentations to divide the ADC output into multiple segments and accurately estimates the drift by the Newton iteration. By removing the drifted fundamental from original output, and replacing with a coherent, non-drift estimated fundamental, accurate spectral results can be obtained. Extensive simulation results and error analysis have validated the accuracy of the proposed algorithm. The proposed algorithm can tolerate various test condition variations such as any-level of non-coherency, a wide input frequency range, and different numbers of segmentations, demonstrating that it is accurate and robust. In addition, several measurement results from different ADCs have verified the accuracy of the proposed algorithm, which is

able to accurately obtain spectral performance of an 18-bit high-resolution ADC. Such an algorithm dramatically relaxes the traditional test requirement such as precise control over test signal frequency, amplitude, which greatly reduces the test setup difficulty and test cost. Given that the time complexity of the proposed algorithm is in the order of $O(2M \cdot \log_2 M) + O(M \cdot 4^2)$, where the Newton iteration takes much less time compared with dominating consuming part: FFT and 4 parameter sine fit [21], the proposed algorithm can be implemented for future on-chip BIST solutions.

References

- [1] Y. Zhuang, L. Xu and D. Chen, "Accurate Spectral Testing With Arbitrary Noncoherency in Sampling and Simultaneous Drifts in Amplitude and Frequency," *IEEE Trans. Instrum. Meas.*, vol. 55, no. 5, pp. 1002–1012, Mar. 2017.
- [2] Y. Zhuang and D. Chen, "ADC Spectral Testing with Signal Amplitude Drift and Simultaneous Non-coherent Sampling", *Journal of Electronic Testing: Theory and Applications*, vol.33, no.3, pp. 305-313, Jun.2017.
- [3] R. J. van de Plassche, *CMOS Integrated Analog-to-Digital and Digital-to-Analog Converters*, Boston, MA, USA: Kluwer Academic Publishers, 2003.
- [4] M. J. M. Pelgrom, *Analog-to-Digital Conversion*, 2nd ed. New York, NY, USA: Springer, 2012.
- [5] A. Oppenheim, *Discrete-time Signal Processing*, Englewood Cliffs, NJ, USA: Prentice-Hall, 1999.
- [6] M. Burns and G. W. Roberts, *An Introduction to Mixed-Signal IC Test and Measurement*, New York, NY, USA: Oxford Univ. Press, 2000.

- [7] IEEE Standard for Terminology and Test Methods for Analg-to-Digital Converters, *IEEE Std.1241*, 2010.
- [8] IEEE Standard for Terminology and Test Methods of Digital-to-Analog Converter Devices, *IEEE Std.1658*, 2011.
- [9] IEEE Standard for Digitizing Waveform Recorders, *IEEE Std.1057*, 2007.
- [10] F. J. Harris, "On the use of windows for harmonic analysis with the discrete Fourier transform," *Proc. IEEE*, vol. 66, no. 1, pp. 51–83, Jan. 1978.
- [11] P. Carbone, E. Nunzi, and D. Petri, "Windows for ADC dynamic testing via frequency-domain analysis," *IEEE Trans. Instrum. Meas.*, vol. 50, no. 6, pp. 1571–1576, Dec. 2001.
- [12] S. Raze, D. Dallet, and P. Marchegay, "Non coherent spectral analysis of ADC using FFT windows: An alternative approach," in *Proc. IEEE Workshop Intell. Data Acquisition Adv. Comput. Syst.*, Sep. 2005, pp. 474–478.
- [13] D. Belega, M. Ciugudean, and D. Stoiciu, "Choice of the cosine-class windows for ADC dynamic testing by spectral analysis," *Measurement*, vol. 40, no. 4, pp. 361–371, May 2007.
- [14] O. M. Solomon, "The use of DFT windows in signal-to-noise ratio and harmonic distortion computations," *IEEE Trans. Instrum. Meas.*, vol. 43, no. 2, pp. 194–199, Apr. 1994.
- [15] T. Z. Bilau, T. Megyeri, A. Sarhegyi, J. Márkus, and I. Kollár, "Four-parameter fitting of sine wave testing result: Iteration and convergence," *Comput. Standards Interfaces*, vol. 26, no. 1, pp. 51–56, 2004. 731

- [16] R. Pintelon and J. Schoukens, "An improved sine-wave fitting procedure for characterizing data acquisition channels," *IEEE Trans. Instrum. Meas.*, vol. 45, no. 2, pp. 588–593, Apr. 1996.
- [17] K. F. Chen, "Estimating parameters of a sine wave by separable nonlinear least squares fitting," *IEEE Trans. Instrum. Meas.*, vol. 59, no. 12, pp. 3214–3217, Dec. 2010.
- [18] G. Simon, R. Pintelon, L. Sujbert, and J. Schoukens, "An efficient nonlinear least square multisine fitting algorithm," *IEEE Trans. Instrum. Meas.*, vol. 51, no. 4, pp. 750–755, Aug. 2002.
- [19] D. Belega, D. Dallet, and D. Petri, "Estimation of the effective number of bits of ADCs using the interpolated DFT method," in *Proc. IEEE Instrum. Meas. Technol. Conf.*, May 2010, pp. 30–35.
- [20] S. Sudani, M. Wu, and D. Chen, "A novel robust and accurate spectral testing method for non-coherent sampling," in *Proc. Int. Test Conf.*, Sep. 2011, pp. 1–10.
- [21] S. K. Sudani and D. Chen, "FIRE: A fundamental identification and replacement method for accurate spectral test without requiring coherency," *IEEE Trans. Instrum. Meas.*, vol. 62, no. 11, pp. 3015–3025, Nov. 2013.
- [22] Y. Zhuang and D. Chen, "Accurate spectral testing with non-coherent sampling for large distortion to noise ratios," in *Proc. IEEE 34th VLSI Test Symp. (VTS)*, Apr. 2016, pp. 1–6.
- [23] Y. Zhuang and D. Chen, "New strategies in removing non-coherency from signals with large distortion to noise ratios," in *Proc. IEEE Int. Symp. Circuits Syst. (ISCAS)*, May 2016, pp. 2901.

- [24] Y. Zhuang and D. Chen, "New strategies in removing noncoherency from signals with large distortion-to-noise ratios," *IEEE Trans. Circuits Syst. II, Express Briefs*, vol. 63, no. 12, pp. 1136–1140, Dec. 2016.
- [25] M. H. Ackroyd, "Short-time spectra and time-frequency energy distributions," *J. Acoust. Soc. Amer.*, vol. 50, pp. 1229–1231, Aug. 2005.
- [26] J. K. Hammond and P. R. White, "The analysis of non-stationary signals using time-frequency methods," *J. Sound Vibrat.*, vol. 190, no. 3, pp. 419–447, 1996.
- [27] M. Landisman, A. Dziewonski, and Y. Satô, "Recent improvements in the analysis of surface wave observations," *Geophys. J. Int.*, vol. 17, no. 4, pp. 369–403, 1969.
- [28] L. Griffiths, "Rapid measurement of digital instantaneous frequency," *IEEE Trans. Acoust., Speech, Signal Process.*, vol. 23, no. 2, pp. 207–222, Apr. 1975.
- [29] L. Cohen, "Time-frequency distributions—A review," *Proc. IEEE*, vol. 77, no. 7, pp. 941–981, Jul. 1989.
- [30] T. Dabóczy, "ADC testing using a resonator-based observer: Processing very long time records and/or testing systems with limited stability," *IEEE Trans. Instrum. Meas.*, vol. 62, no. 5, pp. 1166–1173, May 2013.
- [31] T. Dabóczy, "Increasing the robustness of the resonator based ADC testing," in *Proc. IEEE Int. Instrum. Meas. Technol. Conf. (IMTC)*, May 2013, pp. 353–358.
- [32] L. Xu and D. Chen, "Accurate spectral testing of analog-to-digital converters with frequency drift using phase correction and averaging," in *Proc. IEEE Int. Symp. Circuits Syst.*, May 2015, pp. 2265–2268.

- [33] G. C. Cecchi, "Error analysis of the parameters of a least-squares determined curve when both variables have uncertainties," *Meas. Sci. Technol.*, vol. 2, no. 12, pp. 1127–1128, 1991.
- [34] A. Bergamin, G. Cavagnero, and G. Mana, "Accuracy assessment of a least-squares estimator for scanning X-ray interferometry," *Meas. Sci. Technol.*, vol. 2, no. 8, pp. 725–734, 1991.

CHAPTER 4

HIGH-PURITY SINE WAVE GENERATION USING NONLINEAR DAC WITH PRE-DISTORTION BASED ON LOW-COST ACCURATE DAC-ADC CO-TESTING

Data converters are among the most widely used components in modern integrated devices and systems. A major challenge is to characterize their performances accurately and cost-effectively. The ADC standard test requires the input sinusoidal signal to be 3-4 bits better than the ADC under test. Such high-quality sine waves are extremely difficult to generate and challenging to implement cost effectively. This chapter presents a novel method that is capable of generating a high-purity sine wave using a low-cost nonlinear DAC. The purity of generated sine wave is significantly better than the original DAC output. In addition, with the aid of the low-cost DAC-ADC co-testing method, both DAC and ADC linearity information are accurately obtained with only 1 hit per code. Therefore, it is possible to add DAC linearity information to the DAC input codes, which cancels the nonlinearity of the DAC at output to achieve high purity. The proposed method has been validated by extensive simulation and measurement results, which demonstrated its accuracy and robustness against different resolutions, structures, or performance of the ADCs/DACs. With its low cost and easy test setup, such high-purity sine wave can be widely used for various applications where precision testing is required. In addition, the ADC and DAC linearity information are accurately obtained at the same time without any precision instrumentation, which is suitable for accurate DAC-ADC co-testing.

This chapter is mainly based on the paper accepted by *IEEE Trans. Instrum. Meas.* [1].

4.1 Introduction

Data converters characterization and testing have become more important in industry, due to their wide applications and usage. In recent years, data converter performance is improving rapidly, along with the need to test or measure such precision devices accurately [2-4]. The standard test involves high-precision instruments, such as Automatic Test Equipment (ATE) [5], Audio Precision x555 [6], and Data Converter Test Module (DCTM) [7], which can be quite expensive. Such stringent requirements have become increasingly difficult to meet, especially for high-precision testing, where a high-quality test stimulus or system is either extremely difficult to design or to implement cost effectively. Such instruments meant for today's data converter testing may not be able to test future devices accurately, since data converter performance improves rapidly. Therefore, alternative cost-effective solutions are needed to generate high-purity test stimulus to serve high-precision testing.

There are many cases when there are both Digital-to-Analog Converter (DAC) and Analog-to-Digital Converter (ADC) present in some integrated systems, which could be of great advantage to use both together to test the characteristics of the ADC as well as the DAC without any extra test stimulus or instruments. If DAC is used as the test stimulus for the ADC, its performance or linearity, needs to be 3-4 bits better than the ADC [8-10] because the DAC's nonlinearity will be at the same relative level as the ADC's. Thus, the resulting spectrum of the ADC output will include extra distortions coming from the DAC as well as those generated by the ADC under test. Similarly, for the DAC under test, an ADC with much better performance is needed to sample the DAC output, so the ADC nonlinearity is negligible and the DAC performance can be captured accurately. However, it is evident both

ADC and DAC performances cannot be evaluated simultaneously, and in most cases, the DAC and ADC have similar performances, so it is impossible to use traditional methods to accurately test the desired performance of the ADC using the DAC as a signal generator or use ADC to characterize the DAC.

In the past, there have been many studies regarding this issue. One approach is to use a low-cost, lower quality test stimulus to obtain accurate test results of the high-precision device under test (DUT), such as ADC. In [11], a Stimulus Error Identification and Removal (SEIR) method was developed and validated by numerous industrial data. It no longer requires a high-quality/purity source to test the ADC. Rather, a nonlinear signal source can be utilized to accurately determine the integral nonlinearity (INL) and differential nonlinearity (DNL) characteristics of the ADC under test. However, this method targets ADC testing alone and assumes the input signal is spatially smooth and approximates them via low order polynomial or sinusoidal functions. In [12], the nonlinear test signal was passed through two different filters, and the ADC under test sampled the two outputs separately. Since two different filters create different amplitude and phase shift for input harmonics at different frequencies, the source nonlinearity can be separated from ADC nonlinearity. Both simulation and measurement results have validated the accuracy and robustness of the method. However, the filters must be carefully designed, since they cannot introduce extra nonlinearity to the signal.

Another approach is to generate a high-purity test signal to characterize the DUT. Many approaches focus on using an Arbitrary Waveform Generator (AWG) [13-19]. Some of these methods are achieved by applying correction codes to cancel harmonics and spurs. AWG can generate high-purity sine wave for many applications, but the generated harmonics

frequencies cannot exceed the AWG's limit. In [17], pre-distortion codes were applied to an AWG, including an internal DAC, to measure an ADC more accurately. However, this method's goal is to attempt to move un-wanted spurs and push them to a higher frequency for filtering. This method requires more rigorous calculations as well as the addition of filters at the output of the DAC. Another study in [18] showed how pre-distortion codes were applied to a DAC to help correct spectral impurities in a radar system. However, this method uses several filters as well as attempts to correct for other spectral impurities in the entire radar system, not considering the spectral impurities of the DAC and ADC used. In [19], another approach was taken by changing the program of AWG using shift switching technique. With this technique, the 3rd harmonic is cancelled and a low-distortion sine wave is generated by filtering out other high order distortions. However, besides the 3rd harmonic, other low order harmonics might also limit the dynamic range of the generated sine wave. In [20], a novel method that uses two DACs and an ADC is proposed. This method iteratively removes unwanted harmonics from the main DAC output using Cal DAC and generates ultra-pure sine wave after two iterations. However, this method targets the audio frequency application, since it cannot generate ultra-pure sine waves at higher frequencies. Interpolation is another easy way to improve DAC performance. In [21], the authors proposed a linear interpolation approach to improve DAC performance, but the main task was to increase the resolution of the DAC and make the output waveform much smoother than the original signal, not to improve the spectral purity of the output waveform.

As stated above, previous studies suffer from several drawbacks regarding the generation of cost-effective high spectral purity test stimuli, such as sine waves. No previous studies are available for embedded applications, where no accurate instruments are available

to measure DAC distortions and no accurate signal sources are available to test measurement devices (ADC). In this chapter, the proposed method is an attempt to characterize both DACs and ADCs in a single test, with only 1 hit per code, and using the nonlinear DAC on board to generate a high-purity sine wave signal for accurate testing applications, by means of pre-distortion codes obtained without any accurate devices for generating such codes. Furthermore, the proposed method is based on a simple testing system that requires no extra filtering of higher frequency components to achieve accurate test results. This chapter also presents several options for implementing the proposed method based on trade-offs between accuracy requirements, the amount of hardware, and timing overhead that can be sacrificed in the test setup.

The remainder of the chapter is arranged as follows: Section II discusses standard spectral testing and linearity testing of data converters, and their challenges. Section III introduces the proposed method to generate high-purity sine waves using nonlinear DAC, the ways to generate pre-distortion codes, based on accurate linearity estimation of ADC and DAC. Section IV presents the simulation results in MATLAB. Both functionality and robustness of the proposed method are verified. Section V presents the measurement results that validate the proposed method and Section VI concludes this chapter.

4.2 Challenges of the Standard Test

This chapter focuses on the cost-effective approach to generate high-purity sine waves. To achieve this, we need to obtain accurate linearity performance of the ADC and DAC used to generate such high-purity sine waves. In IEEE standards [8-10], there are two ways to characterize the linearity performance of the ADC or DAC: linearity testing and

spectral testing [2,3,22]. The linearity test, or full code linearity testing, requires testing all transition levels, DNL and INL associated with these transition levels. The standard method for linearity testing is the histogram method, where a pure sine wave or ramp is used as the test stimulus to the DUT. The purity of such sine waves or ramp must be significantly better than DUT. Typically, dozens of samples per code are used for the histogram method to average out the effects of noise in the test stimulus. As the performance of the data converter increases, it pushes the test stimulus to have an even better performance in purity, which would be extremely difficult to design a high-performance source generator that meets such requirements and is costly to achieve. If such requirements are not met, using a low purity test stimulus to test the data converters would result in erroneous test results.

Spectral testing, or dynamic testing, is another common test approach to characterize the data converters. The data converters are generally specified in terms of ac performance characteristics, such as Signal-to-Noise Ratio (SNR), Total Harmonic Distortion (THD), Spurious Free Dynamic Range (SFDR), etc. The sine wave is used as the test stimulus, and Discrete Fourier Transform (DFT) or Fast Fourier Transform (FFT) is performed to obtain spectral results. There are several requirements to ensure accurate results. One is the stimulus purity needs to be 3-4 bits better than DUT. For ADC testing, if DAC is used to generate a sine wave to the ADC, its nonlinearity must be much smaller than ADC nonlinearity, so that at the ADC output spectrum, the nonlinearity is truly the ADC's. Similarly, for the DAC under test, the ADC that samples the DAC output waveform must have a much better performance, so its own nonlinearity will not show up as part of the DAC nonlinearity at the output spectrum. Due to the same limitations mentioned previously, it has become more and more challenging to perform accurate spectral testing. To demonstrate this issue, Figure 4.1

shows a 16-bit ADC spectral test using pure and nonlinear sine waves. The extra nonlinearity from the nonlinear sine wave is lumped together with the ADC nonlinearity, and showed up at the ADC output spectrum (green). For the spectrum using pure sine waves, true ADC nonlinearity is shown in red. Figure 4.2 shows a 16-bit DAC output spectrum, sampled by two 20-bit ADCs. ADCa shows much better linearity performance than DAC's, and ADCb shows a similar linearity performance to DAC's. Similarly, erroneous results caused by the extra nonlinearity from the ADC is shown in red, compared with blue, which is sampled by ADCa. Therefore, both linearity and spectral testing require a high-purity source to achieve accurate test results. In addition, for DAC ADC co-testing, if the standard method is utilized, the DAC and ADC performances cannot be evaluated at the same time without any extra test stimulus or instruments, because either DAC can be accurately estimated using a better ADC or vice versa. Therefore, there is a strong need for alternative solutions to obtain accurate ADC and DAC test results.

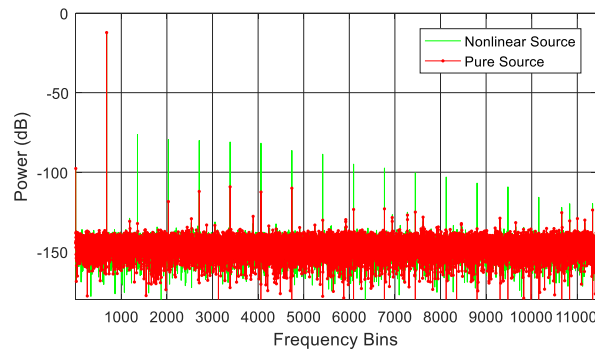


Figure 4.1. ADC spectral testing using: pure and nonlinear sine wave

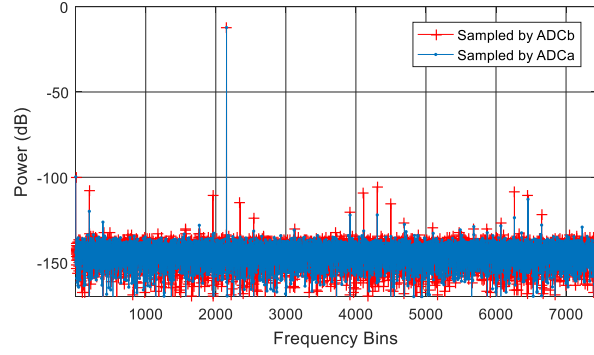


Figure 4.2. DAC output sampled by different ADCs

4.3 Proposed Method

The proposed method is described in detail in this section.

A. ADC Nonlinearity Estimation

The first part of the proposed method involves calculating the ADC's full code INL/DNL, two different ramp signals were applied to an ADC. The ramp signals were both generated identically by the same DAC to produce the voltage V_{out} . The DAC input codes are given by:

$$C_{DAC}(n) = \text{round}(\alpha n \times 2^{N_{DAC}}), \quad (4.1)$$

where $n = 0, 1, 2, \dots, M-1$, M is total data record length; αn is the linear part of the ramp signal; the DAC output range is $[0 V_{RDAC}]$ and has resolution of N_{DAC} bit.

Since the board will add additional gain and offset between the DAC output and the ADC input, we can lump the offset and gain error of the DAC and the board together. This allows the convenience to assume the DAC has no offset and gain error. Hence, the DAC output can be viewed as below:

$$V_{out}(n) = \alpha n + F(n) + w(n), \quad (4.2)$$

where the first two terms on the right-hand side represent the ideal DAC output, $F(n)$ captures the low spatial frequency part of the DAC output errors, and $w(n)$ captures the remaining errors after $F(n)$.

Since $F(n)$ is low frequency, we can use any low frequency basis functions such as polynomials and sinusoids. For example, we choose to approximate $F(n)$ by a finite expansion of sine basis functions, given by:

$$F(n) = \sum_{j=1}^H a_j \cdot \sin(j\pi n) + e(n), \quad (4.3)$$

where only the first H basis functions are included, and $e(n)$ is the residue of nonlinearity that is not modeled by H basis functions.

On the first ramp signal the output voltage of the DAC had a gain factor G and a voltage level shift V_{os} applied to it. On the second ramp signal, only a gain factor was applied. The gain factor is small but identical. The two ramp voltages that are sampled by the ADC can be represented by Eq.(4.4) and Eq.(4.5).

$$V_1(n) = G \cdot V_{out}(n) + V_{os}, \quad (4.4)$$

$$V_2(n) = G \cdot V_{out}(n). \quad (4.5)$$

These two voltages will serve as the two different inputs to the ADC. From the corresponding two ADC output codes, the ADC INL/DNL can be calculated.

The ADC transition level is defined as T_k , and the transition time t_k is defined as the time at which the value of the analog ramp signal equals to T_k , and $k=0,1,\dots,2^N-1$, where N is the resolution of the ADC. They are related by:

$$T_k = G \cdot V_{out}(t_k). \quad (4.6)$$

t_k can be obtained by using the traditional histogram test. Assume C_k is the histogram counts for each ADC code, t_k can be obtained by:

$$t_k = \frac{\sum_{i=1}^k C_i}{\sum_{i=1}^{2^N-2} C_i}. \quad (4.7)$$

Then $INL(k)$ of the ADC can be estimated by:

$$INL(k) = (2^N - 2)t_k + \sum_{j=1}^H a_j \sin(j\pi t_k) - k. \quad (4.8)$$

Since a nonlinear input stimulus is used to test ADC, which has the nonlinearity part of $\sum_{j=1}^H a_j \sin(j\pi t_k)$, if they can be estimated accurately, then the $INL(k)$ of the ADC can therefore be accurately estimated. From the two DAC outputs and two ADC outputs, T_k can be expressed as:

$$T_k = G \cdot V_{out}(t_k^1), \quad (4.9)$$

$$T_k = G \cdot V_{out}(t_k^2) + V_{os}, \quad (4.10)$$

where t_k^1 and t_k^2 are transition times obtained from two ADC output histogram counts, respectively.

For the same ADC under test, the transition level is the same, by equating Eq.(4.9) and Eq.(4.10), Eq.(4.11) can be obtained:

$$(2^N - 2)t_k^1 + \sum_{j=1}^H a_j \sin(j\pi t_k^1) = (2^N - 2)t_k^2 + \sum_{j=1}^H a_j \sin(j\pi t_k^2) - V_{os}. \quad (4.11)$$

Moving all known terms to the left and all unknown terms to the right, Eq.(4.12) can be re-written as:

$$(2^N - 2) \cdot (t_k^1 - t_k^2) = \sum_{j=1}^H a_j \left[\sin(j\pi t_k^1) - \sin(j\pi t_k^2) \right] - V_{os}. \quad (4.12)$$

Since H is much smaller than 2^N , the number of equations is much larger than the number of unknowns, Least Square can be used to estimate the unknowns a_j and V_{os} , given by:

$$\left\{ \hat{a}_1, \hat{a}_2, \dots = \arg \min \left\{ \begin{array}{l} \sum_k (2^N - 2) \cdot (t_k^1 - t_k^2) \\ - \left[\sum_{j=1}^H a_j \left[\sin(j\pi t_k^1) - \sin(j\pi t_k^2) \right] - V_{os} \right]^2 \end{array} \right\} \right\}. \quad (4.13)$$

After the Least Square, the estimated ADC $INL(k)$ is then given by:

$$INL(k) = (2^N - 2)t_k^1 + \sum_{j=1}^H \hat{a}_j \sin(j\pi t_k^1) - k. \quad (4.14)$$

B. DAC Nonlinearity Estimation

With the ADC nonlinearity estimated, it is possible to estimate the DAC's nonlinearity. This is generated as the output voltage of the DAC, which can be viewed as two components. First, the ideal component of this output voltage is due to the input code to the DAC. The second part is the nonlinearity of the DAC, along with the noise of the DAC. Due to the random nature and small quantity, noise is ignored in the following derivations. This second part will then contribute to an error in the output voltage at each input code that corresponds to the INL of each code. These two components consist of the output voltage that will have a gain and/or shift applied to it. From the previous relationship in Eq.(4.2) and Eq.(4.3), Eq.(4.15) and Eq.(4.16) can be combined to relate the input code of the DAC to the output code of the ADC.

$$\left[C_{DAC}(n) + INL_{DAC}(C_{DAC}(n)) \right] \cdot G + V_{os} = C_{ADC1}(n) + INL(C_{ADC1}(n)), \quad (4.15)$$

$$[C_{DAC}(n) + INL_{DAC}(C_{DAC}(n))] \cdot G = C_{ADC2}(n) + INL(C_{ADC2}(n)). \quad (4.16)$$

From these equations, the DAC code, ADC code, and ADC INL are already known. The shift has already been calculated by Least Square in Eq.(4.13). The gain can be calculated as shown by:

$$\hat{G} = [C_{ADC1}(2^N) - C_{ADC1}(1)] / 2^N. \quad (4.17)$$

Once the gain and shift are calculated, either Eq.(4.4) or Eq.(4.5) can be used to solve for the INL of the DAC for each DAC code. This will lead to two supposedly the same solutions as in Eq.(4.18) and Eq.(4.19).

$$INL_{DAC1}(n) = [C_{ADC1}(n) + INL(C_{ADC1}(n)) - V_{os}] / \hat{G} - n, \quad (4.18)$$

$$INL_{DAC2}(n) = [C_{ADC2}(n) + INL(C_{ADC1}(n))] / \hat{G} - n. \quad (4.19)$$

In reality, due to noise, the two solutions might be slightly different. To improve precision, the calculated INL of the DAC can be determined by averaging the two different INL calculations.

$$INL_{DAC}(n) = \frac{INL_{DAC1}(n) + INL_{DAC2}(n)}{2} \quad (4.20)$$

Once the INL of the DAC is estimated, the DAC INL can be added to what the ideal output levels of the DAC. These updated output levels of the DAC will now allow for a better selection of the codes to pass to the DAC to obtain the value closest to the desired output value.

The knowledge of these more accurate output levels is insufficient by itself. It is also necessary to somehow be able to apply this extra knowledge in order to improve the purity of the DAC output. Therefore, different implementation methods are needed in order to accomplish this.

C. Pre-distortion

Now the updated output levels are known, it is possible to select better codes to send to the DAC as pre-distortion codes to obtain new DAC output with significantly improved purity. There are many different methods to apply these pre-distortion codes. The general strategy that should be employed when calculating the pre-distortion codes is to minimize the difference between the calculated output levels of the DAC and the desired analog value.

When this minimization process is optimized, then the best performance can be achieved. To achieve this minimization process there are trade-offs between the increase in performance, and the extra hardware and timing overhead to implement the method. After research and experimentation, two main methods seemed to have the greatest tradeoff potentials.

The first method is to calculate and store all the calculated output levels of the DAC. Then, when a certain output voltage is desired, a search algorithm will find the closest calculated output level to the desired level and then send this code to the DAC. This will have the greatest performance, since it will achieve the best implementation of the minimization of the difference of the calculated output level and the desired analog output. However, it can cause extra overhead, such as area overhead for storing all output voltage levels in memory as well as implementing the search method. Additionally, it costs lots of design effort for hardware implementation, which is not the focus of this chapter. Therefore, this method is not implemented in this chapter.

The second method is to add the estimated DAC's INL at the particular code, then round them to obtain the pre-distortion codes to the DAC. This method can be described by Eq.(4.21) for every n th code that is desired to be seen at the DAC output, where the new

DAC codes $C_{DAC_{new}}(n)$, consist of the original code from the user $C_{user}(n)$, plus the estimated DAC INL at nth code $INL_{DAC}(C_{user}(n))$. In addition, not only the sine wave, but other waveforms can be generated accordingly, like ramp signal, and the output signal purity is significantly improved.

$$C_{DAC_{new}}(n) = \text{round}(C_{user}(n) + INL_{DAC}(C_{user}(n))). \quad (4.21)$$

In our implementation on board, which will be described in section V, the ADC output data are transferred from FPGA to MATLAB, and the proposed method is processed in MATLAB to obtain the estimated ADC, DAC INL, and the pre-distortion codes to the DAC. For implementations where the data are processed on chip or on board, since the estimated INL after the round function is only a few values in LSBs, they can be stored easily without using much memory space. As an option, only the MSB part of the original code can be used to save more memory, and the estimated INL stored can be saved only for the MSB part as well, but as a trade-off, the quantization noise would increase compared with the original code.

The reason for the effectiveness of this method is that the DAC INL curve should be approximately continuous locally. By adding the INL at the originally desired code, this should move the new code very near the most optimal code that was found in the previous method. If the INL was constant across this small range, these methods would be identical. However, since this will not be exactly true, there will be some small deviations from the optimal method. This method will still have increased performance, but not as good as the first method. It will remove most of the harmonic distortions as the systematic error is removed, but there will still be some small errors. This will lead to a little more distortion and noise than the previous method one. It does have some advantages in implementation.

However, if the number of data points for the FFT data is less than the number of codes of the DAC, then the number of INL codes that need to be calculated will be the number of data points. Also, no additional memory would be needed to store the values as they can just be directly added to the previously desired code while sending the data to the DAC, instead of storing and then reading in a search algorithm later.

Figure 4.3 summarizes the flowchart of the proposed method.

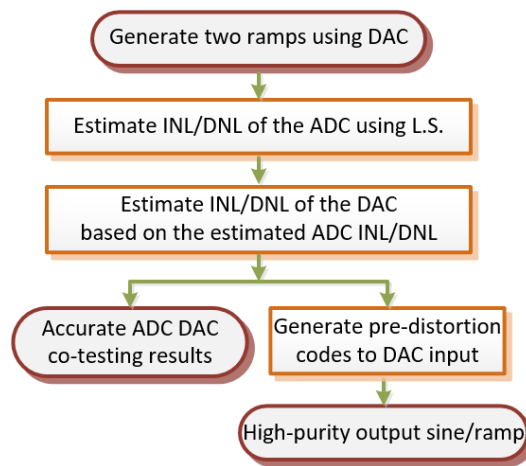


Figure 4.3. Flowchart of the proposed method

4.4 Simulation Results

In this section, simulations results will be shown in order to verify the accuracy of the proposed method in this chapter.

A. Functionality

Firstly, different types and resolutions of DACs and ADCs are used to validated the functionality of the proposed method. In this section, one representative result is shown. One set of result is simulated with a 14-bit nonlinear DAC and ADC, with similar linearity performance. If the standard test method is used, it is impossible to estimate their

performance without using any additional precision test instruments. Using the proposed method, the two nonlinear ramp signals are generated with the DAC and sampled by the ADC, with only 1 hit per code. Then the ADC's INL and the DAC's INL are estimated. From this information and using Eq.(4.21), the DAC's input codes are pre-distorted by DAC's INL information. Figure 4.4 shows the DAC INL estimation and Figure 4.5 shows the ADC INL estimation, respectively. It can be seen that both DAC and ADC linearity information are estimated accurately and they overlap well with their true INLs.

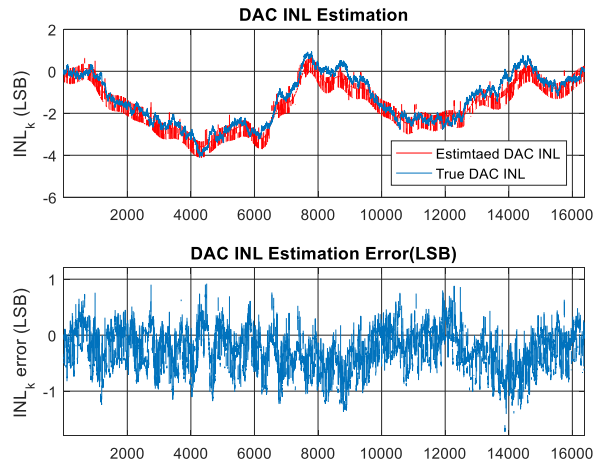


Figure 4.4. DAC INL estimation and estimation error

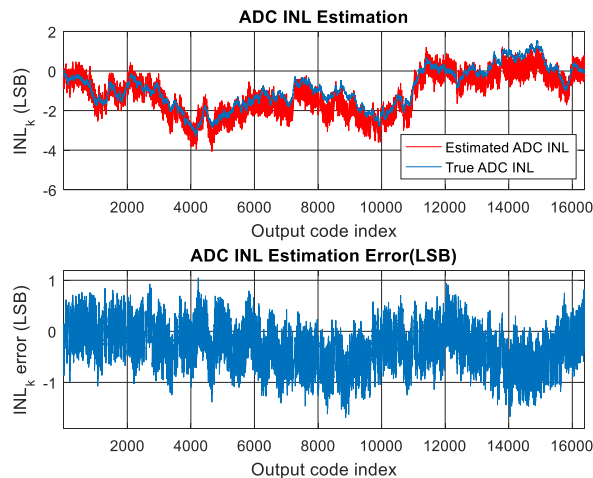


Figure 4.5. ADC INL estimation and estimation error

The DAC's spectral performance is then tested using a perfect ADC with high resolution for the cases when there are no pre-distortion and when pre-distortion codes are applied. The spectrum can be seen in Figure 4.6. As it shows, most of the harmonic distortions at DAC output are removed after applying the pre-distortion codes, the dynamic range as well as purity is significantly improved. Table 4.1 further confirms the test results. As expected, the THD & SFDR can be greatly improved by using the proposed method. The SNR stays at the same level compared to no pre-distortion being applied.

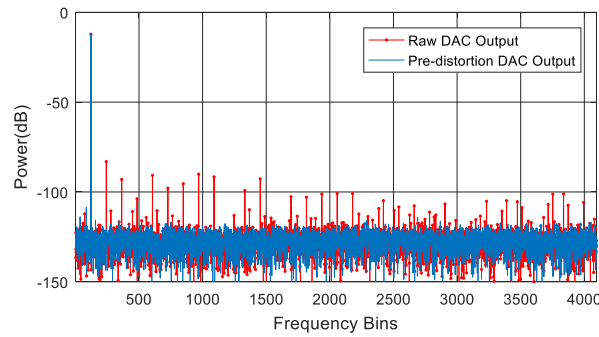


Figure 4.6. Spectrum of the original DAC output versus the spectrum of the pre-distortion DAC output.

Table 4.1. Spectral Specifications of DAC output

DAC Characterization			
Measurement	THD (dB)	SFDR (dB)	SNR (dB)
Original	-66.27	70.12	77.58
Pre-distortion	-88.67	96.36	77.39

B. Robustness:

For further verification purposes, it is also necessary to look at the robustness and repeatability of the proposed method. The proposed method is validated by different test

conditions such as different types, resolution, performance of the converters and different frequencies of generated sine waves. 12, 14 and 16-bit DACs and ADCs are chosen. The ADC is modeled with flash, pipeline and SAR structure, while the DAC is modeled with R-string, R-2R and capacitive binary-weighted structure. For each resolution, 200 cases were simulated, with randomly generated DAC, ADC nonlinearity, different structures and different frequencies of generated the sine wave in each case. The THD and SFDR are used as the criteria to validate the effectiveness of the proposed method. For comparison, in each case, the original DAC output without pre-distortion is also plotted, to serve as a reference and to demonstrate the improvement using the proposed method.

At first, the THD of the DAC output is shown in Figure 4.7, before and after using the proposed method. It is evident to see that after applying the pre-distortion code, the THD of the DAC sine wave output is improved at least 15dB, and the improvement increases as the resolution increases, at 16-bit level, the improvement is even greater, about 30dB. Since most of the harmonics are reduced by the pre-distortion codes, thanks to the accurate estimation of DAC nonlinearity, the DAC output harmonics tend to reduce to the noise floor level. As the resolution increases, the noise floor is reduced, leaving more room for purity improvement.

The SFDR of the DAC output is shown in Figure 4.8. Similarly, after the pre-distortion, the dynamic range is improved significantly. Similarly, as the resolution increases, the improvement increases as well. This is the similar trend seen in Figure 4.7. All of these results have demonstrated that the proposed method is robust against various test setup and test conditions, the estimation to the ADC, DAC nonlinearity are accurate, and the purity of the DAC output after pre-distortion has greatly improved.

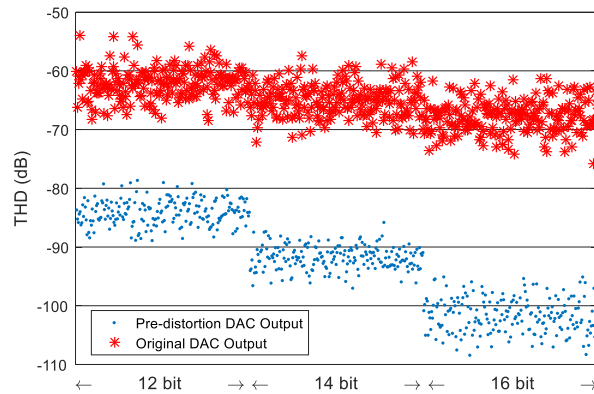


Figure 4.7. Scatter plot showing the THD of various DAC outputs.

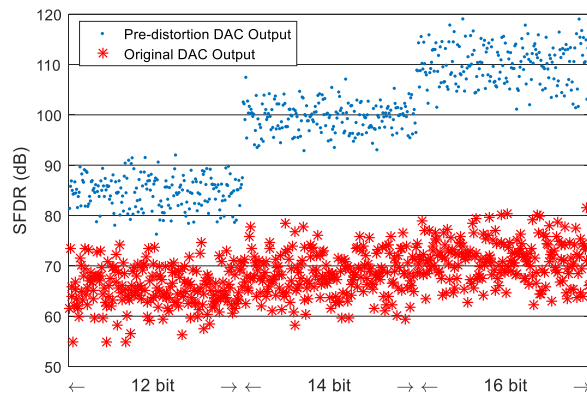


Figure 4.8. Scatter plot showing the SFDR of various DAC outputs.

4.5 Measurement Results

To further validate the proposed method, several measurement results were taken from a custom designed PCB board. The board mainly consists of a 16-bit ADC and multiple DACs. A 20-bit DAC generates the signal that serves as the accurate input stimulus for the ADC testing. To generate the pre-distortion code and validate the proposed method, the 16-bit ADC on board is used to capture the output analog waveform and digitize it to measure its

purity. The test setup with the custom designed board and FPGA board is show in Figure 4.9. The FPGA board is used as the interface between the host computer and the custom designed board. MATLAB first generates the sine wave binary codes for the DAC. Then, the codes are loaded into the FPGA board. After the Verilog code and data are loaded into the FPGA, the FPGA will control the custom designed board and start the testing process. In each conversion, the FPGA transfers a code to the DAC input and the ADC will start the sampling and conversion once the DAC output is ready. After the ADC conversion is complete, the ADC will output an end-of-conversion (EOC) signal for the FPGA to read the ADC outputs. The data received at the FPGA will be saved into the memory in the FPGA board. After all conversions are completed, the data in the FPGA memory will be transferred to the computer as a binary file for the MATLAB to decode.

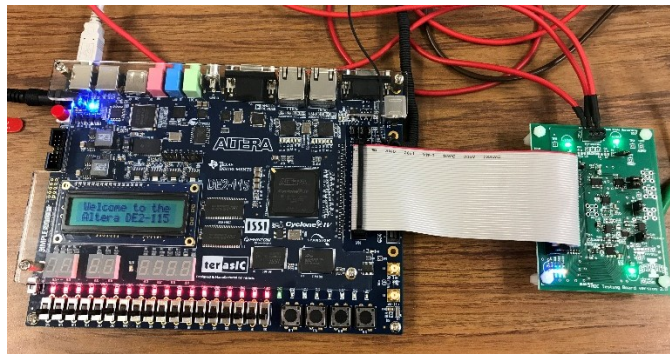


Figure 4.9. Measurement setup with the custom designed board and FPGA.

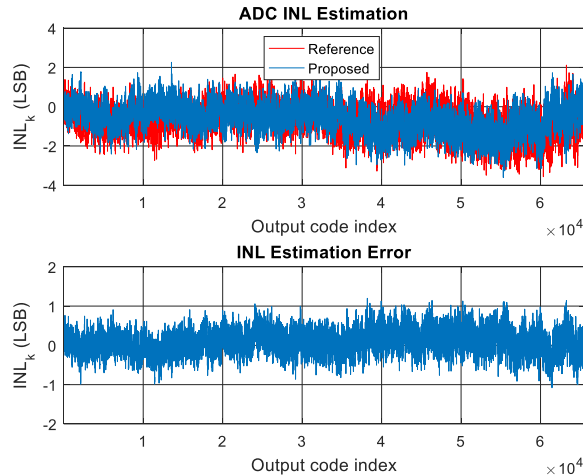


Figure 4.10. ADC INL estimation and estimation error

At first, two nonlinear ramp signals, with an offset in between, are generated by the 16-bit DAC, with only 1 hit per code. After this, the INL of the ADC and INL of the DAC are estimated, respectively based on the proposed method. The calculated INL of the ADC is compared with the traditional histogram measurement results using the 20-bit DAC, with 32 hits per code, which serves as the reference. Their comparison is shown in Figure 4.10, along with the estimation error (lower part). It can be seen that the estimated ADC INL matches well with the reference, the estimation error is mostly within ± 1 LSB.

After the ADC INL is estimated accurately, the DAC INL is estimated to the 16-bit level, which will serve as part of the pre-distortion code to the DAC.

Next comes the validation of the pre-distortion code. Different than the simulation, there is no so-called perfect ADC that can be used to capture the DAC output spectrum. Instead, the 16-bit ADC on board is used to measure the purity of the pre-distorted DAC output, which has 14 and 12 bit resolution. The distortion is worse than the ADC, so the ADC's nonlinearity and quantization noise are much lower, which are negligible compared

with those of the DAC. Then at the ADC output, the spectrum purity is dominated by the DAC output's purity. To relax the input frequency selection requirement, an arbitrary level of non-coherency is allowed. The methods in [23-24] can be utilized to resolve the non-coherency leakage at the output spectrum.

Several sets of data were captured with different input frequencies, DAC resolution, and total data record length, which validated the proposed method. Two preventative results are shown in this section. The first set of data uses 12-bit DAC, with 2^{10} total data record length, and $J_{int}=97$. The ideal sine wave codes generated by MATLAB are sent to the 12-bit DAC, which generates the DAC output captured by the ADC on board. It is shown in Figure 4.11 that the original ADC output spectrum (blue) suffers severe spectrum leakage caused by non-coherent sampling. After implementing the non-coherency correction method [23-24], the leakage is removed, and the true noise and harmonics are revealed from the red spectrum. A certain amount of the harmonic distortions can be viewed from the spectrum and the SFDR of the coherent signal is only 43.12dB. Then, the estimated INL of the DAC quantized to the 12-bit level, is added to the previous ideal sine wave codes. This set of data is the pre-distortion data using the proposed method. The DAC output is captured by the same ADC, whose output spectrum is shown in green, with leakages removed by the same method [23-24]. Most of the harmonic bins are lowered or removed, demonstrating the effectiveness of the proposed method to improve the purity of the DAC signal. The spectral parameters are listed in Table 4.2. The SNR improves before and after using the methods in [23-24], mainly due to the removal of the spectral leakages. However, the dynamic range and THD are still limited by low order harmonics. Although the SNR is in the same level with or without pre-

distortion codes, the THD and SFDR are improved significantly. The SFDR increases to 85.24dB as the dynamic range almost doubles compared with the original DAC output.

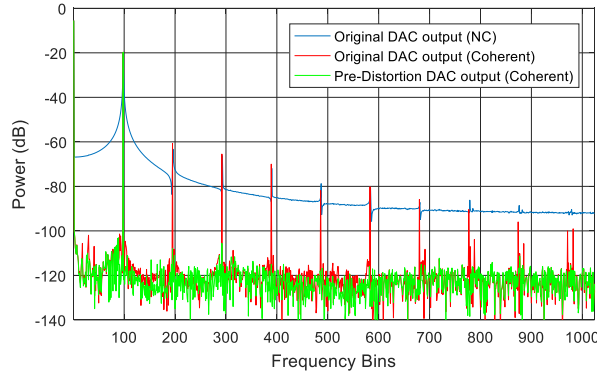


Figure 4.11. 12-bit DAC output spectrum before and after pre-distortion

Table 4.2. Spectral Specifications of the 12-bit DAC output using different methods

Measurement	SNR (dB)	THD (dB)	SFDR(dB)
Original output N.C.	16.92	-39.26	42.65
Raw output + N.C. Algorithm	59.45	-39.57	43.12
Pre-distortion + N.C. Algorithm	60.99	-82.73	85.24

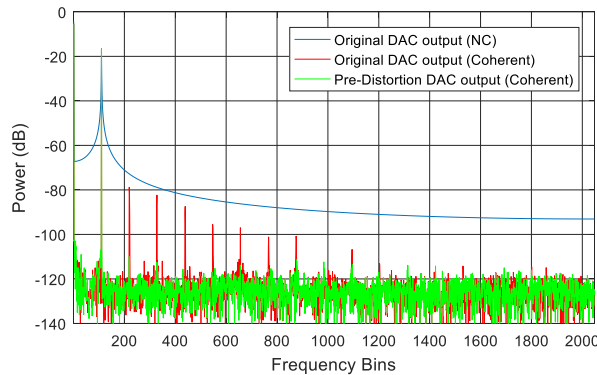


Figure 4.12. 14-bit DAC output spectrum before and after pre-distortion

Table 4.3. Spectral Specifications of the 14-bit DAC output using different methods

Measurement	SNR (dB)	THD (dB)	SFDR(dB)
Original output N.C.	19.74	-42.58	43.89
Raw output + N.C. Algorithm	65.56	-58.43	62.28
Pre-distortion + N.C. Algorithm	65.85	-89.94	92.45

Another set of data is shown, using 14-bit DAC, total data record length became 2^{11} and $J_{int} = 109$. Similar results are shown in Figure 4.12 and Table 4.3. The dynamic range or the purity of the DAC output improved significantly, which again demonstrates the proposed method can generate pre-distorted codes that dramatically improve the purity of the DAC output. All of these measurement data have verified the proposed method is capable of accurately obtaining linearity performance of the ADC, as well as that for the DAC. Moreover, the information for the DAC allows pre-distortion codes at the input for the DAC, significantly improving the dynamic range of the DAC output. Such improvement exceeds the performance of the reported methods mentioned in Section I and is achieved with a low-cost test setup using the proposed method.

In addition, performance comparisons of the proposed method with state-of-the-art methods (measurement results) are summarized in Table 4.4. It shows that the proposed method has achieved better results than most of the state-of-the-art methods except for [20], which requires a more complicated test setup, more calibration, and low frequency operation only. The proposed method has a much simpler, low-cost test setup, without using any precision instruments.

Table 4.4. Comparisons of performance of the proposed method with state-of-the-art methods

Methods	THD (dB)	SFDR(dB)
[13]	NA	* 77
[14]	NA	* 70
[16]	-72	NA
[17]	NA	* 41
[19]	NA	* 85
[20]	-120	124
This work	-90	92

* Approximate value, obtained from graph; NA: not provided in the paper

4.6 Conclusion

In this chapter, a new method capable of generating high-purity sine waves using nonlinear DAC was proposed. The proposed method does not require high-precision instruments to generate high-purity sine waves. Instead, it uses pre-distortion codes to the DAC, with accurately estimated DAC linearity information that cancels nonlinearity of the DAC at output and significantly improves the purity. In addition, both DAC and ADC can be tested accurately at the same time, eliminating the co-testing need for precision instruments or high-quality test stimulus. Extensive simulation results have validated the accuracy and robustness of the proposed method. In addition, the proposed method has been verified by several measurement results and has no requirement on resolution, or performance of the ADC and DAC. With its low-cost test setup, it can serve multiple purposes, such as generating high-purity sinusoidal for high-accuracy applications and accurate testing of data converters.

References

- [1] Y. Zhuang, B. Magstadt, T. Chen, D. Chen, "High-purity Sine Wave Generation Using Nonlinear DAC with Pre-distortion Based on Low-cost Accurate DAC-ADC Co-testing", Submitted to *IEEE Trans. Instrum. Meas.* 2017.
- [2] M. Burns and G.W.Roberts, *An Introduction to Mixed-Signal IC Test and Measurement*, Oxford Univerisity Press, New York, USA, 2012.
- [3] W. Kester, *Data Conversion Handbook*, Analog Devices Inc., Norwood, MA, USA, 2004.
- [4] P. Carbone, S. Kiaei and F. Xu, *Design, Modeling and Testing of Data Converters*, Springer Science & Business Media, Oct 5, 2013.
- [5] K. Brindley, *Automatic Test Equipment*, Elsevier, Oct 22, 2013.
- [6] "APx555 audio analyzer Installation Instructions and Specifications," Audio Precision, Inc, 2014.
- [7] "Precision Data Converter Test Module for X-Series (DCTM)," LTX-Credence Corporation, 2012.
- [8] IEEE Standard for Terminology and Test Methods for Analog-to-Digital Converters, IEEE Standard. 1241-2010.
- [9] IEEE Standard for Terminology and Test Methods of Digital-to-Analog Converter Devices, IEEE Std.1658, 2011.
- [10] IEEE Standard for Digitizing Waveform Recorders, *IEEE Std.1057*, 2007.

- [11] L. Jin, K. Parthasarathy, T. Kuyel, D. Chen and R. Geiger, 'Accurate testing of analog-to-digital converters using low linearity signals with stimulus error identification and removal', *IEEE Trans. Instrum. Meas.*, vol. 54, no. 3, pp. 1188-1199, Jun.2005.
- [12] B. Magstadt, Y. Zhuang and D. Chen, 'Accurate Spectral Testing With Impure Source and Noncoherent Sampling', *IEEE Trans. Instrum. Meas.*, vol. 65, no. 11, pp. 2454-2463, Nov.2016.
- [13] D. Rabijns, W.V. Moer and G.Vandersteen, "Spectrally pure excitation signals: Only a dream?," *IEEE Trans. Instrum. Meas.*, vol. 53, no. 5, pp. 1433–1440, Oct. 2004.
- [14] A. Maeda, "A Method to Generate a Very Low Distortion, High Frequency Sine Waveform Using an AWG," In Proc. *IEEE Int. Test Conf.*, 2008, pp. 1–8.
- [15] S. Shibuya, Y. Kobayashi and H. Kobayashi, "High-frequency low-distortion signal generation algorithm with arbitrary waveform generator", *ASIC (ASICON), 2015 IEEE 11th Int. Conf. on*, Nov. 2015.
- [16] M. Elsayed and E. Sanchez-Sinencio, "A Low THD, Low Power, High Output-Swing Time-Mode-Based Tunable Oscillator Via Digital Harmonic-Cancellation Technique," *IEEE J. Solid-State Circuits*, vol.45, no.5, pp.1061-1071, May 2010.
- [17] K. Wakabayashi, K. Kato, T. Yamada, O. Kobayashi, H. Kobayashi, F. Abe and K. Niitsu, "Low-Distortion Sinewave Generation Method Using Arbitrary Waveform Generator," *J. Electron Testing*, vol.28, no.5, pp.641-651, Oct 2012.
- [18] A. Netterstrom, "Using digital pre-distortion to compensate for analog signal processing errors", In Proc. *IEEE Int. Radar Conf.*, May 1990.

- [19] F. Abe, Y. Kobayashi, K. Sawada, K. Kato, O. Kobayashi and H. Kobayashi, "Low-Distortion Signal Generation for ADC Testing," In Proc. *IEEE Int. Test Conf.*, 2014, pp. 1–10.
- [20] Y. Zhuang, A. Unnithan, A. Joseph, S. Sudani, B. Magstadt and D. Chen, "Low Cost Ultra-Pure Sine Wave Generation with Self Calibration", In Proc. *IEEE Int. Test Conf.*, Nov. 2016.
- [21] H.W. Wang, C.F. Chan and C.S. Choy, "High speed CMOS digital-to-analog converter with linear interpolator", *IEEE Trans. on Cons. Electronics*, vol. 46, no. 4, pp. 1137-1142, Nov.2000.
- [22] A. Oppenheim and R. Schaffer, *Discrete-Time Signal Processing*, Engle-wood Cliffs, NJ, USA: Prentice-Hall, 1999.
- [23] Y. Zhuang and D. Chen, "New Strategies in Removing Non-coherency from Signals with Large Distortion to Noise Ratios", *IEEE Trans. on Circ. and Syst. II: Express Brief*, vol. 63, no. 12, pp. 1136-1140, Dec.2016.
- [24] Y. Zhuang and D. Chen, "Algorithms for Accurate Spectral Analysis in the Presence of Arbitrary Non-coherency and Large Distortion", Accepted by *IEEE Trans. on Instrum. Meas.*, 2017.

CHAPTER 5

LOW COST ULTRA-PURE SINE WAVE GENERATION WITH SELF-CALIBRATION

As data acquisition systems' performance continues to increase, so does the need for a test and characterization solution with a purity input test signal that exceeds currently available state-of-the-art instruments. This chapter presents a new method for generating ultra-pure sine waves used in such applications. The pure sine wave is generated by readily available Digital-to-Analog Converters (DACs) with distortions that may be thousands time worse than the required system's purity. Readily available Analog-to-Digital Converter (ADC) with similar purity as the DAC is utilized to measure the distortions generated by these DACs. An innovative algorithm is used to remove distortions present in the generated sine wave iteratively. Simulation results verify the proposed method by generating a -140dB ultra-pure sine wave using two DACs and an ADC with -85dB Total Harmonic Distortion (THD). A test circuit board has been designed and measurement results demonstrate the generated sine wave has a high purity capable of testing an ADC with -120dB THD accurately.

This chapter is mainly based on the paper published to *IEEE Int. Test Conf. 2016* [1].

5.1 Introduction

Data Converters play a crucial role in electronics field as they bridge the analog world with the digital domain and vice-versa in modern Integrated Circuits (ICs). Over the last decade, significant progress has been achieved in designing high-precision data converters [2]. Currently, 16-bit ADCs and DACs are commonly used in IC design. Applications, such

as precision measurement, seismic signal conditioning, and precision analog microcontrollers, push the designer to achieve even higher performance of data converters [3]. To characterize such sophisticated devices, high-end Automatic Test Equipment (ATE) are now widely used in industrial and consumer products. Among many test mechanisms to quantify the performance of data converters, spectral testing is one of the widely-used mechanisms. Spectral testing involves testing the data converter for dynamic specifications key to determining its performance. Both IEEE standard 1241 [4] and IEEE standard 1057 [5] list several requirements to perform spectral testing accurately. One of the requirements is the input signal for the ADC under test must be 3-4 bits purer than the ADC. This requirement becomes more challenging when the resolution for the ADCs becomes higher.

In the literature, many researchers have proposed methods to generate high-purity, low distortion sine waves. In [10], a high-purity sine wave is generated with an Arbitrary Waveform Generator (AWG). By removing unwanted harmonics and spurs, and applying the correct signal, a high-purity sine wave is generated. Later, Maeda proposed a method to generate very low distortion, high-frequency sine waves [11]. By applying reverse vector calibration signals to the harmonics at output to cancel distortions, a very low distortion sine wave is created. In [12], by changing the AWG program to suppress the third order harmonics and filter spurious components, a low distortion sine wave is generated. In [13], Elsayed et al. proposed an architectural solution for designing low THD oscillators with a digital harmonic-cancellation-block and passive filter; hence, a THD of -73dB is shown at 10MHz . In [14], a method is proposed to generate an ultra-pure sine wave from the outputs of a phase shift oscillator by cancelling the harmonics using weighing and summing of the outputs. A THD smaller than -100dBc was reported. All these methods have demonstrated

their effectiveness via measurements and are easily implemented in standard labs at low cost. However, the generated sine waves' purity, although greatly improved, is still insufficient to meet the current, stringent test requirements.

In industry, several high-performance equipment are widely used to test high-resolution ADCs. The latest Audio Precision APx series signal generator, such as the APx 555, generates very low distortion sinusoidal signals with purity levels of -120dB [6]. This demonstrates its high performance as an analog source and its applications in various high-precision test environments. The Data Converter Test Module (DCTM) instrument also provides capabilities to meet the requirements of a high-precision data converter test. It produces a -120dB low distortion sine wave by utilizing stringent test diagnostics and calibrations [7].

However, such purity level is achieved either through sophisticated circuitry design or complicated calibrations, which require a plethora of design efforts and careful design considerations. This test equipment, although accurate, is large and extremely costly, which limits practical usage in standards labs.

Although costly, such signal generators may not meet stringent requirements, since the device's performance under test becomes higher. For example, an 18-bit ADC would require at least -130dB purity for the input signal. In addition, when the resolution becomes higher, the signal generation equipment may not be available for such high purity. In this case, the ADC output spectrum will no longer contain just ADC nonlinearity, but also contain nonlinearity from the input. The ADC's specifications, such as THD and Spurious Free Dynamic Range (SFDR), cannot be obtained accurately from the output spectrum. Therefore, a method is needed to generate high-purity sinusoidal signals at low cost. This

chapter proposes a signal generator that provides ultra-pure sine waves through novel iterative algorithms with readily available devices. The method is computationally efficient with self-calibration and readily implemented to applications that require high-purity sine waves.

The chapter is arranged as follows. Section II describes the proposed method for generating ultra-pure sine wave. Section III presents the simulation results in MATLAB. Section IV validates the proposed method by measurement results and Section V concludes the chapter.

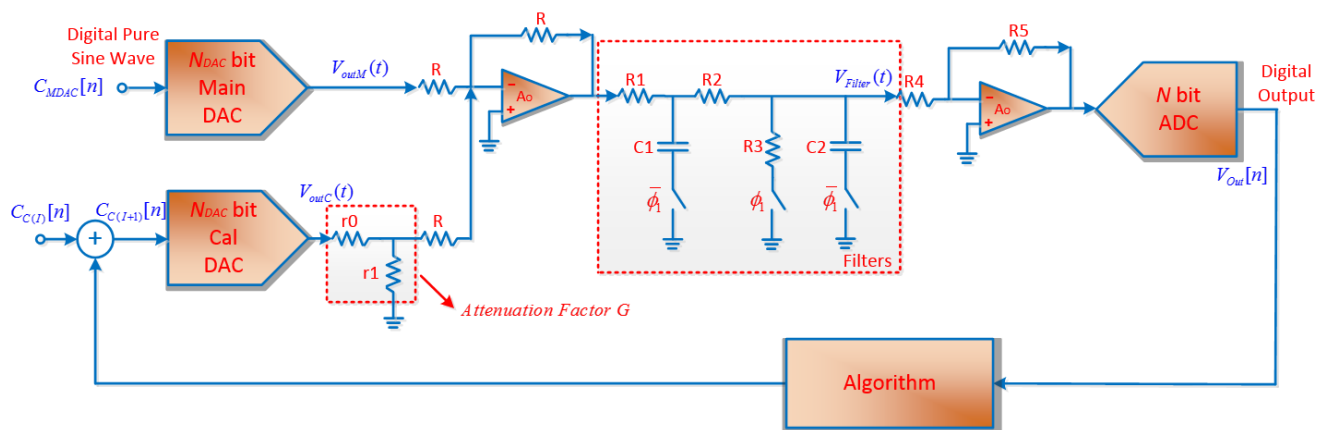


Figure 5.1. Test setup diagram of proposed method

5.2 Proposed Method

The proposed setup is shown in Figure 5.1: two DACs, the Main DAC and the Calibration (Cal) DAC are summed together to achieve the buffered output. The Cal DAC output is attenuated by a simple RR attenuator with an attenuation factor of $G = r0/r1$, whose role is discussed later. Then, two different filters, RR attenuator and RC filter, are connected after the summed buffer. The output for these filters will be the ADC inputs.

When one filter is connected, the other filter is switched off, so the input of both filters is the same, but ADC will have two different inputs spectrally-related, based on the transfer functions of both filters. These two ADC outputs are acquired for further processing.

A. Signal Derivation

At first iteration, the Main DAC generates its nonlinear output signal, later used as the ADC's input signal. The Cal DAC is turned off, so $C_{FDAC(i)} = 0$. The Main DAC input codes $C_{MDAC}(t)$ are given by:

$$C_{MDAC}(t) = \text{round} \left(\left(\frac{V_{RDAC}}{2} + |A| \cos(\omega_o t + \phi) \right) \times 2^{N_{DAC}} \right), \quad (5.1)$$

where $t \in [iT_{sDAC}, (i+1)T_{sDAC})$, $i = 0, 1, 2, \dots, M_{DAC} - 1$, T_{sDAC} stands for DAC sampling period, M_{DAC} is the data record length of DAC input codes, $|A| \leq \frac{V_{RDAC}}{2}$, the DAC output range is $[0 V_{RDAC}]$ and has resolution of N_{DAC} bit, ϕ is the initial phase of the input signal, and $f_{sig} = \frac{\omega_o}{2\pi}$ is the input frequency of the input signal.

The ideal DAC analog output signal is given by:

$$V_{out_ideal}(t) = \frac{C_{in}(t)}{2^{N_{DAC}}} = \frac{V_{RDAC}}{2} + |A| \cos(\omega_o t + \phi) + Q_{DAC}, \quad (5.2)$$

where the quantization error of the DAC is given by:

$$Q_{DAC} = \text{round} \left(\left(\frac{V_{RDAC}}{2} + |A| \cos(\omega_o t + \phi) \right) \times 2^{N_{DAC}} \right) - \frac{V_{RDAC}}{2} - |A| \cos(\omega_o t + \phi). \quad (5.3)$$

In reality, noise and nonlinearities are added to the DAC's output. Since the algorithm cannot distinguish nonlinearities from the Main DAC and its buffer, their noise and nonlinearities

are combined for algorithm estimation and calibration. Therefore, combined with Main DAC and the buffer at output, the output signal is given by

$$V_{outM}(t) = \frac{V_{RDAC}}{2} + |A| \cos(\omega_o t + \phi) + Q_{DAC} + \sum_{k=2}^{+\infty} A_k \cos(k\omega_o t + \phi_k) + w(t), \quad (5.4)$$

where $w(t)$ is the combined noise of Main DAC and the buffer. Eq. (5.4) is rewritten in exponential form:

$$V_{Buffer}(t) = D_0 + \sum_{k=\pm 1}^{\pm H} |D_k| e^{j-k\omega_o t} e^{j\phi_k} + W_{MDAC}(t), \quad (5.5)$$

where $D_0 = \frac{V_{RDAC}}{2}$, $|D_1| = |D_{-1}| = \frac{|A|}{2}$, $|D_k| = |D_{-k}| = \frac{|A_k|}{2}$, and ϕ_1, ϕ_k are fundamental and k^{th} harmonics phase, respectively. $W_{MDAC}(t)$ is the total noise, including quantization and output noises for the Main DAC and buffer. $k = 1, 2, \dots, H$, and first H harmonics are considered for analysis, assuming higher order harmonics have negligible power.

After the buffer, two filters are connected between the Main DAC and the ADC. The filter outputs are given by:

$$V_{Filter1}(t) = D + \sum_{k=\pm 1}^{\pm H} |D_k H_1(jk\omega_o)| e^{j-k\omega_o t} e^{j(\phi_k + \varphi_k)} + W_1(t), \quad (5.6)$$

$$V_{Filter2}(t) = D + \sum_{k=\pm 1}^{\pm H} |D_k H_2(jk\omega_o)| e^{j-k\omega_o t} e^{j(\phi_k + \psi_k)} + W_2(t), \quad (5.7)$$

where D is the offset voltage—approximately the same for both signals. The frequency responses for the filters are $H_1(j\omega)$ and $H_2(j\omega)$, respectively:

$$H_1(j\omega) = |H_1(j\omega)| e^{j\varphi(\omega)} \quad (5.8)$$

$$= \frac{R_3 \parallel R_4}{R_1 + R_2 + R_3 \parallel R_4}. \quad (5.9)$$

$$H_2(j\omega) = |H_2(j\omega)| e^{j\psi(\omega)} \quad (5.10)$$

$$= \frac{1}{\left(\frac{R_1}{R_4} + \frac{R_2}{R_4} + 1\right) + j\omega \cdot \left[R_1 C_1 \left(\frac{R_2}{R_4} + 1\right) + C_2 (R_1 + R_2) \right] + (j\omega)^2 R_1 R_2 C_1 C_2} \quad (5.11)$$

Detailed descriptions regarding these filters will be discussed later.

B. Fundamental Amplitude Match

For the algorithm to work properly, both fundamental signals (the two input signals for the ADC after the two filters) must have the same amplitude. To achieve this, the measured resistor and capacitor with values close to the designed values are selected. Since any level of non-coherency is allowed, by adjusting the input frequency and comparing the two ADC outputs, the two output amplitudes are matched with only several ADC LSBs error. Caution must be taken to avoid signal amplitude clipping when the ADC is sampling both filter outputs.

In designing the filters, passive components are used on the circuit board, these devices are likely from the specification by about 5%. This is not a problem, since input frequency adjusts for fundamental amplitude matching. The exact resistors/capacitors' values are not critical, because in the algorithm, the measured values for the filters will be used to calculate filter transfer function in Eq. (5.8)-(5.11) with sufficient accuracy, which minimizes the estimation error. However, the mismatch between measured and designed resistors/capacitors' values determines how much deviation between designed and actual corner frequencies. In addition, the algorithm has no restriction over input frequency, capable

of generating a wide frequency range of high-purity sinusoidal signals. An array of capacitors can be implemented to adjust filter response according to input frequency.

Another requirement for the filters is the chosen resistors and capacitors must have a good linearity performance because the algorithm cannot differentiate the nonlinearities of the filter from the nonlinearities of both the DAC and the ADC. As a result, if the filters introduce non-negligible nonlinearities, the estimation results could be erroneous.

With amplitudes matched, the ADC outputs are given by

$$V_{out1}[n] = D + \sum_{k=\pm 1}^{\pm H} |D_k H_1(jk\omega_o)| e^{j \cdot k\omega_o n T_{sADC}} e^{j(\phi_k + \varphi_k)} + \sum_{k=\pm 2}^{\pm H} |HD_k| e^{j \cdot k\omega_o n T_{sADC}} e^{j \cdot k(\phi_1 + \varphi_1) + \gamma_k} + W_{ADC1}[n] \quad , \quad (5.12)$$

$$V_{out2}[n] = D + \sum_{k=\pm 1}^{\pm H} |D_k H_2(jk\omega_o)| e^{j \cdot k\omega_o n T_{sADC}} e^{j(\phi_k + \psi_k)} + \sum_{k=\pm 2}^{\pm H} |HD_k| e^{j \cdot k\omega_o n T_{sADC}} e^{j \cdot k(\phi_1 + \psi_1) + \gamma_k} + W_{ADC2}[n] \quad , \quad (5.13)$$

where higher order harmonics caused by the interactions between harmonics of the source and the ADC are neglected, since they contribute smaller harmonics terms compared with source and ADC harmonics. This is also analyzed and verified in [15].

C. Fundamental Phase Match

For the algorithm to work correctly, the fundamental phase also must be matched for both ADC outputs. Since the input codes for the Main DAC for these two sets of data are the same, the output after both filters is different due to different phase shifts of the filter transfer function. To achieve the best phase matching possible, first, after acquiring the RR attenuator output from the ADC $V_{out1}[n]$, the first five consecutive points are chosen—

$x_1[1], x_1[2], x_1[3], x_1[4], x_1[5]$. This phase must be chosen from the data points that are settled, which means the initial data points in the transient process are discarded. Second, after acquiring the RC filter output of the ADC with the same length compared with the RR attenuator output for the ADC, the first quarter portion of the data is chosen. Among these data points, the best matching the first five points of the RR attenuator are determined by minimizing the square root mean:

$$x_{\min} = \sqrt{\left. \begin{aligned} &(x_2[i] - x_1[1])^2 + (x_2[i+1] - x_1[2])^2 + (x_2[i+2] - x_1[3])^2 \\ &+ (x_2[i+3] - x_1[4])^2 + (x_2[i+4] - x_1[5])^2 \end{aligned} \right|_{Min}}. \quad (5.14)$$

After the index, i , is calculated, the new RC filter output data start from i to the end, M , the total data record length. The data record length, $M-i+1$, and the RR attenuator output are also shortened to $M-i+1$ from $x_1[1]$ to $x_1[M-i+1]$. Here, the phase difference introduced by harmonics are sufficiently small to be considered negligible compared with the phase difference for the fundamental. Therefore, once the ADC output data's phase is matched, it means the fundamental initial phase is matched. Two new sets are given by:

$$\begin{aligned} V_{out1_new}[n] = & D+ |D_1 H_1(j\omega_o)| e^{j\omega_o n T_{sADC}} e^{j(\phi_1 + \phi_1)} + |D_{-1} H_1(-j\omega_o)| e^{-j\omega_o n T_{sADC}} e^{j(\phi_1 + \phi_1)} \\ & + \sum_{k=\pm 2}^{\pm H} |D_k H_1(jk\omega_o)| e^{j k \omega_o n T_{sADC}} e^{j(\phi_k + \phi_k)} + \sum_{k=\pm 2}^{\pm H} |HD_k| e^{j k \omega_o n T_{sADC}} e^{j k (\phi_1 + \phi_1) + \gamma_k} + W_{ADC1}[n], \end{aligned} \quad (5.15)$$

$$\begin{aligned} V_{out2_new}[n] = & D+ |D_1 H_2(j\omega_o)| e^{j\omega_o n T_{sADC}} e^{j(\phi_1 + \phi_1)} + |D_{-1} H_2(-j\omega_o)| e^{-j\omega_o n T_{sADC}} e^{j(\phi_1 + \phi_1)} \\ & + \sum_{k=\pm 2}^{\pm H} |D_k H_2(jk\omega_o)| e^{j k \omega_o n T_{sADC}} e^{j(\phi_k + \psi_k + k(\phi_1 - \psi_1))} + \sum_{k=\pm 2}^{\pm H} |HD_k| e^{j k \omega_o n T_{sADC}} e^{j k (\phi_1 + \phi_1) + \gamma_k} + W_{ADC2}[n]. \end{aligned} \quad (5.16)$$

Now, the initial phase is matched, meaning the fundamental of these two different filter outputs entering the ADC are approximately the same, but with different nonlinearities. Since the nonlinearities' power is small compared with that of the fundamental, the differences caused are sufficiently small to be negligible. Therefore, it is assumed the two

filter output signals entering the ADC are approximately the same. As a result, the errors caused by the ADC, mainly nonlinearities, are the same.

D. Non-coherent Fundamental Identification

The first step of the algorithm involves fundamental identification and removal, like the FIRE method [9]. The FIRE method is developed under the assumption the harmonics powers are smaller than the power of the fundamental. Although the harmonics power leakage, due to non-coherent sampling, will be overlap with the fundamental power leakage, their spectral leakage is below the noise floor. Thus, the fundamental estimation will not be affected by harmonics leakage. In addition, the error in estimating the harmonics power using DFT is mainly due to the non-coherency of the fundamental [8]. However, this assumption is no longer true if the harmonics power reaches a certain level. In this case, the harmonics power leakage will be above the noise floor and will introduce error to the fundamental estimation. If the fundamental estimation is inaccurate, the fundamental removal is not complete, which, in return, will introduce error to harmonics power estimation. Thus, an iterative method introduced in [16] is used for fundamental and harmonics estimations. The detailed steps are not repeated in this chapter.

After identification, the estimated fundamental is given by:

$$\hat{V}_{Fund}[n] = \hat{A} \sin\left(\frac{2\pi(J_{int} + \hat{\delta})}{M} n + \hat{\phi}\right) + V_{os}, \quad (5.17)$$

where J_{int} stands for the integer part of the sampled periods, $\hat{\delta}$ is the estimated fractional part of the sampled periods, \hat{A} is the estimated fundamental amplitude, $\hat{\phi}$ is the estimated initial phase, and V_{os} is the estimated DC offset.

E. DAC Nonlinearity Estimation

After the fundamentals in both outputs are estimated, they are subtracted from the two outputs.

$$r_1[n] = V_{out1_new}[n] - \hat{V}_{Fund}[n]. \quad (5.18)$$

$$r_2[n] = V_{out2_new}[n] - \hat{V}_{Fund}[n]. \quad (5.19)$$

Since the two outputs have the same ADC nonlinearities, when subtracting the two residues, the ADC nonlinearities are subtracted, leaving only DAC's nonlinearities.

$$R_3[n] = r_1[n] - r_2[n]. \quad (5.20)$$

Now, $R_3[n]$ is viewed as the summations of a fundamental and harmonics in the form of sines and cosines. By using least squares again without the error introduced by the leakage of the fundamental, the accurate estimation for each harmonic component is obtained similarly. Again, the detailed steps are not repeated here. The estimated harmonics are given by:

$$xh_2[n] = \sum_{k=2}^H \left[\hat{a}_k \cos\left(2\pi k \frac{(J_{int} + \hat{\delta})}{M} n\right) + \hat{b}_k \sin\left(2\pi k \frac{(J_{int} + \hat{\delta})}{M} n\right) \right]. \quad (5.21)$$

The estimated k^{th} harmonic component is given by $|\sqrt{\hat{a}_k^2 + \hat{b}_k^2}| e^{j\theta_k}$, where $\theta_k = \tan^{-1}\left(\frac{\hat{b}_k}{\hat{a}_k}\right)$.

By subtracting Eq. (5.15) and (5.16) from Eq. (5.6) and (5.7), respectively, the ADC introduced errors are subtracted, as well as the fundamental and DC components, leaving only subtractions of nonlinearities from these two outputs. For $k = 2, 3, \dots, H$, each k^{th} nonlinearity subtraction is obtained by $|\sqrt{\hat{a}_k^2 + \hat{b}_k^2}| e^{j\theta_k}$, derived above. Ignoring the noise effect and re-arranging terms, the DAC nonlinearity is estimated:

$$2|\hat{D}_k|e^{j\hat{\phi}_k} = \frac{|\sqrt{\hat{a}_k^2 + \hat{b}_k^2}|e^{j\theta_k}}{|\hat{H}_1(jk\omega_o)|e^{j(\hat{\phi}_k - k\hat{\phi}_1)} - |\hat{H}_2(jk\omega_o)|e^{j(\hat{\psi}_k - k\hat{\psi}_1)}}, \quad (5.22)$$

where k^{th} DAC's harmonic amplitude and phase is $2|\hat{D}_k|$, $\hat{\phi}_k$, respectively.

F. Cal DAC Calibration

Now the Cal DAC input codes are the estimated Main DAC nonlinearity divided by an estimated attenuation factor \hat{G} .

$$C_{CDAC}(t) = \text{round}\left(\left(-\hat{G} \times \sum_{k=2}^H 2|\hat{D}_k| \cos(k\omega_o t + \hat{\phi}_k) + \frac{V_{RDAC}}{2}\right) \times 2^{N_{DAC}}\right). \quad (5.23)$$

Similar to Main DAC output, the Cal DAC output is given by

$$\begin{aligned} V_{outC}(t) \approx & \frac{V_{RDAC}}{2} + (-\hat{G}) \times \sum_{k=2}^H 2|\hat{D}_k| \cos(k\omega_o t + \hat{\phi}_k) \\ & + \sum_{k=2}^H A_{CDACK} \cos(k\omega_o t + \phi_{CDACK}) + W_{CDAC}(t) \end{aligned}, \quad (5.24)$$

where $W_{CDAC}(t)$ contains noise and quantization errors of the Cal DAC.

After attenuation, the buffered Cal DAC output is given by:

$$V_{Buffer_C}(t) = D_C - \frac{\hat{G}}{G} \times \sum_{k=\pm 2}^{\pm H} |\hat{D}_k| e^{j\cdot k\omega_o t} e^{j\cdot \hat{\phi}_k} + E_{CDAC}(t) / G. \quad (5.25)$$

$$E_{CDAC}(t) = \sum_{k=2}^H A_{CDACK} \cos(k\omega_o t + \phi_{CDACK}) + W_{CDAC}(t). \quad (5.26)$$

Eq.(5.25) shows the error introduced by the Cal DAC is attenuated by the factor G , the error introduced by Cal DAC is sufficiently small, so the combined DAC output signal will not be affected by the Cal DAC errors.

Note that the attenuation must be controlled to certain level so the input codes' range will near the full range of the Cal DAC input. However, if the attenuation factor is too large, the Cal DAC input will be clipped and lead to incorrect output. Not only the nonlinearities for the Main DAC will not be cancelled, but extra distortions to the combined signal will be introduced.

After attenuation, the combined DACs output is given by

$$V_C(t) = D_0 - D_C + |D_1| (e^{j \cdot k \omega_o t} + e^{-j \cdot k \omega_o t}) e^{j \cdot \phi_k} + \sum_{k=\pm 2}^{\pm H} \left(|D_k| e^{j \cdot k \omega_o t} e^{j \cdot \phi_k} - (1 + GE_F) \times \left(-\frac{\hat{G}}{G} \right) \times |D_k| e^{j \cdot k \omega_o t} e^{j \cdot \phi_k} \right) + W_{MDAC}(t) - E_{CDAC}(t) / G \quad (5.27)$$

Once the input codes are fed into the Main DAC and the devices are turned on accordingly, the entire iteration for generating Cal DAC codes will be automatically performed to produce ultra-pure sine wave. Thus, the proposed method is capable of self-calibration.

G. Ultra-pure Signal Capturing

The combined signal now should have most of the nonlinearities cancelled. A high-resolution ADC is used to capture this high-purity combined signal. A band-pass filter also is used to filter output from other frequency components except for fundamental signals. If the purity of the combined signal is beyond the purity of the ADC used to capture it, alternatively, the high purity of the combined signal is demonstrated by accurately evaluating the performance of high-performance ADC under test.

If the signal still has residual nonlinearities, as mentioned previously, more iterations is utilized to improve signal purity.

H. Iterations and Convergence

In this section, a mathematical analysis will demonstrate the iteration process is guaranteed to converge and the source nonlinearity will eventually calibrate that only limited by noise. Let $HD_{k,i}$ stands for k^{th} input harmonic distortion in i^{th} iteration ($i = 1, 2, \dots$). At the first iteration, the true value of k^{th} input harmonic distortion is $HD_{k,1} = |D_k| e^{j \cdot k \omega_o t} e^{j \cdot \phi_k}$.

The estimated k^{th} input harmonic distortion is given by:

$$HD_{k,1} = |\hat{D}_{k,1}| e^{j \cdot \hat{\phi}_{k,1}} \quad (5.28)$$

$$= \frac{|\sqrt{\hat{a}_{k,1}^2 + \hat{b}_{k,1}^2}| e^{j \cdot \hat{\theta}_{k,1}}}{2 \left(|\hat{H}_1(jk\omega_o)| e^{j \cdot (\hat{\phi}_k - k\hat{\phi}_1)} - |\hat{H}_2(jk\omega_o)| e^{j \cdot (\hat{\psi}_k - k\hat{\psi}_1)} \right)}. \quad (5.29)$$

At the second iteration, the true value of k^{th} input harmonic distortion is given by:

$$HD_{k,2} = HD_{k,1} - \frac{\hat{G}}{G} \times HD_{k,1} + \frac{|D_{CDACK}| e^{j \cdot k \omega_o t} e^{j \cdot \phi_{CDACK}}}{G}. \quad (5.30)$$

Therefore, at the $(i+1)^{\text{th}}$ iteration, the k^{th} harmonic distortion is:

$$HD_{k,i+1} = HD_{k,i} - \frac{\hat{G}}{G} \times HD_{k,i} + \frac{|D_{CDACK}| e^{j \cdot k \omega_o t} e^{j \cdot \phi_{CDACK}}}{G}. \quad (5.31)$$

Assume:

$$HD_{k,i} = HD_{k,i} + \Delta HD_{k,i}, \quad (5.32)$$

where $\Delta HD_{k,i}$ contain the i^{th} iteration's estimation. Then, Eq. (5.31) is rewritten as:

$$HD_{k,i+1} = \left(1 - \frac{\hat{G}}{G}\right) HD_{k,i} + \frac{\hat{G} \cdot \Delta HD_{k,i} + |D_{CDACK}| e^{j \cdot k \omega_o t} e^{j \cdot \phi_{CDACK}}}{G}. \quad (5.33)$$

$HD_{k,i}$ also is given by

$$HD_{k,i} = \frac{|\sqrt{a_{k,i}^2 + b_{k,i}^2}| e^{j\theta_{k,i}}}{2\left(|H_1(jk\omega_o)| e^{j(\varphi_k - k\varphi_1)} - |H_2(jk\omega_o)| e^{j(\psi_k - k\psi_1)}\right)} + W_{HD_ADC+N}, \quad (5.34)$$

where W_{HD_ADC+N} contains the ADC harmonics and noise subtraction between the two ADC outputs, and error from the true and estimated filters values. On the numerator,

$|\sqrt{a_{k,i}^2 + b_{k,i}^2}| e^{j\theta_{k,i}}$ is linearly proportional to $HD_{k,i}$. Let: $|\sqrt{a_{k,i}^2 + b_{k,i}^2}| e^{j\theta_{k,i}} = \beta \cdot HD_{k,i}$ and

$\frac{1}{\alpha} = 2\left(|H_1(jk\omega_o)| e^{j(\psi_k - k\psi_1)} - |H_2(jk\omega_o)| e^{j(\varphi_k - k\varphi_1)}\right)$, which is independent of iterations.

Similarly, let $\alpha = \hat{\alpha} + \Delta\alpha$, $\beta = \hat{\beta} + \Delta\beta$. $\Delta\alpha$ contains the estimation error from a minor inequality of the two outputs for ADC nonlinearity; $\Delta\beta$ contains the estimation error from FIRE and least squares computational errors.

Then, Eq. (5.34) is written as:

$$HD_{k,i} = \alpha \cdot \beta \cdot HD_{k,i} + W_{HD_ADC+N} \quad (5.35)$$

$$\approx HD_{k,i} + (\Delta\alpha + \Delta\beta) \cdot HD_{k,i} + W_{HD_ADC+N} \cdot \quad (5.36)$$

Inserting Eq. (5.36) into Eq. (5.33), we have:

$$|HD_{k,i+1}| = \left| \frac{\Delta G + \hat{G} \cdot (\Delta\alpha + \Delta\beta)}{G} \right| \cdot |HD_{k,i}| + \left| \frac{\hat{G} \cdot W_{HD_ADC+N} + |D_{CDACK}| e^{j \cdot k\omega_o t} e^{j \cdot \phi_{CDACK}}}{G} \right|, \quad (5.37)$$

where $0 < \left| \frac{\Delta G + \hat{G} \cdot (\Delta\alpha + \Delta\beta)}{G} \right| \ll 1$ and $\varepsilon = \left| \frac{\hat{G} \cdot W_{HD_ADC+N} + |D_{CDACK}| e^{j \cdot k\omega_o t} e^{j \cdot \phi_{CDACK}}}{G} \right|$ is the

small error term due to various error sources mentioned previously. Therefore, we have:

$$\lim_{i \rightarrow \infty} |HD_{k,i}| = \varepsilon. \quad (5.38)$$

This demonstrates as the iteration process continues, eventually the source nonlinearity will be calibrated and converge.

5.3 Simulation Results

The proposed method is first validated by simulations done in MATLAB. A 16-bit nonlinear ADC with THD of -85dB and two 16-bit nonlinear DACs (THD of -85dB) are modeled in MATLAB. The input codes are also generated in MATLAB: the ideal sinewave with amplitude near the full range of ADC and DAC. The number of period J in the input codes is integer 331. Later, the resistors and capacitors are modeled with 5% value mismatch, which serve as the RR and RC filter components in the actual circuit. The output of the Main DAC is then transformed via FFT to the frequency domain and multiply the transfer function of both filters. The time domain output of both filters is acquired by taking the IFFT of the modified output data. These steps will model the output time domain signal after the filters, which is the input of the ADC. Because the filter component has a mismatch after obtaining two outputs from the ADC, the calibration steps described in Section II.B are used to match the amplitude of both ADC outputs. The frequency of the input is now changed, meaning J will no longer be an integer. The signal will be non-coherently sampled by the ADC. This will not introduce additional problems, since the algorithm can tolerate any level of non-coherency. After using the algorithm, two DAC outputs are combined to obtain the combined ultra pure signal and the two iterations are performed in the simulation.

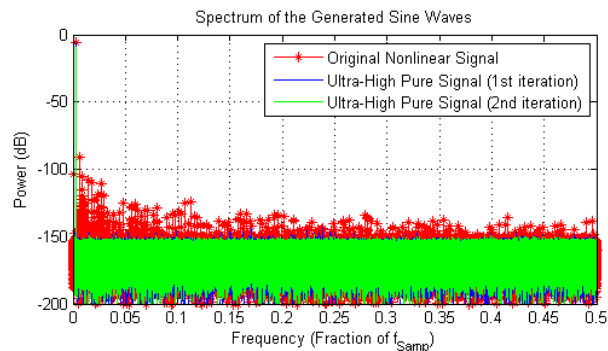


Figure 5.2. Spectrum of the generated sine waves

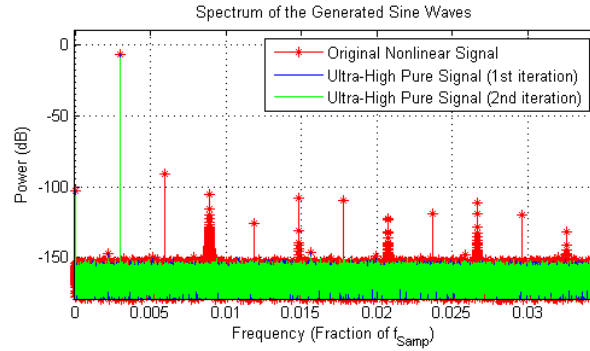


Figure 5.3. Zoomed spectrum of the generated sine waves showing fundamental and first 10 harmonics in Figure 5.2

Figure 5.2 shows the spectrum of the original Main DAC output (red), and the generated ultra-pure signal output by the proposed method (blue and green), 2 iteration results are shown, respectively. Figure 5.3 shows the zoomed spectrum for fundamental and the first 10 harmonics. In simulations, the true spectrum of the signal is obtained by taking the FFT of the signal, assuming the ADC capturing these signals has infinite resolution. In actual measurement, discussed in detail in Section IV, this generated ultra-pure signal is used to test a commercial high-performance ADC. Figure 5.2 shows after the first iteration, most of the harmonics are cancelled, but still there are some at higher frequencies not accurately estimated and completely removed (blue). After the first iteration, the residue harmonics that failed capture are removed during the second iteration (red), resulting in a signal purity (THD) around -140dB.

5.4 Measurement Results

A Print Circuit Board (PCB) is designed to validate the proposed method, Figure 5.4. The motherboard is shown (Figure 5.4) with an Opel Kelly FPGA connected to the PC via a

USB 2.0 connector. This FPGA is used to generate common mode signals and other control signals. The ultra-pure sine wave board is the circuit board custom-designed for this project housing two DACs (DAC8831), filter block and an 18-bit ADC (ADS9110). The Main DAC (DAC8831) is used for a 2kHz and 4.169kHz impure sinusoidal signal with 1.25 or 2.5Vpp. High-precision/low distortion capacitors and resistors are used to design the RR and RC filters. For the RR attenuator, the resistor values are $R1=R2 = 1.1k$, $R3=2.2k$; for RC filter, the capacitor values are $C1=C2=47nF$.

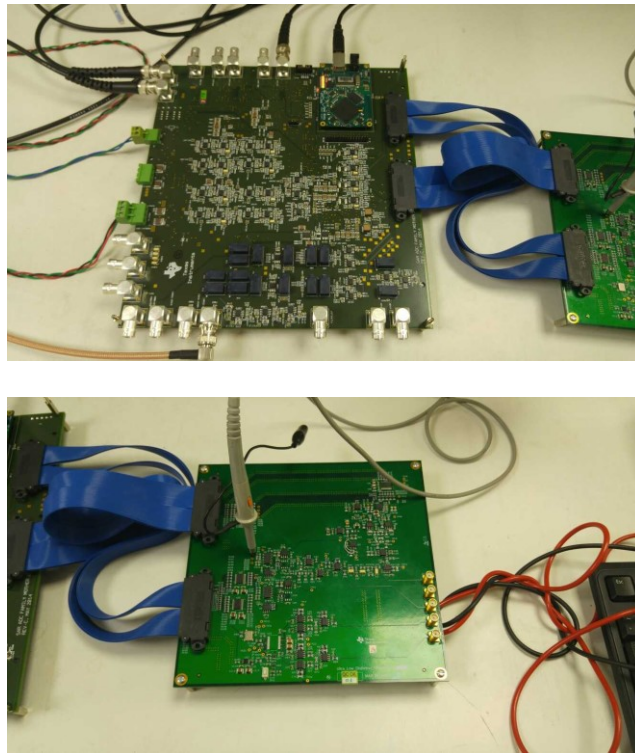


Figure 5.4. Designed printed circuit board: motherboard with FPGA (above) and custom ultra-pure sine wave board with DACs/ADC (below)

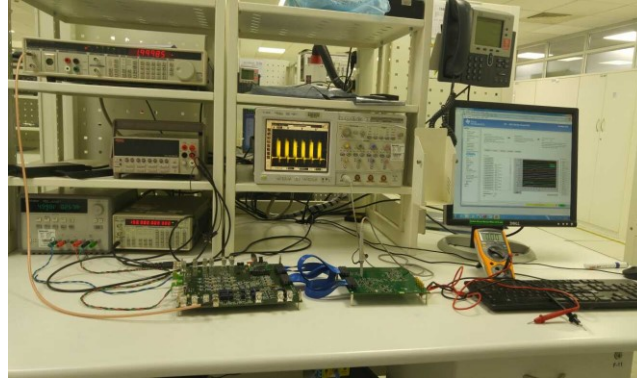


Figure 5.5. Test setup of the board

For DACs, the Main DAC serves as the signal generator and the Cal DAC serves as the calibration device. These two DACs are not relevant to this study because they serve different purposes. They could be in different structures or provide different resolutions. The selection of the DACs depends on the frequency of the generated ultra-pure sine wave and should generate sine waves of such frequency. There is a trade-off between speed and accuracy of the DAC. For the best performance of the DAC, the DAC's maximum output frequency is more than 10 times the generated sine wave. Thus, the sine wave is viewed as pseudo static. For the ADC, depending on how many orders of harmonics needed for the sample, it should be capable of sampling fundamental and harmonics of the input sine wave. Similarly, there is a trade-off between speed and accuracy of the ADC. The buffers must have good linearity performance, especially the one before the ADC. It should contribute negligible nonlinearity to the system compared with source nonlinearity and ADC nonlinearity. The op amps that serve as buffers at the output of DAC and input of the ADC are OPA211.

Figure 5.5 shows the test setup to validate the proposed method. The steps for running the test are described as follows:

1. The first step involves filter characterization, sine waves, and various harmonics frequencies generated that pass through the filters. Accurate filters that transfer function is obtained.

2. Using the approach described in Section II.B, the fundamental amplitude can match the accuracy level. Labview™ is used to generate 2^{16} unique points for a sine wave feed to the Main DAC using SDI with the help of FPGA. This output is first passed through the RR attenuator and then the RC filter. These two outputs are captured using the ADC and frequency is adjusted slightly so the two fundamentals have the same amplitude. Once this frequency is determined, the test can begin.

3. The sine waves with the previously adjusted frequencies were generated by the Main DAC, Cal DAC is fed with all zeros once the DACs are settled. The two DAC outputs are combined and then pass through the RR and RC filters, respectively. ADC is used to capture these two outputs, respectively.

4. The proposed algorithm is used to obtain an estimation of the Main DAC nonlinearity and generate the Cal DAC calibration code accordingly.

5. The same input codes are given to Main DAC, while the Cal DAC's input is estimated Main DAC nonlinearity. Then, the combined output is passed through the RR and RC filters, and the ADC captures the two outputs, which are sent to the proposed algorithm. This iterative process is repeated until the purity of the generated sine wave is sufficiently high.

Since the generated sine waves possess a high purity that no lab equipment can accurately characterize to evaluate the generated sine wave and claim its high purity, the ADC on board (ADS9110) is used as a measurement device. The ADC output spectrum

using the generated sine wave as an input source is compared with the reference spectrum that uses the state-of-the-art test setup, including high-purity source, coherent sampling, etc. The ADC on board has a low distortion, which has optimized the THD of -120dB level at 2kHz input frequency. If this ADC is tested accurately by the generated sine wave, the input source purity is 15~20dB beyond distortions of the ADC. Hence, it is demonstrated to have an ultra-high purity.

Figure 5.6 shows the spectrum results for ADS9110, using the generated sine wave and state-of-the-art source, which serves as the reference. The input frequency is around 2kHz for the generated sine wave with 1.25Vpp. For reference, the input frequency must be precisely controlled (2.00081kHz) to achieve coherent sampling. Figure 5.6 shows both blue and red spectra match well on fundamental harmonics bins and noise level. Table 5.1 further validates the accuracy of the proposed method as the spectral performance of the ADC under test is close to the reference. Figure 5.7 shows another set of results and Table 5.2 shows the spectral performance of ADC under test, whose input frequency is around 4.17kHz with 2.5Vpp, while the reference frequency is precisely controlled as 4.16946kHz. Similarly, spectrum and the spectral performance of ADC under test matches well after using generated ultra-pure sine waves with the reference. These two sets of measurement results demonstrated that generated sine waves possess ultra-high purity beyond -120dB and accurately obtained spectral performance of high-performance ADCs.

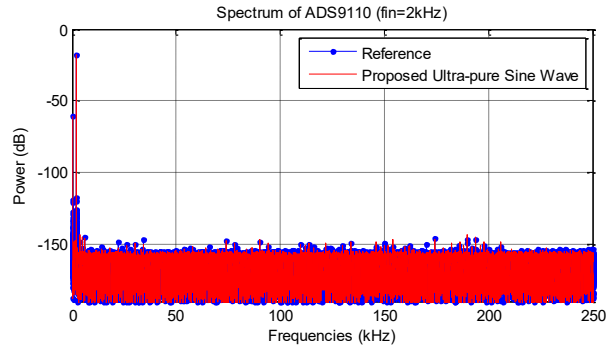


Figure 5.6. ADS9110 ($f_{in}=2\text{kHz}$) spectrum using: (blue) reference, (red) generated sine waves as input

Table 5.1. Spectral Specifications of ADS9110 ($f_{in}=2\text{kHz}$)

Input Signal	THD(dB)	SFDR(dB)	SNR(dB)
Reference	-120.42	124.85	97.13
Proposed	-120.05	124.31	96.74

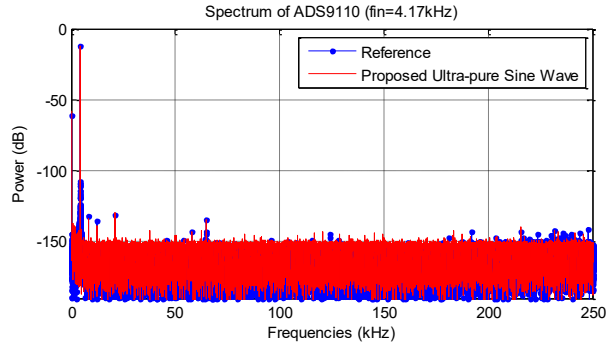


Figure 5.7. ADS9110 ($f_{in}=4.17\text{kHz}$) spectrum using: (blue) reference, (red) generated sine waves as input

Table 5.2. Spectral Specifications of ADS9110 ($f_{in}=4.17\text{kHz}$)

Input Signal	THD(dB)	SFDR(dB)	SNR(dB)
Reference	-115.61	118.05	97.35
Proposed	-114.98	117.64	96.88

5.5 Conclusion

A new method capable of generating ultra-pure sine waves using two DACs and an ADC with distortions thousands time worse than the generated signal was proposed. This method performs in-situ calibrations by innovatively estimating and removing distortions present in the generated sine waves through iterations. Simulation results demonstrated the generated signal purity approaches -140dB. Measurement results showed the generated sine waves test an ADC with -120dB THD accurately, which demonstrates its high purity. The proposed method can also tolerate any level of non-coherency, making it robust against non-coherent sampling. The main advantage of this method is it performs in-situ calibration and generates an ultra-pure sine wave using low-cost DACs and ADCs, which is utilized in various high-precision circuitry and systems with much lower test setup cost.

References

- [1] Y. Zhuang, A. Unnithan, A. Joseph, S. Sudani, B. Magstadt and D. Chen, "Low Cost Ultra-Pure Sine Wave Generation with Self Calibration," in Proc. *Int. Test Conf.*, Nov. 2016, pp. 1–9.
- [2] M. Burns and G.W.Roberts, *An Introduction to Mixed-Signal IC Test and Measurement*, Oxford Univerisity Press, New York, USA, 2012.
- [3] IEEE Standard for Terminology and Test Methods for Analg-to-Digital Converters, *IEEE Std.1241*, 2010.
- [4] IEEE Standard for Terminology and Test Methods of Digital-to-Analog Converter Devices, *IEEE Std.1658*, 2011.

- [5] IEEE Standard for Digitizing Waveform Recorders, *IEEE Std.1057*, 2007.
- [6] "APx555 audio analyzer Installation Instructions and Specifications," Audio Precision, Inc, 2014.
- [7] "Precision Data Converter Test Module for X-Series (DCTM)," LTX-Credence Corporation, 2012.
- [8] S. Sudani, M. Wu, and D. Chen, "A novel robust and accurate spectral testing method for non-coherent sampling," In Proc. *IEEE Int. Test Conf.*, 2011, pp. 1–10.
- [9] S. Sudani, D. Chen, "FIRE: A Fundamental Identification and Replacement Method for Accurate Spectral Test Without Requiring Coherency," *IEEE Trans. Instrum. Meas.*, vol. 62, no. 11, pp. 15–25, Nov. 2013.
- [10] D. Rabijns, W.V. Moer and G.Vandersteen, "Spectrally pure excitation signals: Only a dream?," *IEEE Trans. Instrum. Meas.*, vol. 53, no. 5, pp. 1433–1440, Oct. 2004.
- [11] A. Maeda, "A Method to Generate a Very Low Distortion, High Frequency Sine Waveform Using an AWG," In Proc. *IEEE Int. Test Conf.*, 2008, pp. 1–8.
- [12] F. Abe, Y. Kobayashi, K. Sawada, K. Kato, O. Kobayashi and H. Kobayashi, "Low-Distortion Signal Generation for ADC Testing," In Proc. *IEEE Int. Test Conf.*, 2014, pp. 1–10.
- [13] M. Elsayed and E. Sanchez-Sinencio, "A Low THD, Low Power, High Output-Swing Time-Mode-Based Tunable Oscillator Via Digital Harmonic-Cancellation Technique," *IEEE J. Solid-State Circuits*, vol.45, no.5, pp.1061-1071, May 2010.
- [14] B.K. Vasan, S. Sudani, D. Chen, and R. Geiger, "Low-Distortion Sine Wave Generation Using a Novel Harmonic Cancellation Technique," *IEEE Trans. Circuits Syst. I, Reg. Papers*, vol.60, no.5, pp.1122-1134, May 2013.

- [15] S. Sudani, "Accurate spectral test algorithms with relaxed instrumentation requirements," Graduate Theses and Dissertations, Iowa State University, 2013.
- [16] Y. Zhuang and D. Chen, "Accurate Spectral Testing with Non-coherent Sampling for Large Distortion to Noise Ratios," In Proc. *IEEE 34th VLSI Test Symp.*, 2016, pp. 1-6.

CHAPTER 6

ACCURATE SPECTRAL TESTING WITH NON-COHERENT SAMPLING FOR MULTI-TONE TEST

The multi-tone test has gained popularity among current test methods, since it offers flexibility in characterizing systems whose nonlinearities vary over signal frequency. Thus, it is impractical to test using the single tone test. For multi-tone, non-coherent sampling is the major issue to perform accurate spectral testing, since precise control over each test tone frequency is very challenging to achieve. Such control may not be possible for on-chip testing. This chapter proposes a new method to resolve such issues. Based on the closed form initial estimation of non-coherent fundamentals, more accurate estimation of non-coherent fundamentals is obtained. By replacing non-coherent fundamentals with coherent fundamentals, accurate spectral results are achieved. The accuracy and robustness of proposed method are examined extensively by simulation and measurement results. Comparisons are made with the different methods. Combined with high accuracy, robustness, and computational efficiency, the proposed method is implemented for high-precision spectral testing, which relaxes the requirement of coherent sampling for multi-tone tests. In addition, this new method is also suitable for accurate signal spectral analysis when coherent sampling is not achieved.

This chapter is mainly based on the paper published to *IEEE* in *Proc. IEEE Int. Symp. Circuits Syst. [1]* and *IEEE Trans. Circuit & Systems II [2]*.

6.1 Introduction

Spectral testing has become a major way of characterizing circuits and systems, such as amplifiers and Analog-to-Digital Converters (ADCs) [3-4]. Both single tone and multi-

tone are widely used for spectral testing. Since ADC nonlinearity is known to vary with signal frequency [5], if the single tone test is performed, it cannot cover other frequencies. To test other frequency ranges, the single tone sweep test is used, which consists of dozens of frequencies over the signal bandwidth. However, before starting each measurement, it has to wait for settling of the system. This can be time consuming and impractical for laboratory use. Rather, a multi-tone test can reduce the test time required. One example of multi-tone test is for the digital TV tuner, where each ADC is required to sample many different channels with each channel tested using multiple tone. Therefore, it is important to perform accurate multi-tone spectral testing.

To perform accurate spectral testing, the IEEE standards [6-7] recommend coherent sampling. As the performance of the ADC improves, the requirements for the test setup, especially for coherent sampling, becomes more challenging. For the multi-tone test, it is even more difficult to maintain coherent sampling for each tone, since selecting the appropriate frequencies and their ratios of multi-tone can become tedious and time consuming. Locked frequency synthesizers are required to maintain the exact frequency ratios, which makes the test setup more difficult when compared with the single tone test. In addition, such solutions may not be possible for future on-chip low cost tests. If the ADC is non-coherently sampled, fundamental signals will produce spectrum leakages. They mask the true harmonics and noise information of the ADC and produce erroneous spectral results of the ADC. The situation is worse for multi-tone tests, as multiple fundamentals have leakages that overlap each other, making it difficult to resolve and obtain accurate, ADC spectral performance.

Currently, there are two methods widely used to resolve the non-coherent sampling issue: windowing and four-parameter sine fit. Windowing relies on the power of its secondary lobes on the spectrum to remove spectrum leakage, which is challenging for high-resolution and high-performance ADCs [8]. Prior knowledge about the different types of windows is needed to obtain accurate results. This makes the results window dependent [8,14]. Thus, all of these properties compromise the practical usage of windows for high-accuracy spectral testing. The advantage of the four-parameter sine fit lies in its accuracy and robustness to the noise [9,10]. It is computationally inefficient when the full spectrum test is performed to find non-harmonics components [14]. In the past few years, 2-D FFT [11], filter bank method [12], interpolating DFT (IpDFT) method [13], the Fundamental Identification and Replacement (FIRE) method [14], and the two-step method [15-16] were proposed to resolve non-coherent sampling issues. These methods are accurate and robust to any level of non-coherency, which demonstrates their capability for high-accuracy spectral testing. However, none of these methods is applied to the multi-tone test where multiple fundamental leakages are present at the output spectrum instead of only one fundamental leakage, and the overlap of these leakages makes it more difficult to resolve. Therefore, a new method is needed that can work with a multi-tone test situation where coherent sampling is not achieved for the ADC under test.

This chapter introduces a new method that serves such a purpose. First, the closed form estimations for each fundamental's amplitude, phase, and frequency are obtained to serve as an initial estimation. Then, comparing output with the estimated fundamentals, a more accurate estimation of the fundamentals is obtained simultaneously by a Newton iteration. After all the non-coherent fundamentals are estimated, they are replaced with

coherent fundamentals to obtain a new output, which will have no leakages. Hence, performing FFT on such output will result in correct spectral performance for the ADC. The functionality and robustness of the proposed method are verified in depth by both simulation and measurement results.

The chapter is organized as follows. Section II discusses the multi-tone spectral testing issue with non-coherent sampling. Section III introduces the proposed method. Section IV provides extensive simulations of the proposed method for both functionality and robustness. Section V presents the measurement results and Section VI concludes the chapter.

6.2 Non-Coherent Sampling for Multi-Tone Test

For the L tone sinusoidal, the input for the ADC, the time domain representation is:

$$x(t) = \sum_{i=1}^L A_i \cos(2\pi f_i t + \phi_i), \quad (6.1)$$

where $i=1,2,\dots,L$, A_i is the amplitude of the i^{th} tone's fundamental, f_i is the input signal frequency for the i^{th} tone, and ϕ_i is the initial phase of the i^{th} tone.

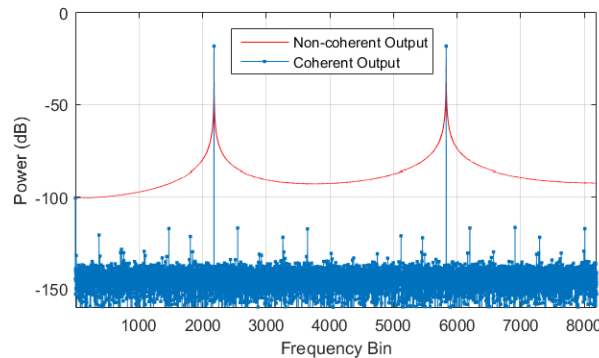


Figure 6.1. Spectrum of an ADC output with coherent sampling (blue) and non-coherent sampling (blue) ($J_{int1}=2179$, $J_{int2}=5827$).

The input frequency, f_i , sampling frequency of ADC, f_s , total number of data record lengths, M , and number of periods, J , satisfy such relations:

$$\frac{J}{M} = \frac{f_i}{f_s} \Rightarrow f_i = \frac{J}{M} f_s. \quad (6.2)$$

If coherent sampling happens, J is an integer and co-prime with M . If not, J is no longer be an integer.

Define $x[n]$ as the analog interpretation of the digital output of the ADC whose gain error and offset have been calibrated. $x[n]$ is given by

$$x[n] = \sum_{i=1}^L A_i \cos(2\pi \frac{J_i}{M} n + \phi_i) + H.D. + I.M.D. + w[n], \quad (6.3)$$

where $n = 0, 1, \dots, M-1$, $H.D.$ is the harmonics distortions of the ADC, $I.M.D.$ is the inter-modulation of the ADC, and $w[n]$ is the noise at the output.

By taking the Discrete Fourier Transform (DFT), the spectral parameters are obtained. The DFT of $x[n]$ is given by

$$X_k = \frac{1}{M} \sum_{n=0}^{M-1} x[n] e^{-j \frac{2\pi k n}{M}}, \quad (6.4)$$

where $k = 0, 1, \dots, M-1$, which represents the frequency bin's index. If coherent sampling conditions are met, for example, $k = hJ_i$ is the frequency bin of the h^{th} harmonic for the i^{th} fundamental and $k = J_i$ is the frequency bin for the i^{th} fundamental.

As mention previously, if the coherent sampling is not satisfied, meaning J is not an integer, then it is separated into two parts: the integer part J_{int} and fraction part δ ($-0.5 \leq \delta \leq 0.5$), where $J = J_{\text{int}} + \delta$. The effects of non-coherent sampling are shown in Figure 6.1, with the two-tone test. Severe leakages may be observed from each fundamental

bin. The leakages overlap each other, which makes fundamental identification and removal difficult for traditional methods, such as windowing and FIRE method.

6.3 Proposed Method

In this section, the proposed method is described in detail in the following subsections to resolve non-coherent sampling issue for the multi-tone test.

A. Fundamentals Initial Estimation

Since the main leakages source comes from the non-coherent fundamentals, estimating them accurately and efficiently is the main goal. For high-performance, high-resolution ADCs, the power of harmonics and inter-modulations are smaller than the fundamentals, whose effects on estimating fundamentals are sufficiently small to be ignored [15,17].

Expanding Eq. (6.3) into Eq. (6.4), and neglecting the noise from the following derivations, X_k is given by

$$X_k = \sum_{i=1}^L \left(\frac{A_i}{2M} \frac{\sin(\pi(J_i - k))}{\sin\left(\frac{\pi(J_i - k)}{M}\right)} e^{j(a(J_i - k) + \phi_i)} + \frac{A_i}{2M} \frac{\sin(\pi(J_i + k))}{\sin\left(\frac{\pi(J_i + k)}{M}\right)} e^{-j(a(J_i + k) + \phi_i)} \right), \quad (6.5)$$

where $a = \pi M / (M - 1)$.

As initial estimations to obtain the closed form solution for the fundamentals' amplitudes, phases, and frequencies, the terms containing $e^{-j(a(J_i + k) + \phi_i)}$ are very small so they are ignored [14]. However, these terms are later considered in the expression to calculate more accurate estimations in the next step. Then, Eq. (6.5) is simplified to:

$$X_k \approx \sum_{i=1}^L \frac{A_i}{2M} \frac{\sin(\pi(J_i - k))}{\sin\left(\frac{\pi(J_i - k)}{M}\right)} e^{j(a(J_i - k) + \phi_i)}. \quad (6.6)$$

The h^{th} fundamental bin and its two nearby bins, $k = J_{\text{int},h}$, $J_{\text{int},h} + 1$ and $J_{\text{int},h} - 1$, is expressed as

$$X_{J_{\text{int},h}} = \frac{A_h e^{j\phi_h}}{2M} \frac{1 - e^{j2\pi\delta_h}}{1 - e^{j\frac{2\pi\delta_h}{M}}} + \sum_{\substack{i=1 \\ i \neq h}}^L \frac{A_i}{2M} \frac{\sin(\pi(J_i - J_{\text{int},h}))}{\sin(\frac{\pi(J_i - J_{\text{int},h})}{M})} e^{j(a(J_i - J_{\text{int},h}) + \phi_i)}, \quad (6.7)$$

$$X_{J_{\text{int},h}+1} = \frac{A_h e^{j\phi_h}}{2M} \frac{1 - e^{j2\pi\delta_h}}{1 - e^{j\frac{2\pi(\delta_h-1)}{M}}} + \sum_{\substack{i=1 \\ i \neq h}}^L \frac{A_i}{2M} \frac{\sin(\pi(J_i + 1 - J_{\text{int},h}))}{\sin(\frac{\pi(J_i + 1 - J_{\text{int},h})}{M})} e^{j(a(J_i + 1 - J_{\text{int},h}) + \phi_i)}, \quad (6.8)$$

$$X_{J_{\text{int},h}-1} = \frac{A_h e^{j\phi_h}}{2M} \frac{1 - e^{j2\pi\delta_h}}{1 - e^{j\frac{2\pi(\delta_h-1)}{M}}} + \sum_{\substack{i=1 \\ i \neq h}}^L \frac{A_i}{2M} \frac{\sin(\pi(J_i - 1 - J_{\text{int},h}))}{\sin(\frac{\pi(J_i - 1 - J_{\text{int},h})}{M})} e^{j(a(J_i - 1 - J_{\text{int},h}) + \phi_i)}. \quad (6.9)$$

For total L tones, there are $3L$ equations with a total of $3L$ unknowns— A_i , ϕ_i , and δ_i for $i=1, 2, \dots, L$. Solving these equations, the initial estimated values for these unknowns are given by

$$\delta_i = \frac{M}{2\pi} \text{imag} \left(\ln \left(\frac{\frac{X_{J_{\text{int},i}}}{X_{J_{\text{int},i}+1}} - \frac{X_{J_{\text{int},i}}}{X_{J_{\text{int},i}-1}}}{\frac{X_{J_{\text{int},i}}}{X_{J_{\text{int},i}+1}} - \frac{X_{J_{\text{int},i}}}{X_{J_{\text{int},i}-1}} + e^{j\frac{2\pi}{M}} - e^{-j\frac{2\pi}{M}}} \right) \right). \quad (6.10)$$

Inserting the δ_i s into Eq. (6.6), the amplitudes, A_i s, are given by

$$A_i = 2M \left| X_{J_{\text{int},i}} \right| \left| \frac{1 - e^{j\frac{2\pi\delta_i}{M}}}{1 - e^{j2\pi\delta_i}} \right|. \quad (6.11)$$

Then ϕ_i is obtained:

$$\phi_i = \frac{M}{2\pi} \text{imag} \left(\ln \left(\frac{2MX_{J_{\text{int},i}}}{A_i} \frac{1 - e^{-j\frac{2\pi\delta_i}{M}}}{1 - e^{-j2\pi\delta_i}} \right) \right). \quad (6.12)$$

B. More Accurate Estimation of the Fundamentals

The initial estimated fundamentals were obtained by ignoring the terms containing $e^{-j(a(J_i+k)+\phi_i)}$ for the high-performance, high-resolution ADC test. Thus, the accuracy of the initial estimations do not meet the requirements. Therefore, they are included in this step for more accurate estimation of the fundamentals. Without neglecting these terms, $X_{J_{\text{int},h}}$ is given by

$$X_{J_{\text{int},h}} = \frac{A_h e^{j\phi_h}}{2M} \frac{1 - e^{j2\pi\delta_h}}{1 - e^{\frac{j2\pi\delta_h}{M}}} + \sum_{\substack{i=1 \\ i \neq h}}^L \frac{A_i}{2M} \frac{\sin(\pi(J_i - J_{\text{int},h}))}{\sin(\frac{\pi(J_i - J_{\text{int},h})}{M})} e^{j(a(J_i - J_{\text{int},h}) + \phi_i)} \\ + \frac{A_h e^{-j\phi_h}}{2M} \frac{1 - e^{-j2\pi(2J_{\text{int},h} + \delta_h)}}{1 - e^{-\frac{j2\pi(2J_{\text{int},h} + \delta_h)}{M}}} + \sum_{\substack{i=1 \\ i \neq h}}^L \frac{A_i}{2M} \frac{\sin(\pi(J_i + J_{\text{int},h}))}{\sin(\frac{\pi(J_i + J_{\text{int},h})}{M})} e^{-j(a(J_i + J_{\text{int},h}) + \phi_i)} \quad (6.13)$$

Equation (6.13) can also be written as real part, $R_{J_{\text{int},h}}$, and imaginary part $I_{J_{\text{int},h}}$:

$$X_{J_{\text{int},h}} = R_{J_{\text{int},h}} + j \cdot I_{J_{\text{int},h}} \quad (6.14)$$

Similarly, all other $2L$ equations are rewritten this way, constructing a total of $6L$ equations:

$$f_{1-L}(A_i, \delta_i, \phi_i) = R_{J_{\text{int},i}}(A_i, \delta_i, \phi_i) - \text{real}(X_{J_{\text{int},i}}), \quad (6.15)$$

$$f_{L+1-2L}(A_i, \delta_i, \phi_i) = I_{J_{\text{int},i}}(A_i, \delta_i, \phi_i) - \text{imag}(X_{J_{\text{int},i}}), \quad (6.16)$$

$$f_{2L+1-3L}(A_i, \delta_i, \phi_i) = R_{J_{\text{int},i+1}}(A_i, \delta_i, \phi_i) - \text{real}(X_{J_{\text{int},i+1}}), \quad (6.17)$$

$$f_{3L+1-4L}(A_i, \delta_i, \phi_i) = I_{J_{\text{int},i+1}}(A_i, \delta_i, \phi_i) - \text{imag}(X_{J_{\text{int},i+1}}), \quad (6.18)$$

$$f_{4L+1-5L}(A_i, \delta_i, \phi_i) = R_{J_{\text{int},i-1}}(A_i, \delta_i, \phi_i) - \text{real}(X_{J_{\text{int},i-1}}), \quad (6.19)$$

$$f_{5L+1-6L}(A_i, \delta_i, \phi_i) = I_{J_{\text{int},i-1}}(A_i, \delta_i, \phi_i) - \text{imag}(X_{J_{\text{int},i-1}}), \quad (6.20)$$

From the actual non-coherent output, $real(X_{J_{int,i}})$ and $imag(X_{J_{int,i}})$ represent the real and imaginary part of $X_{J_{int,i}}$, respectively.

By minimizing these $6L$ nonlinear equations, the differences between calculated and actual output values are minimized. A total $3L$ unknowns A_i , ϕ_i , and δ_i for $i=1,2,\dots,L$, are more accurately estimated by Newton iterations. At $(k+1)^{th}$ iteration, the value for y_{k+1} is given by

$$y_{k+1} = y_k - B_k \backslash F_k, \quad (6.21)$$

where y is the matrix containing $3L$ unknowns, F_k is the vector of $f_{1-6L}(A_i, \delta_i, \phi_i)$, B_k is the Jacobean matrix, and \backslash is the least squares operator. They are shown below:

$$B_k = \begin{bmatrix} \left[\begin{array}{ccc|ccc} \frac{\partial f_1}{\partial A_1} & \frac{\partial f_1}{\partial \delta_1} & \frac{\partial f_1}{\partial \phi_1} & \dots & \dots & \frac{\partial f_1}{\partial \delta_L} & \frac{\partial f_1}{\partial \phi_L} \\ \vdots & \vdots & \vdots & \ddots & \vdots & \vdots & \vdots \\ \frac{\partial f_{6L}}{\partial A_1} & \frac{\partial f_{6L}}{\partial \delta_1} & \frac{\partial f_{6L}}{\partial \phi_1} & \dots & \dots & \frac{\partial f_{6L}}{\partial \delta_L} & \frac{\partial f_{6L}}{\partial \phi_L} \end{array} \right]_{y_k} \end{bmatrix}, \quad (6.22)$$

$$F_k = [f_1 \dots] \quad y_k = \begin{bmatrix} A_i \\ \delta_i \\ \phi_i \end{bmatrix}_k. \quad (6.23)$$

The initial estimated values are used for the initial value of y . Since the initial estimated value is close to actual values, the proposed method needs only a few iterations to reach global minima, and the number of operations are on longer dependent on total data record length M . At each iteration, the proposed method only compute $6L$ equations with $3L$ unknowns, which makes it computationally efficient compared with sine fitting method. In addition, the estimation error is only limited by the noise power per bin as the estimations

only relies on the output data. This will be shown in Section IV to demonstrate that the accuracy of the proposed method is only limited by noise.

C. Coherent Spectrum Construction

After the accurate estimation of all $3L$ unknowns, the estimate non-coherent fundamentals are constructed:

$$x_{F_nc}[n] = \sum_{i=1}^L A_i \cos(2\pi \frac{(J_{inti} + \delta_i)}{M} n + \phi_i). \quad (6.24)$$

They are subtracted from the original ADC output, by adding the estimated coherent fundamentals, the new output without the influence of non-coherent sampling is given by

$$x_{new}[n] = x[n] - x_{F_nc}[n] + x_{F_c}[n], \quad (6.25)$$

where $x_{F_c}[n] = \sum_{i=1}^L A_i \cos(2\pi \frac{J_{inti}}{M} n + \phi_i)$.

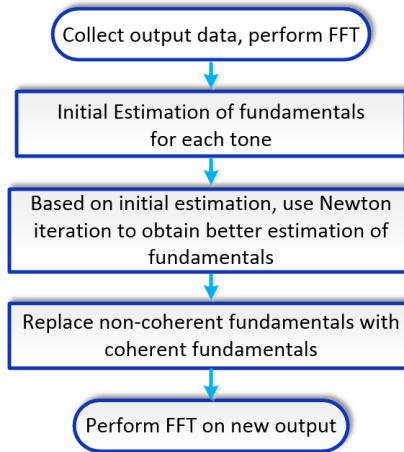


Figure 6.2. Flow chart of the proposed method

Performing FFT on the new output will result in accurate spectral performance of the ADC. The most time-consuming component of the algorithm is performing FFT. The Newtown iteration has less variables to compute compared with the standard sine fitting and the overall time complexity of the method is in the order of $O(M\log(M))$. Figure 6.2 shows the flowchart for the proposed method.

6.4 Simulation Results

In this section, extensive simulations are conducted in MATLAB to evaluate the proposed methods. Comparisons are made with respect to estimation accuracy for the different methods.

A. Functionality

In MATLAB, a 16-bit nonlinear ADC is modeled as the device under test with the full range normalized from 0 to 1 and total data record length (M) of 2^{14} . A multi-tone sinusoidal signal is generated as the input signal to the ADC, whose phases are randomly generated and the total amplitude of the signal is 99% of the full range of the ADC to avoid clipping. The signal noise is modeled as Gaussian noise with rms of 0.5LSB of the ADC. $J_{int1}=2003$, $J_{int2}=4999$, for each tone, the non-coherency, δ , is randomly generated between $[-0.5, 0.5]$.

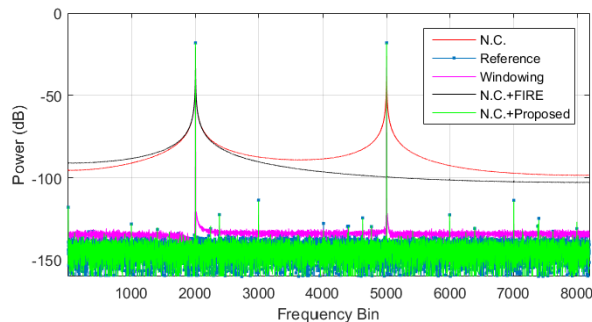


Figure 6.3. ADC output spectrum using different methods (case 1).

Table 6.1. Spectrum performance of the ADC (case 1).

Methods	SNR (dB)	THD (dB)	IMD (dB)
Direct FFT	17.51	-53.26	-48.72
Windowing	77.68	-98.51	-98.14
FIRE	27.65	-67.24	-59.05
Reference	88.79	-101.16	-100.23
Proposed	88.65	-101.35	-100.01

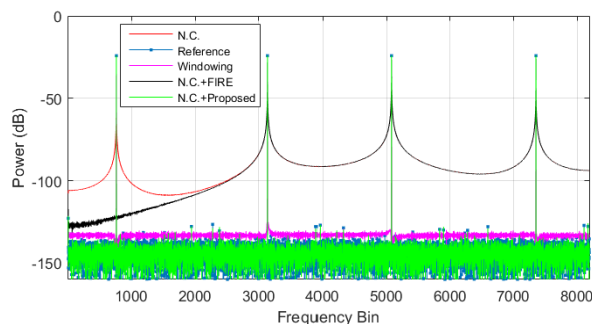


Figure 6.4. ADC output spectrum using different methods (case 2).

Table 6.2. Spectrum performance of the ADC (case 2).

Methods	SNR (dB)	THD (dB)	IMD (dB)
Direct FFT	11.51	-55.26	-50.11
Windowing	68.92	-99.01	-96.58
FIRE	26.74	-68.62	-61.24
Reference	89.15	-100.53	-99.61
Proposed	89.23	-100.42	-99.52

Figure 6.3 shows the ADC output spectrum using different methods. The reference (blue) is obtained when ADC is coherently sampled. Applying direct FFT to the output will result in severe leakage; hence, erroneous spectrum results (red). Applying windowing (pink) will not achieve correct spectrum results. There are still some leakages around the fundamentals and the noise floor is higher. While the FIRE method (black) can remove leakages on one of the fundamentals, it cannot remove leakages from the other fundamental.

The proposed method (green) removes the leakages from both fundamental bins and matches the reference spectrum well. Table 6.1 shows the spectrum parameters using the different methods, which also demonstrate the proposed method can accurately recover the spectrum after non-coherent sampling.

Another nonlinear ADC was modeled in MATLAB using a similar test setup, 4 tones instead of 2 tones are generated as the input to test the ADC ($J_{int1}=757, J_{int2}=3137, J_{int3}=5077, J_{int4}=7351$). Similar results are seen in Figure 6.4. Applying direct FFT will result in severe spectrum leakages around each fundamental bin. Both windowing and the FIRE method do not result in accurate spectra. The proposed method matches the reference spectrum well and an accurate spectral performance of the ADC is provided in Table 6.2.

B. Robustness

To further validate the proposed method versus different test conditions, the robustness of the proposed method is extensively examined. The errors are shown in power scale (dB). The estimated fundamental amplitude, A_{est} , and δ_{est} are chosen and compared with actual values— A and δ . The equations are given by

$$20 \times \log(A_{est} - A), 20 \times \log(\delta_{est} - \delta). \quad (6.26)$$

In the first examination, the proposed method is tested against various levels of non-coherency. For the two-tone test, a total of 1000 runs are simulated. One of the δ is randomly generated from $[-0.5 \ 0.5]$ and fixed for all 1000 runs. However, the other δ is randomly generated at each run from $[-0.5 \ 0.5]$. The input is randomly generated with 0.5LSB rms at each run as well. Other simulation setups are similar to the functionality simulation. Figure 6.5 shows the fundamental amplitude estimation error using the proposed method versus a

different δ . Similar results are shown in Figure 6.6, where the δ estimation error is plotted versus δ . It is seen that all errors are in the level of 10^{-7} (<-120dB) or smaller for different δ , which is the level of added noise. This demonstrates that the estimation on the non-coherent fundamental is accurate and only limited by the noise at the output. The proposed method is robust against any level of non-coherency.

Another set of examinations is performed. Since the proposed method is tested for robustness against non-coherency, this time, for two-tone test, both δ s are randomly generated at each run, and so does input noise. One of the input tone's sampling periods J_{int} is changing at each run from 3 to $M/2$, while the other one is fixed. Both J_{int} s are selected from prime numbers. Other simulation setups are similar to previous simulations. Figures 6.7 and 6.8 show the fundamental amplitude and δ estimation errors using the proposed method versus different J_{int} . Similarly, the errors are only limited by the noise (in the level of 10^{-7} or smaller). This shows the estimations are accurate for various input signal frequencies, meaning the proposed method is insensitive to various input signal frequencies and are used for a wide range of input frequencies.

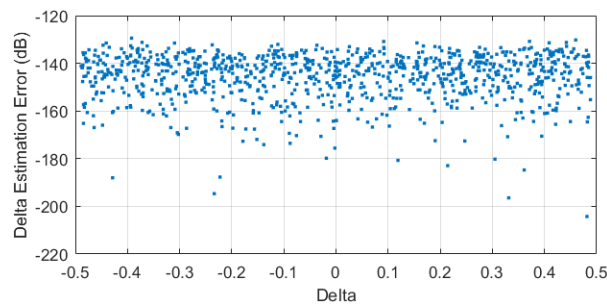


Figure 6.5. Delta estimation error vs. delta ($J_{int1}=2089$, $J_{int2}=5171$).

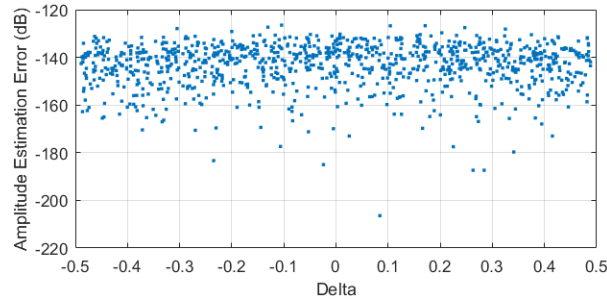


Figure 6.6. Amplitude estimation error vs. delta ($J_{int1}=2089$, $J_{int2}=5171$).

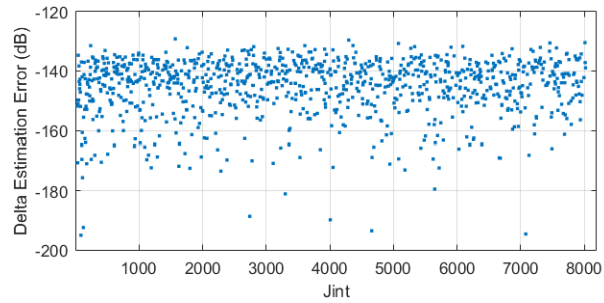


Figure 6.7. Delta estimation error vs. delta ($J_{int1}=2411$, $J_{int2}=3\sim 8191$).

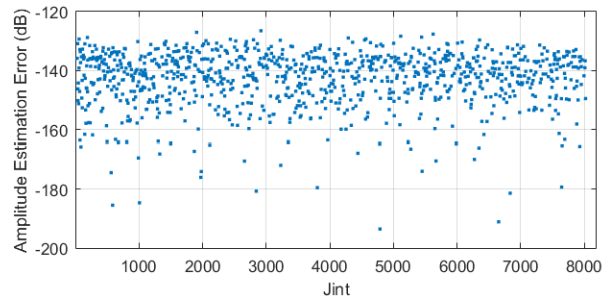


Figure 6.8. Amplitude estimation error vs. delta ($J_{int1}=2411$, $J_{int2}=3\sim 8191$).

6.5 Measurement Results

Several sets of data are taken from different ADCs and verified the proposed method. Due to space limitations, one set of spectrum taken from ADS8881 is shown. A total of 8192 points are sampled for a two-tone test. With 20kHz f_s , the input frequency is roughly controlled, 0.5kHz and 5kHz, while for the reference they are precisely controlled to avoid non-coherent sampling. Both Figure 6.9 and Table 6.3 verified the proposed method, since its

spectrum and spectral performance matched the reference well. Additional data are summarized in Table 6.4.

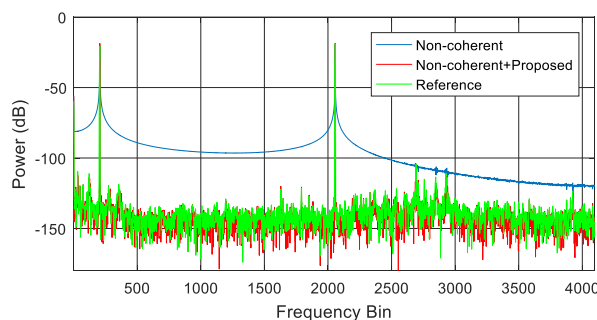


Figure 6.9. ADS8881 output spectrum.

Table 6.3. Spectrum performance of ADS8881.

Methods	SNR (dB)	THD (dB)	IMD (dB)
Direct FFT	16.45	-48.36	-61.68
Reference	82.12	-106.69	-104.81
Proposed	81.85	-106.34	-104.52

Table 6.4. Spectrum performance using proposed method.

Date Set	Methods	SNR(dB)	THD(dB)	IMD(dB)
Set 1	Reference	81.36	-100.52	-102.42
	Proposed	81.24	-100.41	-102.23
Set 2	Reference	80.65	-95.87	-97.69
	Proposed	80.52	-95.68	-97.86
Set 3	Reference	82.68	-102.84	-102.42
	Proposed	82.74	-102.72	-102.63
Set 4	Reference	78.63	-94.26	-93.58
	Proposed	78.54	-94.21	-93.41
Set 5	Reference	75.42	-89.58	-88.47
	Proposed	75.21	-89.37	-88.54

In addition, another 5 sets of data were generated with different input frequencies and sampled based on different ADCs using different sampling rates. Their spectral performances

using the proposed method achieved accurate results compared with the reference and are summarized in Table 6.4. This also validated the accuracy and robustness of the proposed method under different test environments and different ADCs under test.

6.6 Conclusion

A new method was proposed to relax the non-coherent sampling requirements for multi-tone spectral testing. Using vigorous mathematical derivations, this new method estimates the non-coherent fundamentals accurately in two steps and remove them from the original output to eliminate spectrum leakages. The advantages compared to windowing and FIRE methods are shown. Both simulation and measurement results validated the accuracy and robustness of the proposed method, which is robust against any level of non-coherency and capable of tolerating a wide range of input signal frequencies. Combined with its computational efficiency, this new method can be readily implemented into accurate spectral testing and eliminate the need for coherent sampling. This will dramatically relax the test setup for the multi-tone test.

References

- [1] Y. Zhuang and D. Chen, "Accurate Spectral Testing with Non-coherent Sampling for Multi Tone Applications", in Proc. *IEEE Int. Symp. Circuits Syst.*, May. 2017, pp. 1-3..
- [2] Y. Zhuang and D. Chen, "Accurate Spectral Testing with Non-coherent Sampling for Multi Tone Applications", Accepted by *IEEE Trans. on Circ. and Syst. II*, 2017.
- [3] M. Burns and G.W.Roberts, "*An Introduction to Mixed-Signal IC Test and Measurement*," Oxford Univerisity Press, New York, USA, 2012.

- [4] J. Doernberg, H.-S. Lee, and D.A. Hodges, "Full-Speed Testing of A/D Converters," *IEEE J. Solid State Circuits*, SC-19, pp. 820-827, Dec.1984.
- [5] M. Mahoney, "*DSP-Based Testing of Analog and Mixed-Signal Circuits*," Wiley-IEEE Computer Society Press, 1987.
- [6] IEEE Standard for Terminology and Test Methods for Analg-to-Digital Converters, *IEEE Std.1241*, 2010.
- [7] IEEE Standard for Digitizing Waveform Recorders, *IEEE Std.1057*, 2007.
- [8] F. J. Harris, "On the use of windows for harmonic analysis with the discrete Fourier transform," *Proc. IEEE*, vol. 66, no. 1, pp. 51–83, Jan.1978.
- [9] P. Vilmos and K. Istvan, "Acceleration of the ADC Test With Sine-Wave Fit," *IEEE Trans. Instrum. Meas.*, vol. 62, no. 5, pp. 880–888, May 2013.
- [10] H. Peter, "Properties of the IEEE-STD-1057 Four-Parameter Sine Wave Fit Algorithm," *IEEE Trans. Instrum. Meas.*, vol. 49, no. 6, pp. 1189–1193, Dec. 2013.
- [11] X.M. Gao et al., "Analysis of second-order harmonic distortion of ADC using bispectrum," *IEEE Trans. Instrum. Meas.*, vol. 45, no. 1, pp. 50-55, 1996.
- [12] C. Rebai, D. Dallet, and P. Marchegay, "Noncoherent Spectral Analysis of ADC Using Filter Bank," *IEEE Trans. Instrum. Meas.*, vol. 53, no. 3, pp 652-660, 2004.
- [13] D. Belega, D. Dallet, and D. Stoiciu, "Choice of the Window Used in the Interpolated Discrete Fourier Transform Method," *Revue Roumaine des Sciences Techniques Serie Electrotechnique et Energetique*, vol. 54 , no. 4, 365–374, 2009.
- [14] S. Sudani and D. Chen, "FIRE: A Fundamental Identification and Replacement Method for Accurate Spectral Test without Requiring Coherency," *IEEE Trans. Instrum. Meas.*, vol. 62, no. 11, pp. 15–25, Nov. 2013.

- [15] Y. Zhuang and D. Chen, "Accurate Spectral Testing with Non-coherent Sampling for Large Distortion to Noise Ratios," *IEEE 34th VLSI Test Symp.*, pp. 1-6, April 2016.
- [16] Y. Zhuang and D. Chen, "New Strategies in Removing Non-coherency from Signals with Large Distortion to Noise Ratios," in *Proc. IEEE Int. Symp. Circuits Syst.*, pp. 1-3, May 2016.
- [17] Y. Zhuang and D. Chen, "New Strategies in Removing Non-coherency from Signals with Large Distortion to Noise Ratios", *IEEE Trans. on Circ. and Syst. II: Express Brief*, vol. 63, no. 12, pp. 1136-1140, Dec.2016.

CHAPTER 7**ACCURATE SPECTRAL TESTING WITH IMPURE TEST STIMULUS FOR
MULTI-TONE TEST**

Analog-to-Digital Converters (ADCs) are among one of the world's largest volume devices. ADCs are a necessary, vital mixed-signal integrated circuit (IC) component in almost every electrical device and system. One of the challenges is to accurately and cost-effectively test the continually better performance ADCs. For spectral testing of the ADC, one of the goals is to obtain dynamic performance of the ADC under test. The conventional test has become extremely difficult to implement accurately and cost-effectively, since the test stimulus to the ADC must have an even better purity than ADC under test with continuously higher performance. In addition, multi-tone tests require harmonics and spur, as well as the intermodulation must be accurately tested without influence from impure test stimuli. To resolve this issue, this chapter proposes a new method. This method uses the low purity test stimulus instead of a high-precision test stimulus, passes the signal to two different cost-effective filters, and the output signals are then sampled by the ADC, by separating the nonlinearity from the source, the true ADC nonlinearity is accurately estimated. Then the dynamic performance of the ADC under test can be obtained. Extensive simulation results validate the functionality and robustness of the proposed method with different levels of impure test stimulus and different types or resolutions of the ADC under test. The proposed method greatly reduces the requirements on the test stimulus and is implemented into the board level or on-chip high-performance ADC spectral testing and characterization.

This chapter is mainly based on the paper submitted to *IEEE VLSI Test Symp. 2018* [1].

7.1 Introduction

Recent advancements in semiconductor technologies have enabled designers to economically and efficiently design a device with continuously better performance. As the one of the most widely used mixed-signal ICs, ADC testing represents one of the most challenging tasks in mixed-signal testing. Spectral testing has become a major method to characterize ADCs. Due to its advantages, the frequency domain analysis method is widely employed to determine the dynamic performance of the ADCs under test [2-3]. Although the single tone is commonly used in spectral testing of the ADCs, multi-tone is still a necessary testing approach, especially when ADC nonlinearity must be tested at different frequencies and intermodulation must be quantified. Since ADC nonlinearity is known to vary with signal frequency [4-5], for the single tone test, a single test cannot cover other frequencies. To test other frequency ranges, instead of using the single tone to test each frequency multiple times, the multi-tone test is utilized to reduce the test time and cost.

To perform accurate spectral testing, the IEEE standards [6-7] require the input stimuli to the ADC have 3-4 bit better linearity performance. This means about an extra 20dB higher purity for the sine wave. For example, an ADC with a Total Harmonic Distortion (THD) of 100dB would require a test stimulus of about 120dB. This is extremely difficult for the test stimulus to achieve and the test cost would increase substantially. Moreover, as the device performance increases dramatically, especially for Built-In-Self-Test (BIST) solutions, there are no available source on-chip with better purity. Therefore, alternative solutions are needed to solve this bottleneck of high-performance, multi-tone, spectral testing.

In the past, some work has been achieved to relax this difficult requirement. There are mainly two approaches: one approach is to remove the effects of nonlinearity caused by the test stimulus and recover the correct linearity performance for the device under test (DUT). In [8-9], an algorithm was described to use filters on the input signal to obtain accurate results. Simulation results were shown to validate the method. In [10], a novel, robust method is proposed that greatly reduces the test stimulus purity requirements. Another main approach is to generate a high-purity test signal as a test stimulus to test the high-performance DUTs. Many approaches focus on using an Arbitrary Waveform Generator (AWG) [11-14] by applying correction codes or using phase shift to cancel harmonics and spurs in the signal to generate high-purity sine waves that serve high-performance testing. In [15], a novel approach is proposed to generate high-purity sine waves using two DACs. All these approaches have their fields of application and some have been widely adopted for years. Yet, some lack sufficient purity performance, others achieved at a high cost, and, most importantly, many of these methods are targeted for the single tone test. None of the approaches can be directly applied to the multi-tone test. Therefore, a new method is needed to relax the test stimulus purity requirement for the multi-tone test.

The chapter is organized as follows: Section II discusses the issue of impure test stimulus for the multi-tone test. Section III describes the proposed method. Section VI provides extensive examination of the proposed method for both functionality and robustness. Section V concludes the chapter.

7.2 Impure Test Stimulus for Multi-Tone Test

Since sine waves are commonly used for spectral testing, in the following analysis the multi-tone sine wave is the focus. For the ideal L tone sine wave, the time domain representation is given by

$$x(t) = V_{os} + \sum_{l=1}^L A_l \cos(2\pi f_l t + \phi_l), \quad (7.1)$$

where V_{os} is the offset of the signal, A_l , f_l , and ϕ_l are the amplitude, signal frequency, and initial phase of the l^{th} tone's fundamental, respectively.

With the impure test stimulus, harmonics, intermodulation and noise will show up in the signal. Then Eq. (7.1) is re-written as:

$$x(t) = V_{os} + \sum_{l=1}^L A_l \cos(2\pi f_l t + \phi_l) + H.D. + I.M.D. + w, \quad (7.2)$$

where $H.D.$, $I.M.D.$, and w stand for harmonics distortion, intermodulation distortion, and noise present in the multi-tone signal, respectively.

Eq.(7.2) can also be represented by an exponential form as follows, with $\omega = 2\pi f$,

$$x(t) = V_{os} + \sum_{l=1}^L |A_l| e^{j\omega_l t} e^{j\phi_l} + \sum_{k=\pm 2}^{\pm K} \sum_{I \in E(k,L)} |D_{k,I}| e^{j\omega_{k,I} t} e^{j\lambda_{k,I}} + w, \quad (7.3)$$

where $D_{k,I}$, $\lambda_{k,I}$ are k^{th} order tone amplitude and initial phase, respectively.

$E(k,L) = \{[i_1 \cdots \cdots i_k]\}$, $\omega_{k,I} = \sum i_l \cdot \omega_l$. I is the index in the set E , and this E contains combinations of L tones, i_l to I_L , for both harmonics and intermodulation tones up to K^{th} order.

For example, the third order tone where $k=3$, $\sum |i_l| = 3$ can be the third harmonics from any of the L tones. This means only one i is 3, and the remainder are 0. The frequency

is $\omega_{k,l} = 3\omega_l, l = 1, \dots, L$. Or, it can be the third order intermodulation among these L tones, such as $i_1 = 1, i_2 = 2$, with the remainder 0. This third order intermodulation tone frequency is $\omega_{k,l} = \pm\omega_1 \pm 2\omega_2$. Therefore, at the third order, this index, l , has multiple values, depending on the combination of different tones.

After this test stimulus is sampled by the ADC, the ADC output is then given by

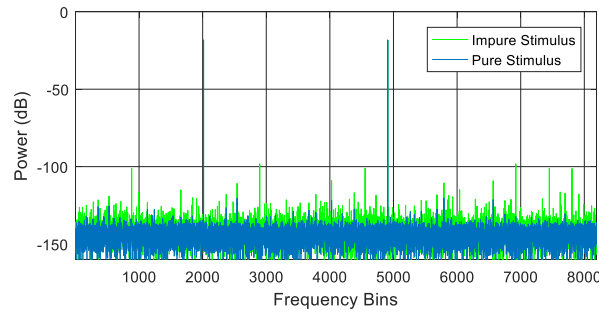


Figure 7.1. Spectrum of an ADC output with pure stimulus (green) and impure stimulus (blue).

$$x[n] = V_{os} + \sum_{l=1}^L |A_l| e^{j\omega_l n T_s} e^{j\phi_l} + N.L.[n] + W[n], \quad (7.4)$$

where $n=0, 1, \dots, M-1$, M is the total data record length, T_s is the ADC sampling period, $N.L.$ contains all nonlinearities from both ADC and the test stimulus, and $W[n]$ is the sampled noise, including signal noise, w , ADC noise, and its quantization noise.

The input frequency, f_l , sampling frequency of ADC, f_s , the total number of data record length, M , and number of periods, J , satisfy such relations [5-7]:

$$\frac{J}{M} = \frac{f_l}{f_s} \Rightarrow f_l = \frac{J}{M} f_s. \quad (7.5)$$

For coherent sampling, J is an integer. It is recommended to choose the input frequency so that J is co-prime with M . By taking Discrete Fourier Transform (DFT), the spectral parameters can be obtained. The DFT of $x[n]$ is given by

$$X[m] = \frac{1}{M} \sum_{n=0}^{M-1} x[n] e^{-j \frac{2\pi m n}{M}}, \quad (7.6)$$

where $m = 0, 1, \dots, M-1$, which represents the frequency bin's index.

To demonstrate the problem of impure test stimuli, an example is provided in Figure 7.1 with a 16-bit ADC under test. The impure stimulus is generated by a low quality DAC, whose nonlinearity is larger than for the ADC. In comparison, the accurate test spectrum (blue) for the ADC is achieved by using the pure test stimulus to the ADC. Clearly, many of the harmonics and intermodulation bins from the green spectrum are higher than those from the blue spectrum, indicating nonlinearity from the impure stimulus corrupts the ADC test results.

7.3 Proposed Method

In this section, the proposed method is described in detail in the following subsections. First, the multi-tone impure stimulus is generated, which will pass through two filters with different amplitudes and phase shift at different frequencies. Second, the ADC under test samples these two signals passed from the filters. Finally, the proposed method uses two ADC outputs, separates the nonlinearity from the stimulus, and obtains the estimated ADC nonlinearity and the spectrum. Figure 7.2 shows the proposed method's test setup.

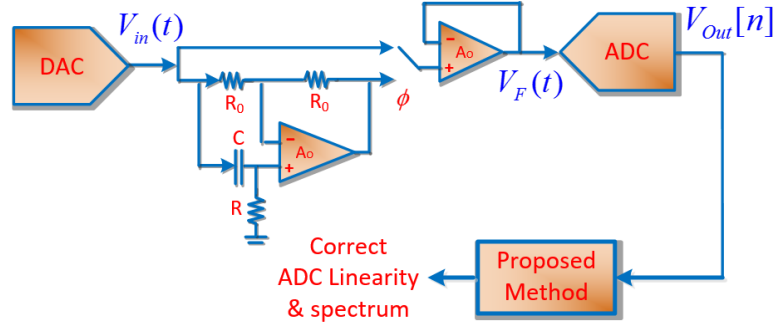


Figure 7.2. Test setup of the proposed method

A. Impure Stimulus

There are several ways to generate the impure test stimulus cost-effectively. One way is to use a nonlinear DAC to produce the impure test stimulus. Since the DAC takes the digital input code, the multi-tone sine waves can be easily programmed with a given amplitude, frequency, and initial phase. In the proposed method's test setup, the nonlinear DAC is used, as shown in Figure 7.2. For two inputs to the filters, V_{in1} is essentially $x(t)$ in Eq. (7.3); on the other hand, V_{in2} has the phase shift for each fundamental tone,

$$V_{in2}(t) = V_{os} + \sum_{l=1}^L |A_l| e^{j\omega_l t} e^{j(\phi_l - \beta_{1,l})} + \sum_{k=\pm 2}^{\pm K} \sum_{l \in E(k,L)} |D_{k,l}| e^{j\omega_{k,l} t} e^{j(\lambda_{k,l} - \varphi_{k,l})} + w, \quad (7.7)$$

where $\beta_{1,l}$ is the phase shift for each fundamental, $\varphi_{k,l}$ is the phase shift on each harmonic/intermodulation, $\varphi_{k,l} = \sum_l i_l \beta_{1,l}$, similar to the case of $\omega_{k,l}$ in the previous section.

B. Two Filters

After the nonlinear DAC generates two outputs, they are passed through two filters. For filter 1, essentially no filtering, $H_1(j\omega) = 1$, the signal goes directly to the ADC. Filter 2 is an all pass filter with its transfer function given by

$$H_2(j\omega) = \frac{j\omega RC - 1}{j\omega RC + 1}. \quad (7.8)$$

It can be seen that the amplitude of the filter 2 is always 1 for different frequencies, but the phase shift will be different.

After two DAC outputs pass through two filters, $V_F(t)$ is obtained:

$$V_{F1}(t) = V_{os} + \sum_{l=1}^L |A_l| e^{j\omega_l t} e^{j\phi} + \sum_{k=\pm 2}^{\pm K} \sum_{l \in E(k,L)} |D_{k,l}| e^{j\omega_{k,l} t} e^{j\lambda_{k,l}} + W_1. \quad (7.9)$$

$$V_{F2}(t) = V_{os} + \sum_{l=1}^L |A_l| e^{j\omega_l t} e^{j(\phi - \beta_{1,l} + \beta_{2,l})} + \sum_{k=\pm 2}^{\pm K} \sum_{l \in E(k,L)} |D_{k,l}| e^{j\omega_{k,l} t} e^{j(\lambda_{k,l} - \phi_{k,l} + \beta_{\omega_{k,l}})} + W_2. \quad (7.10)$$

where W_1 and W_2 are the noises from each filter output, including noise from the DAC and

the filters. $\beta_{\omega_{k,l}} = \angle \frac{1 - j\omega_{k,l} RC}{1 + j\omega_{k,l} RC}$ is the phase shift filter 2 at different frequencies. $\beta_{1,l}$ is the

phase shift of filter 2 at the l^{th} fundamental frequency. This is the same phase shift in each fundamental tone when generating the multi-tone stimulus in the DAC. Thus, it will cancel the phase shift. At filter 2 output, the fundamentals have no phase shift and their phases are the same as filter 1 output. So, both outputs have the same fundamental when sampled by the ADC under test.

Next, both filter outputs are sampled by the ADC under test. The two outputs for the ADC are given by

$$V_{out1}[n] = V_{os} + \sum_{l=1}^L |A_l| e^{j\omega_l n T_{SA}} e^{j\phi} + \sum_{k=\pm 2}^{\pm K} \sum_{l \in E(k,L)} |A_{k,l}| e^{j\omega_{k,l} n T_{SA}} e^{j\gamma_{k,l}} + \sum_{k=\pm 2}^{\pm K} \sum_{l \in E(k,L)} |D_{k,l}| e^{j\omega_{k,l} n T_{SA}} e^{j\lambda_{k,l}} + W_{ADC1}[n]. \quad (7.11)$$

$$\begin{aligned}
V_{out2}[n] = & V_{os} + \sum_{l=1}^L |A_l| e^{j\omega_l n T_{SA}} e^{j\phi_l} + \sum_{k=\pm 2}^{\pm K} \sum_{l \in E(k,L)} |A_{k,l}| e^{j\omega_{k,l} n T_{SA}} e^{j\gamma_{k,l}} \\
& + \sum_{k=\pm 2}^{\pm K} \sum_{l \in E(k,L)} |D_{k,l}| e^{j\omega_{k,l} n T_{SA}} e^{j(\lambda_{k,l} - \varphi_{k,l} + \beta_{\omega_{k,l}})} + W_{ADC2}[n]
\end{aligned} \quad (7.12)$$

where $A_{k,l}$ and $\gamma_{k,l}$ are the amplitude and initial phase of the ADC's k^{th} order harmonics or intermodulation, respectively. Since the fundamentals entering the ADC are the same, the excited ADC nonlinearity is approximately the same for both outputs, despite the small differences of nonlinearity in the impure stimulus.

C. Proposed Method

After the ADC produced two outputs from two filters, the first step is to perform DFT or Fast Fourier Transform (FFT) using Eq. (7.6). Then, the spectrums for the two outputs can be obtained, $X_1[m]$, $X_2[m]$.

Since both ADC and the stimulus nonlinearity can be seen at the ADC output on the spectrum, they are lumped together in the same frequency bins, and the true ADC dynamic performance cannot be directly obtained. To separate the nonlinearity and obtain the correct ADC performance, the second step subtracts the two output spectrum. The residue $R[m]$ is given by:

$$R[m] = X_1[m] - X_2[m]. \quad (7.13)$$

This subtracts the fundamental and nonlinearity of the ADC, leaving only the nonlinearity from the impure stimulus with different phase shifts from the two filter outputs. Since coherent sampling is satisfied at either output spectrum, the multi-tone fundamentals can be easily identified by finding the bins with the largest power except for the DC bin. By using Eq. (7.5), the input frequencies can be calculated. Then, the harmonics and

intermodulation frequencies, $\omega_{k,l}$, are known. Using Eq. (7.5), their bin indices on the spectrum defined as $Z_{k,l}$ are known. Caution is required for frequencies that exceed half of the sampling frequency, when the frequency bins will be aliased back to the first half of the spectrum $[0 fs/2]$ [5-7].

Assuming the noise is excluded, using Eqs. (11)-(13), the subtraction on the spectrum at $Z_{k,l}$ will result in:

$$R[Z_{k,l}] = |D_{k,l}| e^{j\hat{\lambda}_{k,l}} - |D_{k,l} H_2(j\omega_{k,l})| e^{j(\hat{\lambda}_{k,l} - \varphi_{k,l} + \beta_{\omega_{k,l}})}. \quad (7.14)$$

When designing the filters, the component values can be accurately obtained, and thus the transfer function in Eq. (7.8) can be determined.

At each frequency $\omega_{k,l}$, namely each frequency bin $Z_{k,l}$ on the spectrum, with the help of Eq. (7.13) the nonlinearity from the impure stimulus can be given by

$$|\hat{D}_{k,l}| e^{j\hat{\lambda}_{k,l}} = \frac{R[Z_{k,l}]}{1 - |\hat{H}_2(j\omega_{k,l})| e^{j(\beta_{\omega_{k,l}} - \varphi_{k,l})}}. \quad (7.15)$$

The final step of the proposed method is to remove the estimated nonlinearity from the spectrum. Since $V_{out1}[n]$ has no phase shift from the source (DAC) or the filter at its output spectrum, X_I , the estimated nonlinearity from the impure stimulus is removed, given by

$$X_{new}[Z_{k,l}] = X_I[Z_{k,l}] - |\hat{D}_{k,l}| e^{j\hat{\lambda}_{k,l}}. \quad (7.16)$$

Other spectrum information for the ADC, such as the fundamentals, nonlinearity from the ADC and its noise remain intact. Therefore, $X_{new}[Z_{k,l}]$ contains the correct spectral test results of the ADC under test. Figure 7.3 summarizes the flowchart of the proposed method.

D. Discussion

In the proposed test setup, an impure stimulus: a nonlinear DAC with nonlinearity that can be worse than the ADC under test, is used to test the ADC. This cannot be completed by using a conventional method. Designing a cost-effective filter that creates different phase shifts and uses ADC to sample two outputs, the nonlinearity from the impure stimulus can be separated from the ADC nonlinearity to obtain the ADC's spectral performance.

For the proposed method to work properly, there are several requirements for the filters. They include the designed filter component must possess good linearity, so that it will not add extra nonlinearity to the system. Another critical step is to estimate the phase shift for given nonlinearity frequency. This requires knowledge of the designed filter transfer function. When designing the filter, the value for each component is known to the designer. Therefore, the filter transfer function is known. Other requirements are discussed in detail in [10,15] and will not be repeated here.

Another recommendation is generating the multi-tone sine waves. Besides coherent sampling, each tone's frequency or J is selected such that when considered to K^{th} order nonlinearity, no harmonic bins overlap with intermodulation bins at the same location. Thus, each nonlinearity bin (harmonics and intermodulation) will have its individual frequency and bin on the ADC output spectrum and their phase shift is unique, due to the filter. Otherwise, if a frequency bin on the spectrum belongs to a certain harmonic bin as well as an intermodulation bin, the phase shift cannot be determined using the proposed method. This can be easily avoided by calculating the harmonics and intermodulation bin locations before signal generation by the DAC, given the certain order of harmonics/intermodulation considered in the proposed method.

As it shows, the proposed method has no prior knowledge of the stimulus' purity or knowledge on the ADC. This provides much flexibility as different types, resolutions, or performances of the ADC can be tested accurately, given various levels of purity of the impure stimulus. This will be validated in the next section.

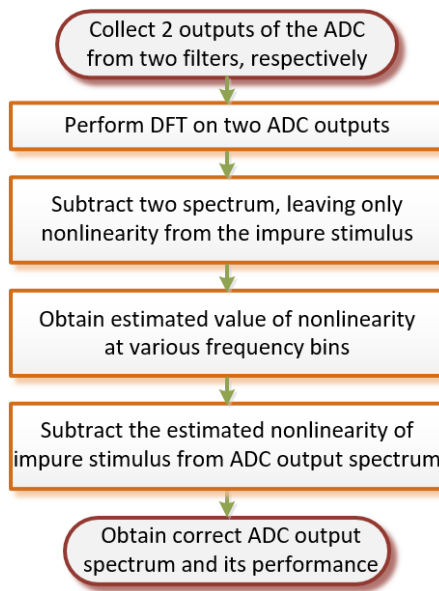


Figure 7.3. Flowchart of the proposed method

More in-depth discussions regarding error analysis and limitations can be done in the future. Hardware implementation is under investigation to obtain more measurement results to further validate the proposed method. Due to space limitation, these are outside the scope of this chapter.

7.4 Simulation Results

In this section, extensive simulations were performed using MATLAB to validate the proposed method.

A. Functionality

First, the functionality of the proposed method is validated, which provided two representative results. In MATLAB, a 16-bit, nonlinear ADC is modeled as the device under test with the full range normalized from 0 to 1 and total data record length (M) of 2^{14} . A two-tone sine wave was generated by a 16-bit nonlinear DAC, whose nonlinearity or purity is worse than the ADC under test. The DAC output will serve as the impure stimulus to the ADC. In comparison, the true ADC performance is tested by an ideal 16-bit DAC with no nonlinearity to serve as the reference result. The ADC sampling frequency is set at 2MHz with $J_{int1}=2003$, $J_{int2}=4999$, at each tone. For filters, the resistors are $100\text{k}\Omega$ and the capacitor is 12.7pF with 1% mismatch. In the proposed method, up to the 20th order of harmonics and 5th order of intermodulation are included for estimation. Figure 7.4 shows the ADC output spectrum with impure stimulus (green) and pure stimulus (blue). Many harmonics and intermodulation bins can be seen at the ADC output spectrum caused by the impure stimulus. Figure 7.5 shows the ADC output spectrum after using the proposed method and the successful removal of nonlinearity from the impure stimulus. The red spectrum matches well with the reference spectrum (blue) for fundamentals, noise, and nonlinearity bins. Table 7.1 further validates the proposed method, as the THD and Intermodulation Distortion (IMD) using proposed method agree with the reference.

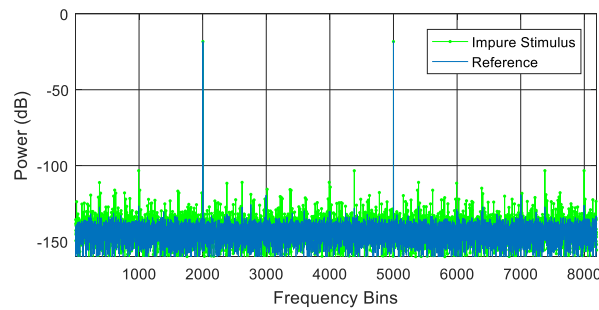


Figure 7.4. Two-tone ADC output spectrum using impure stimulus.

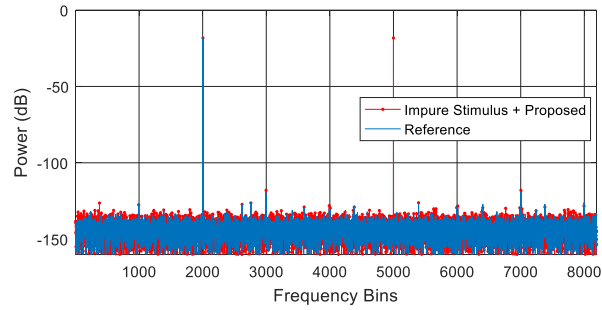


Figure 7.5. Two-tone ADC output spectrum using impure stimulus with the proposed method.

Table 7.1. Spectrum performance of the ADC (case 1).

Methods	THD (dB)	IMD (dB)
Impure Stimulus	-88.01	-74.93
Proposed	-95.14	-90.67
Reference	-95.07	-90.94

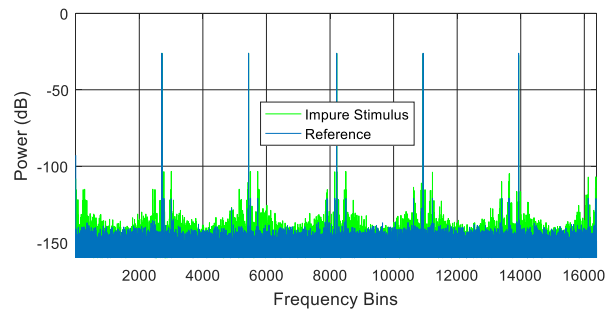


Figure 7.6. Five-tone ADC output spectrum using impure stimulus.

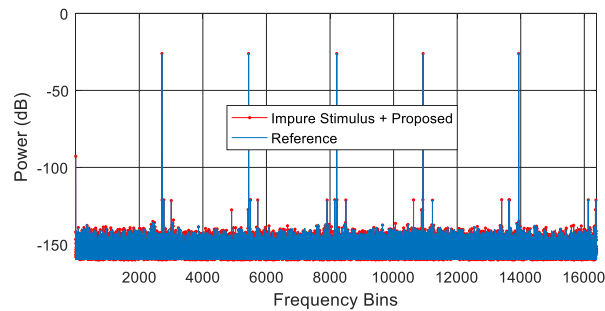


Figure 7.7. Five-tone ADC output spectrum using impure stimulus with the proposed method.

Table 7.2. Spectrum performance of the ADC (case 2).

Methods	THD (dB)	IMD (dB)
Impure Stimulus	-80.64	-66.41
Proposed	-93.09	-84.25
Reference	-93.32	-84.14

Another set of results is shown with five-tone impure sine waves generated by another 16-bit nonlinear DAC, and an 18-bit ADC is tested with $M=2^{15}$ and five fundamentals J_s : 2711, 5437, 8209, 10927, and 13933. Another test setup is similar as previously. Similar results can be seen from Figures. 7.6 and 7.7. The green spectrum using the impure stimulus generated many nonlinearity bins, where the correct ADC spectrum information cannot be obtained. After using the proposed method, the red spectrum removed nonlinearity from the impure stimulus similar to the previous test results and matched well with the reference. Table 7.2 also confirmed the proposed method's accuracy in estimating the THD and IMD.

B. Robustness

The robustness of the proposed algorithm must also be verified. Different types, resolutions, and performances of the DACs and ADCs are generated to validate the robustness of the proposed method under these different test conditions. For DAC, 12–16-bit resolutions were generated with an R-string, R-2R, and binary capacitive DACs, whose nonlinearity varies as well. For ADC, 16–20-bit ADC were generated with pipeline SAR ADCs. M also varies from 2^{13} to 2^{15} . For each test, since high-precision instruments are not available, the DAC nonlinearity is designed worse than the ADC under test, so its nonlinearity will corrupt the test results. The estimated ADC THD and IMD are compared

with their reference values tested by the pure stimulus. Figures 7.8 and 7.9 show the results, which are ordered by the purity of the stimulus, namely the purity of the DAC output signal in dB. These figures show only low purity test stimuli from -90dB to -60dB, the estimated THDs (blue triangles in Figure 7.8) and IMDs (blue triangles in Figure 7.9) lie very closely with the reference values shown as red crosses in both Figure 7.8 and Figure 7.9, respectively. These demonstrate after using the proposed method, it is capable of obtaining correct THD and IMD information for the ADC, given different purity for stimuli, different types, resolutions, or performance of DACs and ADCs.

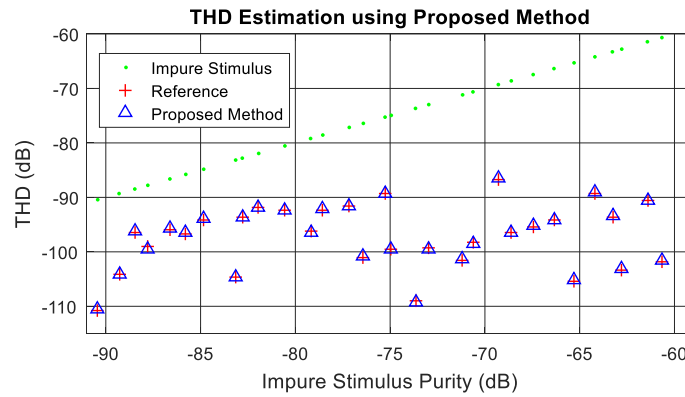


Figure 7.8. THD estimation using the proposed method.

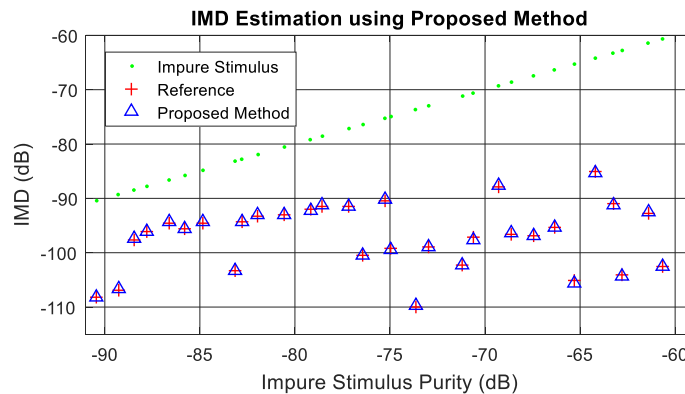


Figure 7.9. IMD estimation using the proposed method.

7.5 Conclusion

This chapter proposed a new method for a cost-effective test system to dramatically relax the linearity requirements for multi-tone spectral testing. This proposed method can separate harmonics and intermodulation of the impure test stimulus from the ADC output spectrum. The design requirements for this cost-effect test system are discussed in detail. Both functionality and robustness of the proposed method are validated, and accuracy and robustness against various test conditions are demonstrated. By using such a cost-effective test system and the proposed method, the need for high-precision, high-purity and costly test stimulus in multi-tone spectral testing is eliminated, which can be implemented into board or chip level multi-tone high-precision spectral testing.

References

- [1] Y. Zhuang and D. Chen, "Accurate Spectral Testing with Impure Source Test Stimulus for Multi-tone Test," submitted to *IEEE VLSI Test Symp. (VTS)* 2018.
- [2] M. Burns and G.W.Roberts, *An Introduction to Mixed-Signal IC Test and Measurement*, Oxford Univerisity Press, New York, USA, 2012.
- [3] J. Doernberg, H.-S. Lee, and D.A. Hodges, "Full-Speed Testing of A/D Converters," *IEEE J. Solid State Circuits*, SC-19, pp. 820-827, Dec.1984.
- [4] M. Mahoney, *DSP-Based Testing of Analog and Mixed-Signal Circuits*, Wiley-IEEE Computer Society Press, 1987.
- [5] Y. Zhuang and D. Chen, "New strategies in removing noncoherency from signals with large distortion-to-noise ratios," Accepted by *IEEE Trans. Circuits Syst. II, Exp. Briefs*, Aug. 2017.

- [6] IEEE Standard for Terminology and Test Methods for Analog-to-Digital Converters, *IEEE Std.1241*, 2010.
- [7] IEEE Standard for Digitizing Waveform Recorders, *IEEE Std.1057*, 2007.
- [8] Z. Yu, D. Chen, and R. Geiger, “Accurate testing of ADC’s spectral performance using imprecise sinusoidal excitations,” in Proc. *IEEE Int. Symp. Circuits Syst.*, vol. 1. May 2004, pp. 645–648.
- [9] D. Slepíčka, “The estimation of test signal quality by means of two simple filters in ADC testing,” *Comput. Standards Interfaces*, vol. 34, no. 1, pp. 156–161, Jan. 2012.
- [10] B. Magstadt, Y. Zhuang and D. Chen, “Accurate Spectral Testing With Impure Source and Noncoherent Sampling,” *IEEE Trans. Instrum. Meas.*, vol. 65, no. 11, pp. 2454-2463, Nov. 2016.
- [11] D. Rabijns, W.V. Moer and G.Vandersteen, “Spectrally pure excitation signals: Only a dream?,” *IEEE Trans. Instrum. Meas.*, vol. 53, no. 5, pp. 1433–1440, Oct. 2004.
- [12] A. Maeda, “A Method to Generate a Very Low Distortion, High Frequency Sine Waveform Using an AWG,” In Proc. *IEEE Int. Test Conf.*, 2008, pp. 1–8.
- [13] M. Elsayed and E. Sanchez-Sinencio, “A Low THD, Low Power, High Output-Swing Time-Mode-Based Tunable Oscillator Via Digital Harmonic-Cancellation Technique,” *IEEE J. Solid-State Circuits*, vol. 45, no. 5, pp.1061-1071, May 2010.
- [14] F. Abe, Y. Kobayashi, K. Sawada, K. Kato, O. Kobayashi and H. Kobayashi, “Low-Distortion Signal Generation for ADC Testing,” In Proc. *IEEE Int. Test Conf.*, 2014, pp. 1–10.

- [15] Y. Zhuang, A. Unnithan, A. Joseph, S. Sudani, B. Magstadt, and D. Chen, "Low Cost Ultra-Pure Sine Wave Generation with Self Calibration," In Proc. *IEEE Int. Test Conf.*, 2016, pp. 1-9.

CHAPTER 8

MULTI-TONE SINE WAVE GENERATION ACHIEVING THE THEORETICAL MINIMUM OF PEAK-TO-AVERAGE POWER RATIO

Multi-tone signals have been widely used in various applications. One of the bottlenecks is how to maximize the signal power given a certain peak range, namely achieving the minimum peak-to-average power ratio (PAPR). In this chapter, a novel strategy is proposed to achieve the minimum PAPR for multi-tone sine waves. By properly selecting each tone's frequency and initial phase, the multi-tone sine waves can achieve the minimum amplitude, while maintaining total signal power, without power loss during signal generation. It is rigorously proved that the proposed method can achieve the theoretical minimum of PAPR. Extensive simulation results for various cases are presented that validate the desired property of the generated waveform. Guidelines are provided for practical implementation of the multi-tone sine waves, such as signal and system spectral testing, maximizing power amplifier transmission efficiency, multi-carrier transmission, orthogonal frequency-division multiplexing (OFDM), and other wireless communication systems.

This chapter is mainly based on the paper submitted to *IEEE Trans. Circ. Syst. I* [1].

8.1 Introduction

Sine waves are among the most widely used signals in communications, system analysis, and many other applications. Often, single-tone sine waves are used, such as the test stimulus for dynamic testing of data converters, transceivers, power amplifiers (PAs), other devices, systems, etc. [2-5]. They also serve as a carrier wave in a global system for mobile (GSM) transmissions [6], as well as the fields of material and chemical spectroscopy

measurements. For the multi-tone signal, especially the multi-tone sine wave, has attracted a lot of attention during the past decades. For example, characterizing a wideband circuit and system often requires the frequency response across the entire bandwidth, which is challenging for single-tone test [7]. One widely adopted approach is using the multi-tone test signal, since it reduces the test time compared with multiple measurements using a single tone. Moreover, as the performance of the circuit and system tends to vary with frequency, using a multi-tone signal is more practical in real laboratory and production testing. In communications systems, intermodulation distortion (IMD) is a key specification to determine the linearity performance of the systems, which also requires multi-tone signals [8-10, 33]. As the interest in multi-carrier transmission grows, multi-carrier modulation (MCM) and OFDM have been proposed and deployed in many wireless communication standards [11-13], where the carriers and the representation of the transmitted signals in the time domain are often multi-tone sine waves.

Apart from the wide applications for multi-tone sine waves, how to reduce and minimize the PAPR is still a challenging task. One example would be the usage of PAs in the transceivers normally working in a linear region to achieve best power efficiency, and to prevent spectral growth of multi-carriers in the form of intermodulation among subcarriers and out-of-band radiation. If the PAs are operating beyond the linear region due to high PAPR of the input signal, many distortions will be created in the transmitted signal and the drawbacks of high PAPR often outweigh the benefits of multi-carrier transmission systems. Therefore, it is vital to control the signal peak values within the PA's saturation region, while maximizing the output power for transmission. Another example is in the testing of systems like transceivers, data converters, operational amplifiers, etc., to achieve best Signal-to-Noise

Ratio (SNR) possible. The signal's power must be maximized, so the test stimulus often reaches the full range of the system input. If the multi-tone signal has a high PAPR without clipping the signal at the input, it would compromise the signal power; hence, decrease the measured performance of the systems. Therefore, it is crucial to find solutions that can achieve minimum PAPR for multi-tone signals, especially for multi-tone sine waves.

In the past, many methods have been proposed to deal with the PAPR issue [14-30]. In the application of OFDM, some use amplitude clipping and filtering [16-17]. Coding [18-22], tone reservation, and tone injection [23] are used to reduce PAPR. Selected mapping (SLM) [24-25] and partial transmit sequences (PTS) are also used [26-27]. Based on [14-16], these methods are capable of reducing PAPR, but at the cost of data rate loss, increasing computational complexity, average power increase, etc. A novel circuit for reducing the crest factor of a multi-tone data signal is proposed [28], where the correction signal is subtracted from the original multi-tone signal. In [29], a novel, improved method for generating the reduced peak amplitude high data rate channels is proposed. This consists of several lower rate channels with phase rotated before summed and transmitted. However, none of these methods discussed the application for multi-sine waves amplitude reduction. In [30], an optimal multi-sine design is proposed with either logarithmically or equally-spaced frequencies. It appropriately selected the phases to compress the amplitude; however, it becomes more difficult as the number of tones increases to select the optimal phases. In industry, to create low PAPA multi-tone signals, one of the most widely used approaches is to vary the phase from 0 to 360 degrees between adjacent single tones and it is recommended to vary the tone phases randomly. This approach has been adopted for many years and been used by many researchers and engineers. However, it is time consuming, especially with

more tones. Therefore, a new method is necessary and vital to find the optimal PAPR for multi-tone sine waves.

The remainder of the chapter is arranged as follows. Section II discusses multi-tone sine waves and their challenges to achieve small PAPR. Section III introduces the proposed method to generate multi-tone sine waves with the theoretical minimum PAPR. Section IV presents the simulation results in MATLAB to validate the proposed method to generate multi-tone sine waves with minimum PAPR. Section V concludes this chapter.

8.2 Multi-tone Sine Waves and PAPR

In this section, the definition of multi-tone sine waves and PAPR are provided. The problems of a high PAPR for multi-tone sine waves are illustrated.

OFDM signals can be written as:

$$v(t) = \frac{1}{\sqrt{N}} \sum_{k=0}^{N-1} X_k e^{j2\pi f_k t}, \quad 0 \leq t \leq NT, \quad (8.1)$$

where N is the number of symbols, X is the block of N symbols: $X = \{X_k, k = 0, 1, \dots, N-1\}$ in the frequency domain with each symbol modulating one set of subcarriers: $f_k = k\Delta f$, $\Delta f = 1/NT$, and T is the original symbol period.

This low-pass signal can be either real or complex. Real valued low-pass equivalent signals are typically transmitted at baseband, such as wireline applications. For wireless applications, the transmitted signal is up converted to carrier frequency, f_c . In general, the transmitted signal can be written as:

$$s(t) = R\{x(t)e^{j2\pi f_c t}\}. \quad (8.2)$$

It can also be represented as:

$$s(t) = \sum_{k=0}^{N-1} |X_k| \cos(2\pi |f_c + k/T| t + \arg[X_k]). \quad (8.3)$$

The transmission signal can be viewed as a summation of N -tone sine waves with different frequencies, namely multi-tone sine waves. For simplicity in this chapter, each considered tone has an equal amplitude, but arbitrary initial phase.

In the time domain, the N -tone sine wave with normalized amplitude is given by:

$$x(t) = \sum_{i=1}^N \cos(2\pi f_i t + \phi_i), \quad (8.4)$$

where f_i and ϕ_i are each tone's frequency and initial phase, respectively.

The PAPR is defined as the peak amplitude squared divided by the rms value squared:

$$PAPR = \frac{|x|_{peak}^2}{x_{rms}^2}. \quad (8.5)$$

It can also be expressed in dB:

$$PAPR_{dB} = 10 \log_{10} \frac{|x|_{peak}^2}{x_{rms}^2}. \quad (8.6)$$

For a single-tone sine wave, whose amplitude is normalized to 1, the rms value is $1/\sqrt{2}$, while its peak value is 1. Then, the PAPR is $\sqrt{2}$ or 3.01dB. For multi-tone sine waves, the rms value is $\sqrt{N/2}$ and the peak value at worst case scenario becomes N . Then, the PAPR comes to $2N$ or $10 \log_{10} 2N$ in dB, which worsens as the number of tones increases. For the best case where the power remains the same, while the peak reaches the theoretical minimum of \sqrt{N} , the PAPR reaches the minimum like for the single-tone case: $\sqrt{2}$ or 3.01dB. Therefore, the goal essentially is to find the minimum peak value of the multi-tone sine wave, while maintaining the signal power.

In recent years, such multi-tone signals are achieved by Arbitrary Waveform Generators (AWGs) and Digital-to-Analog Converters (DACs). In Automatic Test Equipment (ATE) the signal generation pattern is by digitized or sampled signal with low-pass or band-pass filtering. In the future, it can be envisioned that all waveforms will be digitally-generated or synthesized.

The sampled or discrete multi-tone sine wave is given by:

$$x[n] = \sum_{i=1}^N \cos(2\pi f_i n T_s + \phi_i) + w[n], \quad (8.7)$$

where $n = 0, 1, \dots$, M is the total data record length, T_s is the sampling period, f_s is the sampling rate and $T_s = 1/f_s$, $w[n]$ contains signal noise, input referred noise from the digitizer, and quantization noise of the digitizer. Since it is not related to this chapter's focus, for simplification purposes the noise term is ignored in the following derivations.

If the coherent sampling condition is met [31-33], the integer number waveform cycles in the data record is J , the input and sampling frequency, and the total data record length satisfies the following relationship:

$$f_i = J \frac{f_s}{M}. \quad (8.8)$$

Therefore, frequency selection is essentially selecting the J and M is usually selected as a power of 2 for faster processing of the Fast Fourier Transform (FFT). Usually, f_i is selected not to be a sub-harmonic of f_s , then the quantization error is random and uncorrelated with f_i . If this condition is not satisfied, it will cause the quantization noise energy to be concentrated at harmonics of the fundamental frequency, thereby producing distortion—an artifact of the sampling process rather than nonlinearity of the Analog-to-Digital Converter (ADC) or signal [3]. J is preferred chosen to be an odd number. In

addition, if the input frequency exceeds half of the sampling frequency, aliasing will occur on the spectrum and the fundamental tone will be reflected back according to $|n.f_s - f_i|$ at frequency range: $[0 f_s/2]$, viewed as a low frequency fundamental. For this reason, in the following analysis, only the non-aliasing input frequency is selected, meaning J is smaller than $M/2$. From this discussion, it can be seen that to satisfy these conditions, J cannot be arbitrarily selected. Hence, the frequency for each tone cannot be arbitrarily selected either.

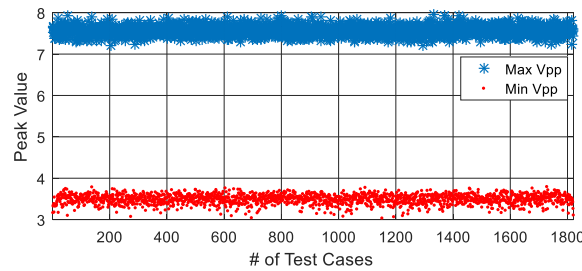


Figure 8.1. 8-tone sine wave maximum and minimum peak values.

Using Eq. (8.8), replace f_i with J_i , Eq. (8.7) can be re-written as:

$$x[n] = \sum_{i=1}^N \cos\left(2\pi \frac{J_i}{M} n + \phi_i\right). \quad (8.9)$$

In the following derivations, the frequency selection essentially becomes selecting the proper J . Using Eq. (8.9) as a starting point, derive all the following multi-tone cases. To illustrate the issue of high PAPR, namely the high peak value, an 8-tone sine wave is generated. Each tone's J is selected for coherent sampling and odd numbers are randomly selected among $[0 M/2]$. A total of more than 1800 test cases were performed. Once the frequencies are selected, their initial phases are randomly generated from $[0 2\pi]$ for a total of 10,000 runs to generate 1000 8-tone sine waves with different peak values. This is the

conventional method mentioned in Section I. Figure 8.1 shows the maximum and minimum peak values for these 10,000 sine waves at each test case. Even though each case has 10,000 runs with different initial phases, for many test cases the maximum peak values are near 8. However, minimum peak values never reach the theoretical minimum of $\sqrt{8}$. This implies without the careful selection of the tone frequency and their initial phases, it would be extremely difficult to calculate the minimum PAPR for multi-tone sine waves.

8.3 Proposed Strategy

The statement in the previous section leads to the need for the proposed method to generate the multi-tone sine wave with minimum PAPR, which will be described in detail in this section. Since the rms of the signal needs to maintain the same level of $\sqrt{N/2}$ without losing power to reach the theoretical minimum PAPR, the generated multi-tone signal amplitude must be \sqrt{N} . Therefore, the proposed method seeks a way to generate a minimum peak value of \sqrt{N} without losing power.

A. 2^z Multi-Tones

The first part of the proposed method focuses on finding the minimum PAPR for multi-tone sine waves, using 2^z number of tones, since this number of tones is commonly used in communication applications such as OFDM.

1) 2-tone

Starting with a 2-tone sine wave $x_2[n]$:

$$x_2[n] = \cos(\omega_1 n + \phi_1) + \cos(\omega_2 n + \phi_2), \quad (8.10)$$

where $\omega_1 = 2\pi \frac{J_1}{M}$ and $\omega_2 = 2\pi \frac{J_2}{M}$.

$x_2[n]$ can be written as:

$$x_2[n] = 2 \cos\left(\frac{(\omega_1 + \omega_2)n + \phi_1 + \phi_2}{2}\right) \cos\left(\frac{(\omega_1 - \omega_2)n + \phi_1 - \phi_2}{2}\right). \quad (8.11)$$

We propose the 2-tone has the relationship given by $J_1 + J_2 = M/2$. $x_2[n]$ is then given by:

$$x_2[n] = 2 \cos\left(2\pi \frac{J_1}{M} n + \frac{\phi_1 - \phi_2 - n\pi}{2}\right) \cos\left(\frac{\phi_1 + \phi_2}{2} + \frac{\pi}{2} n\right). \quad (8.12)$$

Since the goal is to find the peak value for the first cos term, the peak value is 1. The second cos term, given a different n , can be categorized into four groups:

$$\cos\left(\frac{\phi_1 + \phi_2}{2} + \frac{\pi}{2} n\right) = \begin{cases} \cos\left(\frac{\phi_1 + \phi_2}{2}\right), & \text{if } n = 0, 4, 8, \dots \\ \sin\left(\frac{\phi_1 + \phi_2}{2}\right), & \text{if } n = 1, 5, 9, \dots \\ -\cos\left(\frac{\phi_1 + \phi_2}{2}\right), & \text{if } n = 2, 6, 10, \dots \\ -\sin\left(\frac{\phi_1 + \phi_2}{2}\right), & \text{if } n = 3, 7, 11, \dots \end{cases}. \quad (8.13)$$

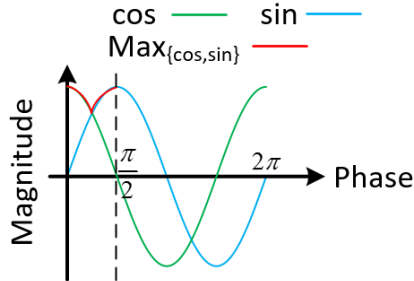


Figure 8.2. Illustration of Eq. (8.13) for minimum peak value

For the peak value, it is evident for the cos term or the sin term, the value is 1. Since we are looking for the minimum peak value, due to its symmetry in Eq. (8.13) without loss of

generality within one period $[0, 2\pi]$, assume $\cos(\frac{\phi_1 + \phi_2}{2}) > 0$ and $\sin(\frac{\phi_1 + \phi_2}{2}) > 0$. The peak

value is illustrated in Figure 8.2 along the red curve, whose minimum value occurs at $\frac{\pi}{4}$,

which is $\frac{1}{\sqrt{2}}$. By symmetry, the minimum peak also occurs at $\frac{5\pi}{4}$, meaning that if

$\frac{\phi_1 + \phi_2}{2} = \frac{\pi}{4} + j\pi$, $j = 0, \pm 1, \pm 2, \dots$. Since the sine waves are periodic, for simplicity in the

following derivations, assume the first tone's initial phase is 0: $\phi_1 = 0$. Then ϕ_2 can be $\frac{\pi}{2}$. A 2-

tone sine wave will have a minimum peak value of $\sqrt{2}$, if each tone's amplitude is 1.

2) 4-tone

For the 4-tone case:

$$x_4[n] = \cos(\omega_1 n + \phi_1) + \cos(\omega_1' n + \phi_1') + \cos(\omega_2 n + \phi_2) + \cos(\omega_2' n + \phi_2'). \quad (8.14)$$

Similarly, we propose two pairs of frequencies: $J_1 + J_1' = M/2$ and $J_2 + J_2' = M/2$,

whose initial phases sum to either 0 or π . If $\phi_1 = 0$, then assume $\phi_1' = \pi$, $\phi_2 = -\phi_2'$, $x_4[n]$ is

given by:

$$\begin{aligned} x_4[n] = & \cos(2\pi \frac{J_1}{M} n) + \cos(2\pi \frac{M/2 - J_1}{M} n + \pi) \\ & + \cos(2\pi \frac{J_2}{M} n + \phi_2) + \cos(2\pi \frac{M/2 - J_2}{M} n - \phi_2') \end{aligned}, \quad (8.15)$$

which can be further simplified to $x_4[n] = \cos \omega_1 n [1 + \cos(n+1)\pi] + \cos(\omega_2 n + \phi_2) [1 + \cos n\pi]$.

If n is an even number, $x_4[n]$ becomes $2 \cos(\omega_2 n + \phi_2)$. If n is an odd number, $x_4[n]$

becomes $2 \cos \omega_1 n$. Therefore, the proposed 4-tone sine wave can achieve a minimum peak

value of 2.

3) 8-tone

For the 8-tone sine wave, the J_s will have four pairs. Each sums to $M/2$: $J_1 + J'_1 = M/2$, $J_2 + J'_2 = M/2$, $J_3 + J'_3 = M/2$ and $J_4 + J'_4 = M/2$. For their initial

phases, we propose such a relationship: $\phi_1 = \phi'_1 = 0, \phi_2 = 0, \phi'_2 = \pi, \phi_3 = \frac{\pi}{2},$

$\phi'_3 = -\frac{\pi}{2}, \phi_4 = 0, \phi'_4 = -\pi$. Using this information, the 8-tone sine wave is given by:

$$\begin{aligned} x_8[n] = & \cos(2\pi \frac{J_1}{M} n) + \cos(2\pi \frac{M/2 - J_1}{M} n) + \cos(2\pi \frac{J_2}{M} n) + \cos(2\pi \frac{M/2 - J_2}{M} n + \pi) \\ & + \cos(2\pi \frac{J_3}{M} n + \frac{\pi}{2}) + \cos(2\pi \frac{M/2 - J_3}{M} n - \frac{\pi}{2}) + \cos(2\pi \frac{J_4}{M} n) + \cos(2\pi \frac{M/2 - J_4}{M} n - \pi) \end{aligned} \quad (8.16)$$

To further simplify the frequency terms, we propose:

$$J_3 = J_1 + M/4, \quad (8.17)$$

$$J_4 = J_2 + M/4. \quad (8.18)$$

Then, Eq. (8.16) can be written as:

$$\begin{aligned} x_8[n] = & \cos(2\pi \frac{J_1}{M} n) + \cos(2\pi \frac{J_1}{M} n - n\pi) + \cos(2\pi \frac{J_2}{M} n) + \cos(2\pi \frac{J_2}{M} n - (n+1)\pi) \\ & + \cos(2\pi \frac{J_1 + M/4}{M} n + \frac{\pi}{2}) + \cos(2\pi \frac{M/4 - J_1}{M} n - \frac{\pi}{2}) \\ & + \cos(2\pi \frac{J_2 + M/4}{M} n) + \cos(2\pi \frac{M/4 - J_2}{M} n - \pi) \end{aligned} \quad (8.19)$$

Further simplification leads to:

$$x_8[n] = \left[\cos(\omega_1 n) + \cos\left(\omega_1 n + \frac{(n+1)\pi}{2}\right) \right] [1 + \cos n\pi] + \left[\cos(\omega_2 n) + \cos\left(\omega_2 n + \frac{n\pi}{2}\right) \right] [1 + \cos(n+1)\pi] \quad (8.20)$$

The 8-tone sine wave can be categorized into four groups:

$$x_8[n] = \begin{cases} 2 \cos \omega_1 n - 2 \sin \omega_1 n, & \text{if } n = 0, 4, 8, \dots \\ 2 \cos \omega_2 n - 2 \sin \omega_2 n, & \text{if } n = 1, 5, 9, \dots \\ 2 \cos \omega_1 n + 2 \sin \omega_1 n, & \text{if } n = 2, 6, 10, \dots \\ 2 \cos \omega_2 n + 2 \sin \omega_2 n, & \text{if } n = 3, 7, 11, \dots \end{cases} \quad (8.21)$$

It is evident each of these four groups will lead to a peak value of $\sqrt{8}$ for the proposed 8-tone sine wave.

4) 16-tone

A similar theory is applied to the 16-tone sine wave, where we have eight pairs of J_s .

Each sums to $M/2$. For initial phases, we propose: $\phi_1 = \phi'_1 = 0, \phi_2 = \phi'_2 = 0, \phi_3 = 0, \phi'_3 = \pi,$

$$\phi_4 = \phi'_4 = -\frac{\pi}{2}, \phi_5 = \phi'_5 = 0, \phi_6 = \phi'_6 = -\pi, \phi_7 = 0, \phi'_7 = \pi, \phi_8 = \phi'_8 = \frac{\pi}{2}.$$

The 16-tone sine wave can be given by:

$$x_{16}[n] = \cos\left(2\pi \frac{J_1}{M} n\right) + \cos\left(2\pi \frac{M/2 - J_1}{M} n\right) + \cos\left(2\pi \frac{J_2}{M} n\right) + \cos\left(2\pi \frac{M/2 - J_2}{M} n\right) + \cos\left(2\pi \frac{J_3}{M} n\right) + \cos\left(2\pi \frac{M/2 - J_3}{M} n + \pi\right) + \cos\left(2\pi \frac{J_4}{M} n - \frac{\pi}{2}\right) + \cos\left(2\pi \frac{M/2 - J_4}{M} n - \frac{\pi}{2}\right) + \cos\left(2\pi \frac{J_5}{M} n\right) + \cos\left(2\pi \frac{M/2 - J_5}{M} n\right) + \cos\left(2\pi \frac{J_6}{M} n - \pi\right) + \cos\left(2\pi \frac{M/2 - J_6}{M} n - \pi\right) + \cos\left(2\pi \frac{J_7}{M} n\right) + \cos\left(2\pi \frac{M/2 - J_7}{M} n + \pi\right) + \cos\left(2\pi \frac{J_8}{M} n + \frac{\pi}{2}\right) + \cos\left(2\pi \frac{M/2 - J_8}{M} n + \frac{\pi}{2}\right) \quad (8.22)$$

If only the first four terms are examined:

$$x_{16,1}[n] = \cos(2\pi \frac{J_1}{M} n) + \cos(2\pi \frac{M/2 - J_1}{M} n) + \cos(2\pi \frac{J_2}{M} n) + \cos(2\pi \frac{M/2 - J_2}{M} n). \quad (8.23)$$

If J_2 is related to J_1 given by:

$$J_2 = J_1 + M/4, \quad (8.24)$$

Then Eq. (8.23) can be simplified to:

$$x_{16,1}[n] = \cos(\omega_1 n)(1 + \cos n\pi)(1 + \cos \frac{n}{2} \pi). \quad (8.25)$$

It is clear to see that its peak value only equals 4, if $n=0,4,8\dots$, and the remainder of the ns will result in 0. Similarly, the second four terms will produce the peak value of 4 with a different frequency, if $n=1,5,9\dots$. Thus, $x_{16}[n]$ is simplified to:

$$x_{16}[n] = \begin{cases} 4 \cos \omega_1 n, & \text{if } n = 0, 4, 8, \dots \\ 4 \cos \omega_3 n, & \text{if } n = 1, 5, 9, \dots \\ 4 \cos \omega_5 n, & \text{if } n = 2, 6, 10, \dots \\ 4 \cos \omega_7 n, & \text{if } n = 3, 7, 11, \dots \end{cases} \quad (8.26)$$

By dividing the 16 tones into four groups, each group is only non-zero at 1 of every 4 ns . There are no non-zero values summing among different groups, which is similar to the idea of interleaving among the four different sine waves. Moreover, as shown in Eq. (8.26), there are no relationships among the four group frequencies and $\omega_1, \omega_3, \omega_5, \omega_7$ will have many selection choices. This adds flexibility to the proposed strategy, as more frequency choices can be selected that will lead to the minimum peak value of 4 for the 16-tone sine wave.

5) 32-tone

Then for the 32-tone case, we can use a similar approach as for the 8-tone case: with term $\cos \omega_1 n$. Find $\sin \omega_1 n$ that can add a peak value of $\sqrt{2}$. Since we know from the 16-tone

that it can be divided into four groups, each group has a peak value of 4 and only shows every 1 of 4 n . We can again divide the 32-tone into four groups, each with eight tones.

Assume the first group already has 4-tone $\cos(\omega_1 n) + \cos(\omega_1 n - n\pi) + \cos(\omega_1 n + \frac{n\pi}{2}) + \cos(\omega_1 n - \frac{n\pi}{2})$, equivalent to Eq. (8.25). Another 4-tone configuration is needed to obtain

the $\sin \omega_1 n$ term. Then, like Eq. (8.25), the proposed additional 4-tone

is $\cos(\omega_1 n + \frac{n+2}{4}\pi)[1 + \cos n\pi][1 + \cos \frac{n}{2}\pi]$. Expanding this term leads to:

$$\begin{aligned} & \cos(\omega_1 n + \frac{n+2}{4}\pi)[1 + \cos n\pi][1 + \cos \frac{n}{2}\pi] \\ &= \cos(\omega_1 n + \frac{n+2}{4}\pi) + \cos(\omega_1 n - \frac{3n-2}{4}\pi) + \cos(\omega_1 n + \frac{3n+2}{4}\pi) + \cos(\omega_1 n + \frac{n-2}{4}\pi) \end{aligned} \quad (8.27)$$

Hence, another four sine waves in this group can be determined with their J s related to J_1 given by:

$$J_3 = J_1 + \frac{M}{8}, \quad (8.28)$$

$$J_4 = J_2 + \frac{M}{8}. \quad (8.29)$$

These four sine waves can be paired to two pairs. Each adds up to $M/2$ like all previous cases: $J_3 + J_3' = M/2$ and $J_4 + J_4' = M/2$. With all known information, the first group of 8-tone sine waves can be given by:

$$x_{32,1}[n] = \left[\cos(\omega_1 n) + \cos(\omega_1 n + \frac{n+2}{4}\pi) \right] (1 + \cos n\pi)(1 + \cos \frac{n}{2}\pi). \quad (8.30)$$

This only equals to $4\sqrt{2}$ at $n=0, 4, \dots$. The remainder are 0. From Eq. (8.30), the initial

phases can be obtained: $\phi_1 = \phi_1' = 0, \phi_2 = \phi_2' = 0, \phi_3 = \phi_4 = \frac{\pi}{2}, \phi_3' = \phi_4' = -\frac{\pi}{2}$.

The remaining three groups can be constructed in a similar way. The 32-tone sine wave is therefore given by:

$$x_{32}[n] = \begin{cases} 4 \cos \omega_1 n \pm 4 \sin \omega_1 n, & \text{if } n = 0, 4, 8, \dots \\ 4 \cos \omega_5 n \pm 4 \sin \omega_5 n, & \text{if } n = 1, 5, 9, \dots \\ 4 \cos \omega_9 n \pm 4 \sin \omega_9 n, & \text{if } n = 2, 6, 10, \dots \\ 4 \cos \omega_{13} n \pm 4 \sin \omega_{13} n, & \text{if } n = 3, 7, 11, \dots \end{cases} \quad (8.31)$$

Therefore, the proposed 32-tone sine wave can generate the minimum peak value of $4\sqrt{2}$.

6) 64-tone

Based on the 4-tone and 16-tone results, use the same idea by adding another term to: $(1 + \cos n\pi)(1 + \cos \frac{n}{2}\pi)$ and making it only non-zero at 1 of every 8 n . Thus, for 64 tones, by dividing them into eight groups, each group is only non-zero at 1 of every 8 n , with no non-zero values summing among the different groups. The proposed solution in the first group can be:

$$x_{64,1}[n] = \cos(\omega_1 n)(1 + \cos n\pi)(1 + \cos \frac{n}{2}\pi)(1 + \cos \frac{n}{4}\pi). \quad (8.32)$$

By expanding Eq. (8.32), the end result is a group of eight tones:

$$\begin{aligned} x_{64,1}[n] = & \cos(\omega_1 n) + \cos(\omega_1 n - n\pi) + \cos(\omega_1 n + \frac{n}{2}\pi) + \cos(\omega_1 n - \frac{n}{2}\pi) \\ & + \cos(\omega_1 n + \frac{n}{4}\pi) + \cos(\omega_1 n - \frac{n}{4}\pi) + \cos(\omega_1 n + \frac{3n}{4}\pi) + \cos(\omega_1 n - \frac{3n}{4}\pi) \end{aligned} \quad (8.33)$$

Then, we propose their frequency relationships similar to previous cases with each pair sums to $M/2$: $J_1 + J'_1 = M/2$, $J_2 + J'_2 = M/2$, $J_3 + J'_3 = M/2$ and $J_4 + J'_4 = M/2$. In addition, an offset of $M/4$ and $M/8$ are among J_2 , J_3 and J_4 , represented by Eqs. (8.24), (8.28)-(8.29).

Their initial phases are all 0 for this group. Then, the remaining of seven groups can be constructed similarly, which leads to the proposed 64-tone sine waves:

$$x_{64}[n] = \begin{cases} 8 \cos \omega_1 n, & \text{if } n = 0, 8, \dots \\ 8 \cos \omega_3 n, & \text{if } n = 1, 9, \dots \\ 8 \cos \omega_9 n, & \text{if } n = 2, 10, \dots \\ 8 \cos \omega_{13} n, & \text{if } n = 3, 11, \dots \\ 8 \cos \omega_{17} n, & \text{if } n = 4, 12, \dots \\ 8 \cos \omega_{21} n, & \text{if } n = 5, 13, \dots \\ 8 \cos \omega_{25} n, & \text{if } n = 6, 14, \dots \\ 8 \cos \omega_{29} n, & \text{if } n = 7, 15, \dots \end{cases} \quad (8.34)$$

From Eq. (8.34), it is clear to see the proposed 64-tone sine wave can achieve a minimum peak value of 8.

From these results, we hypothesis:

1. For 4^y number of tones where $y=1,2,3,\dots$, we categorize them into 2^y groups according to different n s. They are non-zero only at certain locations, none of the groups show as non-zero at the same time. This can be accomplished by multiplying the term $1 + \cos \frac{n}{2^y} \pi$ to Eq. (8.32). With proper frequency and phase selection, this will guarantee the multi-tone sine waves with a minimum peak value of 2^y .

2. For other cases $2 \cdot 4^y$, such as 8, 32, ..., they can be separated into 2^y groups. With proper frequency and phase selection, they sum similar to the 2-tone case in the form of $2^y (\cos \omega n \pm \sin \omega n)$ to achieve a minimum peak value of $\sqrt{2} \cdot 2^y$.

B. Low Order Multi-Tones

In addition to multi-tones with 2^z number of tones, other low order multi-tone sine waves are studied, such as the commonly used 3-tone and 5-tone.

1) 3-tone

The 3-tone can be derived from the 2-tone case. Two tones are paired with $J_1 + J_2 = M/2$, and the third tone's J_3 has an offset of $M/4$ with J_1 , which can be represented by Eq. (8.17). Their initial phases include: first two tones sum to $\frac{\pi}{2}$ and the third tone has an offset of $\frac{\pi}{4}$ with the first tone. Assuming the first tone has $\phi_1 = 0$ initial phase, then $\phi_2 = \frac{\pi}{2}$, $\phi_3 = \frac{\pi}{4}$. Thus, the 3-tone is given by:

$$x_3[n] = \cos(2\pi \frac{J_1}{M} n) + \cos(2\pi \frac{J_1}{M} n - n\pi - \frac{\pi}{2}) + \cos(2\pi \frac{J_1}{M} n + \frac{n}{2}\pi + \frac{\pi}{4}). \quad (8.35)$$

It can be categorized into four groups:

$$x_3[n] = \begin{cases} \cos \omega_1 n + \sin \omega_1 n + \cos(\omega_1 n + \frac{\pi}{4}), & n = 0, 4, \dots \\ \cos \omega_1 n - \sin \omega_1 n - \sin(\omega_1 n + \frac{\pi}{4}), & n = 1, 5, \dots \\ \cos \omega_1 n + \sin \omega_1 n - \cos(\omega_1 n + \frac{\pi}{4}), & n = 2, 6, \dots \\ \cos \omega_1 n - \sin \omega_1 n + \sin(\omega_1 n + \frac{\pi}{4}), & n = 3, 7, \dots \end{cases}. \quad (8.36)$$

From Eq. (8.36), it is evident each group can be combined into a single sine wave, with the peak value of $\sqrt{3}$. Therefore, the proposed 3-tone sine wave can achieve the minimum peak value of $\sqrt{3}$ given proper frequency and phase selections.

2) 5-tone

The 5-tone case is derived from the 4-tone case, where it has two pairs of tones, $J_1 + J_1' = M/2$ and $J_2 + J_2' = M/2$, whose initial phases add to either 0 or $\pm\pi$. If $\phi_1 = 0$, then

we assume $\phi_1' = 0, \phi_2 = \phi_2' = -\frac{\pi}{2}$. If we assume $J_1 = 3J_2 - M/4$ and $J_3 = M/4 - J_1 = M/2 - 3J_2$,

with initial phase of $-\frac{\pi}{2}$, the 5-tone can then be given by:

$$x_5[n] = \cos \omega_1 n (1 + \cos n\pi) + \cos(\omega_2 n - \frac{\pi}{2})(1 + \cos(n+1)\pi) + \cos(3\omega_2 n + \frac{\pi}{2} - n\pi). \quad (8.37)$$

It has two categories:

$$x_5[n] = \begin{cases} 2 \cos \omega_1 n - \sin 3\omega_2 n, & n = 0, 2, 4, \dots \\ 2 \sin \omega_2 n + \sin 3\omega_2 n, & n = 1, 3, 5, \dots \end{cases} \quad (8.38)$$

When n is even, the first term in Eq. (8.38) can be re-written as:

$$x_5[n] = 2 \cos(3\omega_2 n - \frac{n}{2}\pi) - \sin 3\omega_2 n, \quad n = 0, 2, 4, \dots, \quad (8.39)$$

which will lead to $\pm 2 \cos 3\omega_2 n - \sin 3\omega_2 n$ and eventually becomes one sine term, with peak value of $\sqrt{5}$. When n is odd, we know:

$$\sin 3\omega_2 n = 3 \sin \omega_2 n - 4 \sin^3 \omega_2 n. \quad (8.40)$$

Substitute Eq. (8.40) into the second term in Eq. (8.38), which will be:

$$x_5[n] = -4 \sin^3 \omega_2 n + 5 \sin \omega_2 n, \quad n = 1, 3, 5, \dots \quad (8.41)$$

By finding the maximum value when $-1 \leq \sin \omega_2 n \leq 1$, it can be proven the maximum value is $\frac{5\sqrt{15}}{9}$ and smaller than the peak value of $\sqrt{5}$ when n is even. Therefore, the proposed 5-tone

sine wave can achieve the minimum peak value of $\sqrt{5}$.

C. Discussion

In this section, several examples of the commonly used multi-tone sine waves are studied, and the strategies to achieve the theoretical minimum peak value are provided and proven mathematically. This is accomplished by appropriately selecting each tone's frequency and the initial phase, instead of randomly varying the tone phases randomly and selecting the one with the minimum peak value. Since they are generated digitally, such multi-tone sine waves can be easily generated by a DAC or AWG. This will reduce most of the computation time and complexity to generate such multi-tone sine waves. In addition, there are many frequency and initial phase choices that meet the proposed strategy's criteria, which provide much better flexibility to implement the proposed strategy, if the user wants to generate multi-tones with evenly spaced frequencies that can also be completed using the proposed strategy. Since the proposed tone frequencies are not fixed, simple calculations and validation on the multi-tone sine wave spectrum can lead to frequency selection with evenly spaced frequencies. One exception in our example is the 5-tone case, due to its unique frequency relationship of the five tones. All discussions are validated in section IV. In addition, the user can also select the logarithmically-distributed multi-tone sine wave, it can be achieved with the flexibility of the proposed strategy. Detailed discussions are not in the scope of this chapter.

Although this section provided several examples of multi-tone sine wave generation, based on these strategies a more detailed study regarding other low order multi-tones can also be done in the future.

Table 8.1 summarizes the proposed strategy for generating different multi-tone sine waves, assuming the first tone has 0 initial phase.

Table 8.1. Proposed strategy for multi-tone sine wave with minimum PAPR

Tone	Frequency	Initial Phase
2	$J_1 + J_2 = M/2$	$\phi_1 = 0, \phi_2 = \pi/2$
3	$J_1 + J_2 = M/2, J_3 = J_1 + M/4$	$\phi_1 = 0, \phi_2 = \pi/2$ $\phi_3 = \pi/4$
4	$J_1 + J'_1 = M/2, J_2 + J'_2 = M/2$	$\phi_1 = \phi'_1 = 0$ $\phi_2 = \phi'_2 = \pi/2$
5	$J_1 + J'_1 = M/2, J_2 + J'_2 = M/2$ $J_1 = 3J_2 - M/4, J_3 = M/4 - J_1$	$\phi_1 = \phi'_1 = 0$ $\phi_2 = \phi'_2 = \phi_3 = -\pi/2$
8	$J_l + J'_l = M/2, l = 1, 2, 3, 4$ $J_3 = J_1 + M/4, J_4 = J_2 + M/4$	$\phi_1 = \phi'_1 = \phi_2 = 0, \phi'_2 = \pi$ $\phi_3 = \pi/2, \phi'_3 = -\pi/2$ $\phi_4 = 0, \phi'_4 = -\pi$
16	$J_l + J'_l = M/2, l = 1, 2, \dots, 8$ $J_{l+1} = J_l + M/4, l = 1, 3, 5, 7$	$\phi_l = 0, \phi'_l = (l-1)\pi/2$ $\phi_{l+1} = \phi'_{l+1} = -(l-1)\pi/4$ $l = 1, 3, 5, 7$
32	$J_l + J'_l = M/2, l = 1, 2, \dots, 16$ $J_{l+1} = J_l + M/4, l = 1, 5, 9, 13$ $J_{l+2} = J_l + M/8, l = 1, 5, 9, 13$ $J_{l+3} = J_{l+1} + M/8, l = 1, 5, 9, 13$	$\phi_l = 0, \phi'_l = (l-1)\pi/4$ $\phi_{l+1} = \phi'_{l+1} = -(l-1)\pi/8$ $\phi_{l+2} = \pi/2 - (l-1)\pi/16$ $\phi'_{l+2} = -\pi/2 - 3(l-1)\pi/16$ $\phi_{l+3} = -\pi/2 - (l-1)\pi/16$ $\phi'_{l+3} = \pi/2 - 3(l-1)\pi/16$ $l = 1, 5, 9, 13$
64	$J_l + J'_l = M/2, l = 1, 2, \dots, 32$ $J_{l+1} = J_l + M/4, l = 1, 5, \dots, 29$ $J_{l+2} = J_l + M/8, l = 1, 5, \dots, 29$ $J_{l+3} = J_{l+1} + M/8, l = 1, 5, \dots, 29$	$\phi_l = 0, \phi'_l = (l-1)\pi/4$ $\phi_{l+1} = \phi'_{l+1} = -(l-1)\pi/8$ $\phi_{l+2} = \phi'_{l+3} = -(l-1)\pi/16$ $\phi'_{l+2} = \phi_{l+3} = -3(l-1)\pi/16$ $l = 1, 5, 9, \dots, 29$

8.4 Simulation Results

In this section, simulations results are shown to verify the generated multi-tone sine waves by the proposed strategy. Both time and frequency domains of the generated multi-tone sine waves are shown to verify their minimum peak values as well as their powers on

the spectrum. Figures 8.3–8.10 show the results for each of the multi-tone sine waves mentioned in Section III, from 2-tone through 64-tone. It is clearly shown in the time domain, each of the generated sine waves achieved the theoretical minimum peak value of \sqrt{N} . The spectrum in the lower part of each figure shows they are all near the 0dB level, meaning each tone in the generated multi-tone sine wave has the same power and there is no power loss in any case. These demonstrate the proposed strategy generates multi-tone sine waves with minimum PAPR. In addition, every spectrum is shown to have evenly spaced tones except for Figure 8.6, the 5-tone case, as mentioned in Section III.C. So, by properly selecting the frequencies, the proposed strategy can generate evenly spaced multi-tones. Additionally, the user can generate other multi-tone sine waves with different frequencies based on the proposed strategy, which offers more flexibility in generating multi-tone sine waves with minimum PAPR.

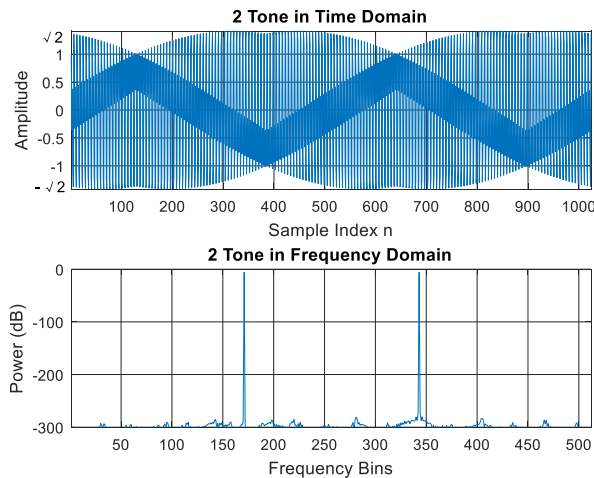


Figure 8.3. Proposed 2-tone sine wave in both time and frequency domain.

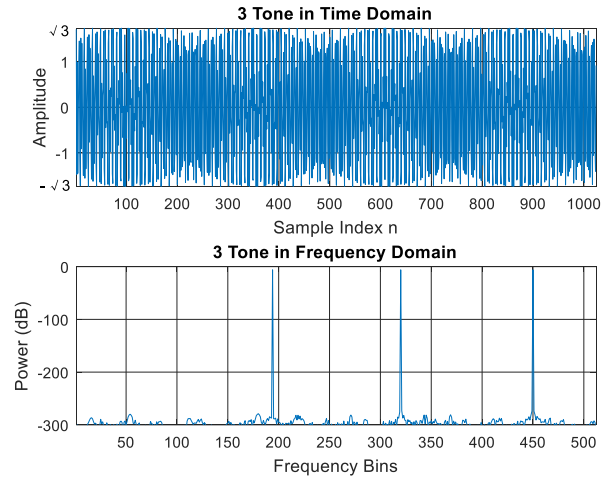


Figure 8.4. Proposed 3-tone sine wave in both time and frequency domain.

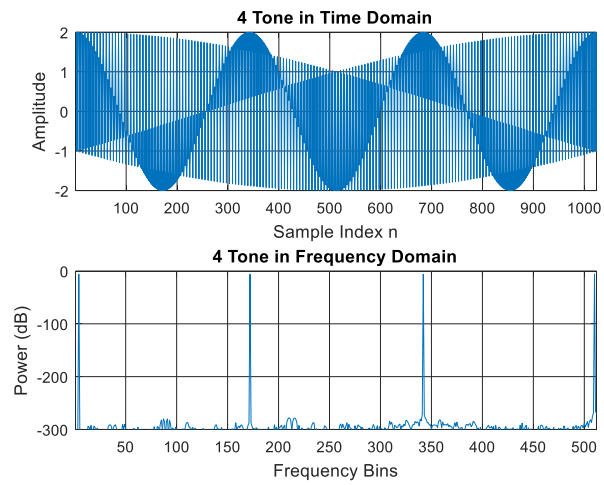


Figure 8.5. Proposed 4-tone sine wave in both time and frequency domain.

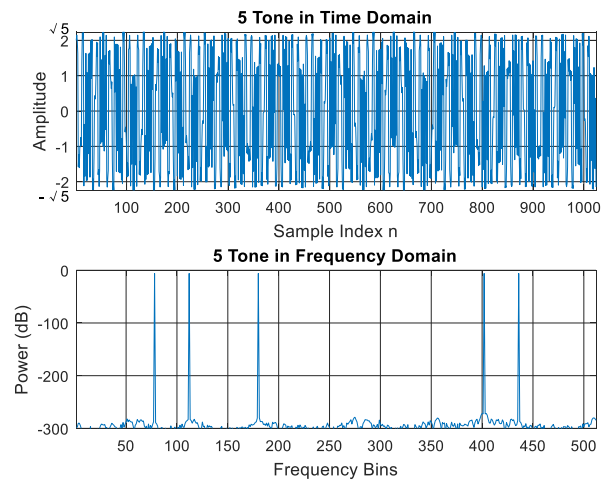


Figure 8.6. Proposed 5-tone sine wave in both time and frequency domain.

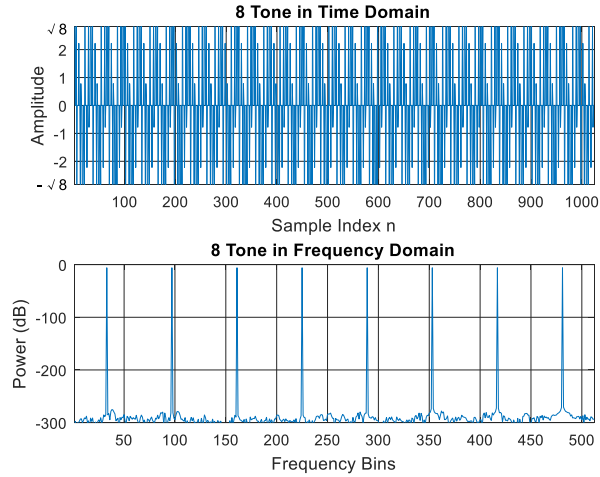


Figure 8.7. Proposed 8-tone sine wave in both time and frequency domain.

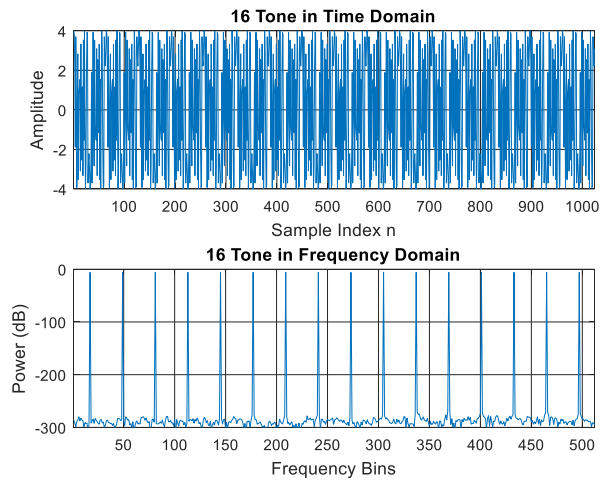


Figure 8.8. Proposed 16-tone sine wave in both time and frequency domain.

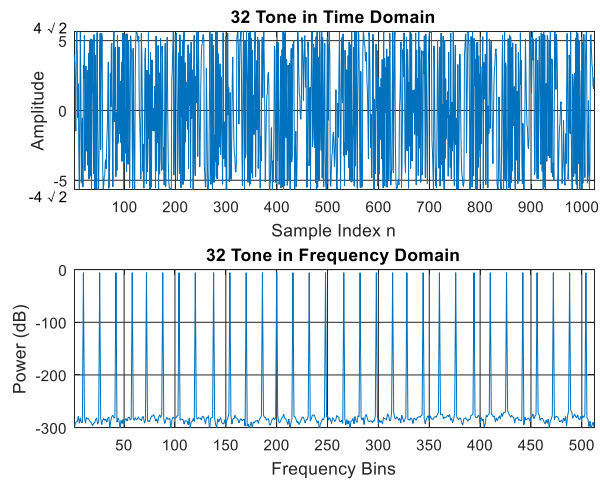


Figure 8.9. Proposed 32-tone sine wave in both time and frequency domain.

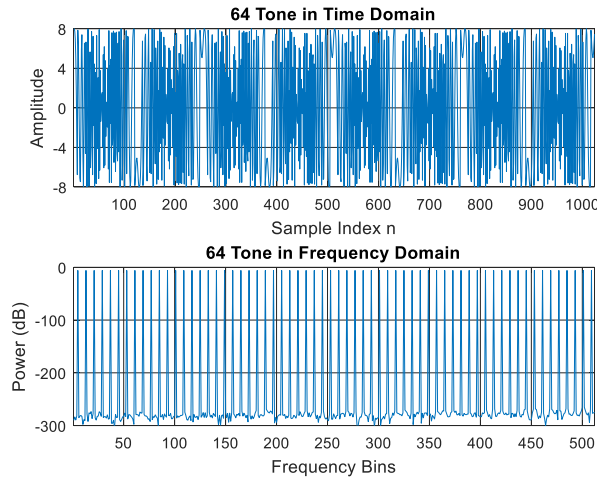


Figure 8.10. Proposed 64-tone sine wave in both time and frequency domain.

8.5 Conclusion

In this chapter, a new strategy for generating multi-tone sine waves with theoretical minimum PAPR is described. By properly selecting each tone's frequency and initial phase, the multi-tone sine waves can achieve the theoretical minimum amplitude without signal power loss. Rigorous mathematical analysis and simulation results both validated the effectiveness of the proposed strategy, which showed the proposed strategy can generate different numbers of multi-tone sine waves. Moreover, it also generalized the strategy of generating a high order of multi-tone sine waves beyond 64 tones and offers much flexibility in its frequency selection. Such strategy can be readily implemented into various fields of applications, such as signal and system testing, PA power efficiency improvement, OFDM, and other wireless communication systems.

References

- [16] Y. Zhuang and D. Chen, "Multi-Tone Sine Wave Generation Achieving the Theoretical Minimum of Peak-to-Average Power Ratio," submitted to *IEEE Trans. Circ. Syst. I*, 2017.
- [17] M. Burns and G.W.Roberts, "*An Introduction to Mixed-Signal IC Test and Measurement*," Oxford Univerisity Press, New York, USA, 2012.
- [18] W. Kester, "*Data Conversion Handbook*," Analog Devices Inc., Norwood, MA, USA, 2004.
- [19] M. Kahrs and K. Brandenburg, "*Applications of Digital Signal Processing to Audio and Acoustics*," Springer Science & Business Media, Apr.18, 2006.
- [20] R. Sobot, "*Wireless Communication Electronics: Introduction to RF Circuits and Design Techniques*," Springer Science & Business Media, Feb.21, 2012.
- [21] J. Eberspächer, H.J. Vögel, C. Bettstetter and C. Hartmann, "*GSM - Architecture, Protocols and Services*," John Wiley & Sons, Dec.23, 2008.
- [22] M. Mahoney, "*DSP-Based Testing of Analog and Mixed-Signal Circuits*," Wiley-IEEE Computer Society Press, 1987.
- [23] K. Kato, F. Abe, K. Wakabayashi, C. Gao, T. Yamada, H. Kobayashi, O. Kobayashi and K. Niitsu, "Two-Tone Signal Generation for Communication Application ADC Testing," in *Proc. IEEE 21st Asian Test Symposium (ATS)*, Nov.19-22 2012.
- [24] R. Hajji, F. Beauregard and F.M. Ghannouchi, "Multi-tone transistor characterization for intermodulation and distortion analysis," in *Proc. Microwave Symposium Digest, IEEE MTT-S International*, Jun.17-21 1996.

- [25] J.C. Pedro and N.B. Carvalho, "Analysis and measurement of multi-tone intermodulation distortion of microwave frequency converters," in *Proc. Microwave Symposium Digest, IEEE MTT-S International*, Aug.06 2002.
- [26] L. J. Cimini, Jr., "Analysis and Simulation of a Digital Mobile Channel using Orthogonal Frequency Division Multiplexing," *IEEE Trans. Commun.*, vol. 33, no. 7, July 1985, pp. 665–75.
- [27] U. Reimers, "Digital Video Broadcasting," *IEEE Commun. Mag.*, vol. 36, no. 10, June 1998, pp. 104–10.
- [28] B. R. Saltzberg, "Comparison of Single-Carrier and Multitone Digital Modulation for ADSL Applications," *IEEE Commun. Mag.*, vol. 36, no. 11, Nov. 1998, pp. 114–21.
- [29] T. Jiang and Y. Wu, "An Overview: Peak-to-Average Power Ratio Reduction Techniques for OFDM Signals," *IEEE Trans. Broadcasting*, vol. 54, no. 2, pp. 1–12, Jun. 2008.
- [30] S. H. Han and J. H. Lee, "An overview of peak-to-average power ratio reduction techniques for multicarrier transmission," *IEEE Personal Communications*, vol. 12, no. 2, pp. 56–65, Apr. 2005.
- [31] X. Huang, J. Lu, J. Zheng, K.B. Letaief and J. Gu, "Companding Transform for Reduction in Peak-to-Average Power Ratio of OFDM Signals," *IEEE Trans. on Wireless Commun.*, vol. 03, no. 6, pp. 2030-2039, Nov.2004.
- [32] R. O'Neill and L. B. Lopes, "Envelope Variations and Spectral Splatter in Clipped Multicarrier Signals," in *Proc. IEEE PIMRC*, Toronto, Canada, Sept. 1995, pp. 71–75.

- [33] J. Armstrong, "Peak-to-Average Power Reduction for OFDM by Repeated Clipping and Frequency Domain Filtering," *IEEE Elect. Lett.*, vol. 38, no. 8, Feb. 2002, pp. 246–47.
- [34] P. Y. Fan and X. G. Xia, "Block coded modulation for the reduction of the peak to average power ratio in OFDM systems," *IEEE Trans. Consumer Electronics*, vol. 45, no. 4, pp. 1025–1029, Nov. 1999.
- [35] T. Ginige, N. Rajatheva, and K. M. Ahmed, "Dynamic spreading code selection method for PAPR reduction in OFDM-CDMA systems with 4-QAM modulation," *IEEE Commun. Lett.*, vol. 5, no. 10, pp. 408–410, Oct. 2001.
- [36] K. Yang and S. Chang, "Peak-to-average power control in OFDM using standard arrays of linear block codes," *IEEE Commun. Lett.*, vol. 7, no. 4, pp. 174–176, Apr. 2003.
- [37] S. B. Slimane, "Reducing the peak-to-average power ratio of OFDM signals through precoding," *IEEE Trans. Vehicular Technology*, vol. 56, no. 2, pp. 686–695, Mar. 2007.
- [38] J. Tellado, "*Peak to Average Power Ratio Reduction for Multicarrier Modulation*," PhD thesis, University of Stanford, Stanford, 1999.
- [39] H. Breiling, S. H. Müller-Weinfurtner, and J. B. Huber, "SLM Peak-Power Reduction without Explicit Side Information," *IEEE Commun. Lett.*, vol. 5, no. 6, June 2001, pp. 239–41.
- [40] S. Goff, S. Al-Samahi, B. Khoo, C. Tsimenidis and B. Sharif, "Selected Mapping without Side Information for PAPR Reduction in OFDM," *IEEE Trans. on Wireless Commun.*, vol. 8, no. 7, pp. 3320-3325, Jul.2009.

- [41] S. H. Müller and J. B. Huber, "OFDM with Reduced Peak-to-Average Power Ratio by Optimum Combination of Partial Transmit Sequences," *IEEE Elect. Lett.*, vol. 33, no. 5, Feb. 1997, pp. 368–69.
- [42] S. H. Han and J. H. Lee, "PAPR Reduction of OFDM Signals Using a Reduced Complexity PTS Technique," *IEEE Sig. Proc. Lett.*, vol. 11, no. 11, Nov. 2004, pp. 887–90.
- [43] P. Laaser, "Method And Apparatus for Reducing A Crest Factor of A Multi-Tone Data Signal," *U.S. Patent 7,286,605 B2*, Oct. 23, 2007.
- [44] E. G. Tiedemann Jr., R. Rezaifar, O. Glauser and T. Chen, "Reduced Peak-to-Average Amplitude Multichannel Link," *U.S. Patent 6,535,478 B2*, Mar. 18, 2003.
- [45] B. Sanchez, G. Vandersteen, R. Bragos and J. Schoukens, "Optimal multisine excitation design for broadband electrical impedance spectroscopy," *Meas. Sci. Technol.* vol. 22, no. 11, pp. 1-11, Sept. 2011.
- [46] Y. Zhuang and D. Chen, "New Strategies in Removing Non-coherency from Signals with Large Distortion to Noise Ratios", *IEEE Trans. Circ. Syst. II: Express Briefs*, vol. 63, no. 12, pp. 1136-1140, Dec. 2016.
- [47] Y. Zhuang and D. Chen, "Algorithms for Accurate Spectral Analysis in the Presence of Arbitrary Non-coherency and Large Distortion", *IEEE Trans. Instrum. Meas.*, vol. 66, no. 10, pp. 2556-2565, Oct. 2017.
- [48] Y. Zhuang and D. Chen, "Accurate Spectral Testing with Non-coherent Sampling for Multi Tone Applications", Accepted by *IEEE Trans. Circ. Syst. II*, 2017.

CHAPTER 9**ACCURATE LINEARITY TESTING USING LOW PURITY STIMULUS ROBUST
AGAINST FLICKER NOISE**

Accurately characterizing linearity performance of high-resolution Analog-to-Digital Converters (ADCs) has been a challenging task for many years, since providing input signals whose purity is beyond ADC under test becomes more difficult as the ADC performance becomes better. Previously, the Stimulus Error Identification and Removal (SEIR) method used two low purity ramps with an offset in between. It can achieve accurate linearity test results for a high precision ADC, but it is vulnerable to flicker noise inherited in the input signals. This chapter proposes two novel methods that eliminate the influence of flicker noise and accurately obtain linearity performance of ADC under test. Using only -40 to -70dB purity sinusoidal signals, or simple interleaved ramps, the proposed methods are easier to implement and can tolerate the influence of flicker noise, while achieving about 1 least significant bit (LSB) estimation error—the similar level when a pure sinusoidal is used for the same ADC linearity test. The proposed methods are analyzed in detail and comparisons are made between the previous SEIR method. The effectiveness and robustness of the proposed methods against flicker noise are verified through various simulations. The proposed methods help reduce production test cost and simplify the test setup for high-resolution ADC linearity test, suitable for cost-effective on-chip implementation.

This chapter is mainly based on the published paper in *IEEE IEEE Int. Midwest. Symp.* 2015 [1] and *IEEE VLSI Test Symp.* 2016 [2].

9.1 Introduction

Significant progress has been made for high-resolution data converters in past decades. Accurately characterizing such high-performance ADCs has become more challenging in the semiconductor industry. One of these tests is accurate linearity testing of ADCs. To test the linearity performance of the ADC, the traditional histogram ramp test uses a linear ramp or sine signal as a stimulus [3-5]. IEEE standard 1057 and 1241 [6,7] require input signal purity be 3-4 bits more than the ADC under test. As ADC performance continues to increase, so does the need for test stimulus that exceeds such high performance. Achieving accuracy as well as reducing test costs and time has been a well-known problem. In the past, the SEIR method was proposed to resolve this issue [8]. It uses two 7-bit linear ramps as input stimulus of the ADC under test with a constant offset voltage between them. Both simulation and experimental results validated the effectiveness of this method. However, this SEIR method requires the voltage offset be constant during the entire test process, which is vulnerable to a non-stationary test environment. In [9], a new method was proposed to effectively cancel environmental non-stationarity using a CSI pattern [10]. Despite its effectiveness and high accuracy, the complexity of generating such patterns of input ramps and ineffectiveness in canceling flicker noise in the input signals have led us to seek an alternative approach.

In this chapter, two new methods are proposed: the first method involves using 0th order interleaving pattern and chopping input ramps into segments [1]. Compared with SEIR, better results were achieved against flicker noise inherited in the input signals. Nevertheless, using nonlinear interleaved ramps as input did not completely resolve the flicker noise

influence on SEIR, since the flicker noise still accumulates over time and corrupts the accuracy of the Integral Nonlinearity (INL) estimations.

The second method involves using low purity sinusoidal—two sine waves with either offset in between or different amplitudes [2]. The influence of the flicker noise on ADC linearity estimation is further reduced.

The remainder of the chapter is arranged as follows. Section II summarizes the effect of flicker noise on the SEIR method, along with its vulnerability. Section III introduces the proposed methods. Section IV presents MATLAB simulation results and Section V concludes the chapter.

9.2 Flicker Noise Effect on SEIR

Flicker noise is a type of electronic noise with a $1/f$ or pink power density spectrum. There are two major theories to explain the physical origins of flicker noise in metal-oxide-semiconductor field-effect transistors (MOSFETs): the number fluctuation theory based on the McWhorter's charge trapping model [11] and the bulk mobility fluctuation theory based on Hooge's hypothesis [12]. A model that incorporates both the number of fluctuations and the correlated surface mobility fluctuation was described by Hung et al. [13]. Based on this model, the MATLAB simulation results of the sampled flicker noise in both time domain and frequency domain are shown in Figure 9.1. The mean is 0 and the rms value is V , which corresponds to 0.5 LSB for a 16-bit ADC with full input range normalized to 1. The same flicker noise is used later in simulations. From Figure 9.1, flicker noise is a slowly changing function over time. The $1/f$ behavior of flicker noise continues as far as can be seen to lower frequencies with no flattening at low frequency. If this continues to zero frequency, then the

integrated fluctuation is infinite or arbitrarily large, i.e., flicker noise can accumulate to very large numbers over time. This effect is demonstrated by simulation in Figure 9.2.

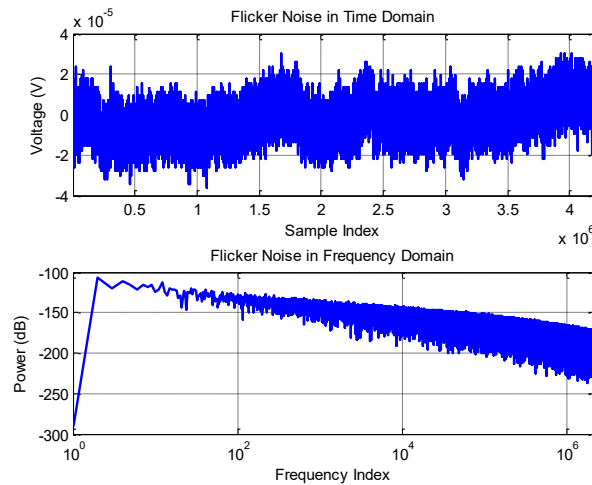


Figure 9.1. Flicker noise in time & frequency domain

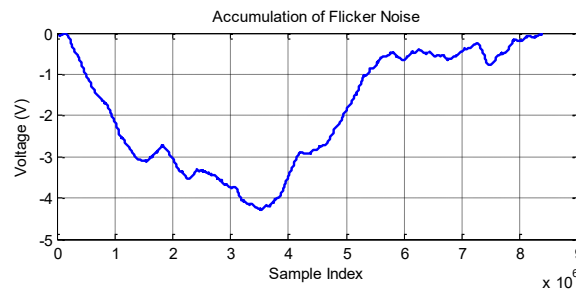


Figure 9.2. Accumulation of flicker noise in time domain

Although flicker noise has zero mean and a small rms value, its accumulation over time can be as large as four times the ADC full input range. The transition level estimation error of SEIR is given by:

$$F(t) = \frac{-1}{\alpha} \int_0^t N(\tau) d\tau, \quad (9.1)$$

where α is the offset between two input ramps and N is the general error term in the SEIR method introduced by all environment error sources. Flicker noise inherited in N will accrue

because of accumulation over time. This accumulation will contribute to a nontrivial amount of error in the SEIR method, as its accrual over time will cause a drift in the constant offset between the two ramps. The INL estimation error can be as large as 12 LSBs as shown in Figure 9.2.

9.3 Proposed Methods

In this section, two methods are proposed to deal with the effects of flicker noise on accurate linearity test.

A. Method 1

First, the original SEIR method was calculated using two nonlinear ramps with a constant offset between them. Two input ramps were modeled the same as in [8].

$$x_1(t) = \alpha [t + \beta(t^2 - t)] + n(t), \quad (9.2)$$

$$x_2(t) = V_{OS} + \alpha [t + \beta(t^2 - t)] + n(t), \quad (9.3)$$

where α, β are unknown to the method. To identify the input nonlinearity, sinusoidal basis functions were utilized.

In [10], CSI was introduced to cancel nonlinear gradients. This CSI pattern was implemented in [9] instead of generating two ramps with an offset. Many triangle waves or short ramps are generated with phase shift and the offset is added to some of them following a given CSI pattern. A third order CSI pattern is implemented in triangle waves shown in Figure 9.3(a). The pattern is “0110100110010110,” where “0” corresponds to a shifted triangle wave and “1” to a non-shifted wave. Now, the input of the ADC is a periodic triangular wave instead of two long ramps. The linearity of these short fast ramps is easier to guarantee compared to the original long ramps. By chopping one long ramp into multiple

triangle waves, flicker noise cannot accumulate over a long period to reduce its accumulation effect on the SEIR method.

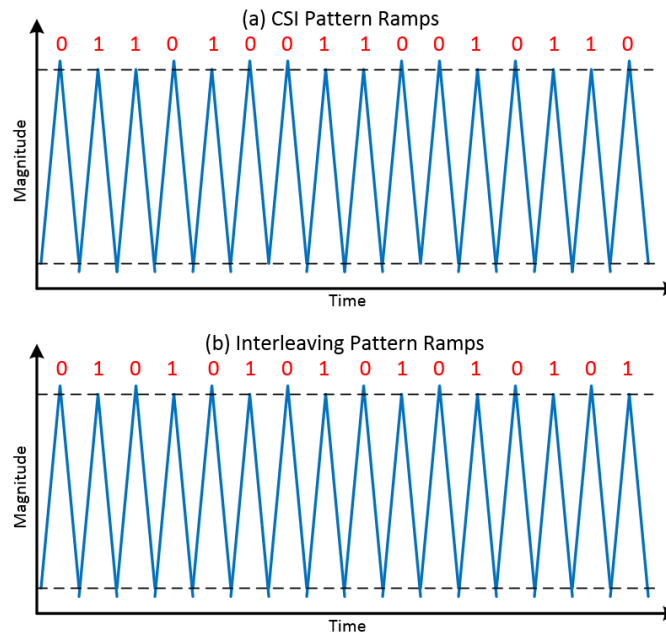


Figure 9.3. Input ramps with CSI pattern (a) and interleaving pattern (b)

As mentioned previously, the CSI pattern can cancel polynomial function drift, but since flicker noise is not polynomial, CSI will not benefit SEIR in canceling flicker noise. Hence, another method, called proposed method 1, to deal with the flicker noise is introduced in Figure 9.3(b), which uses a repeated zero order CSI. This is called interleaving pattern for simplicity in this chapter. Instead of shifting the ramps following the CSI pattern, the triangle wave is shifted every other time.

B. Method 2

Aside from using ramps as input signals, sinusoidal signals are also widely used as a signal source for the ADC linearity test, known as Sinewave Histogram Test (SHT).

Sinusoidal signals, being periodic, inherently have the merit of dispersing time domain samples into different ADC transition levels. This feature is similar to triangular waves, but sinusoidal is much easier to generate. In this case, because consecutively sampled points will be scattered to different ADC transition levels, their sampled flicker noise cannot accumulate over a long period. They are averaged during the sine wave histogram test. This is illustrated in Figure 9.4.

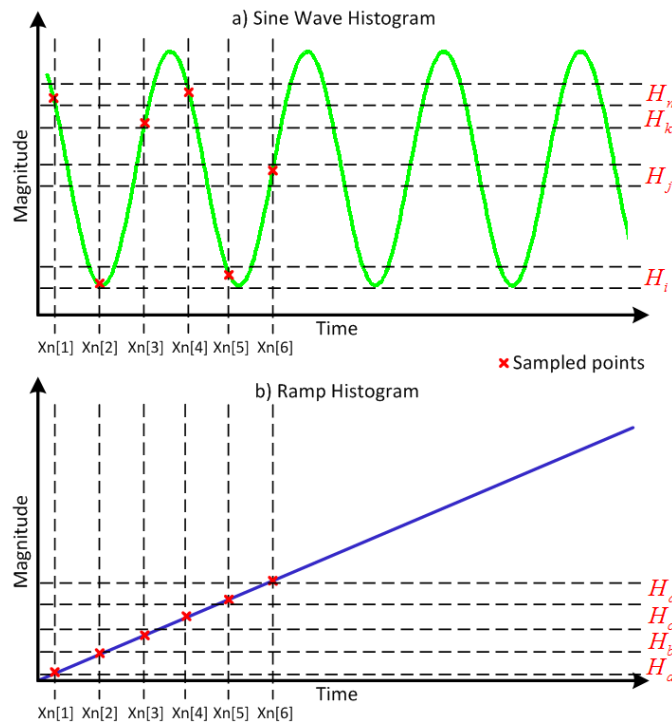


Figure 9.4. a) Sine Wave Histogram compared with b) Ramp Histogram

For ramp input, consecutively sampled points will be in nearby transition levels of the ADC: H_a, H_b, H_c, H_d . In addition, for the real ramp histogram test, one transition level will have several hits per code, like 16, or 64. This will cause the flicker noise to accumulate and affect accuracy of SEIR method. However, for a sinusoidal input, consecutively sampled points are usually in different transition levels that could be far away. When using the

histogram method to estimate transition levels, sampled points from different times are in one transition level. Therefore, their sampled flicker noise will be averaged in the process. Therefore, using sine waves as the input stimulus holds the advantage of reducing the effect of flicker noise on the SEIR method.

This sine wave will replace ramp or interleaved ramps as inputs. To test the high-resolution ADC, high-purity sine waves are still difficult and costly to achieve. To accurately characterize the transition voltages of the ADC, the most critical requirement is the purity of the stimulus. The IEEE standard 1241 requires the input signal to be 3-4 bits purer than the ADC under test. This has become more challenging to achieve, especially when testing high-resolution ADCs. If the stimulus signal exhibits harmonic distortions, the accuracy of the ADC linearity test will be seriously affected. Instead, the proposed method 2 uses two low purity sine wave signals with a constant offset V_{os} in between, shown in blue and red, respectively, in Figure 9.5.

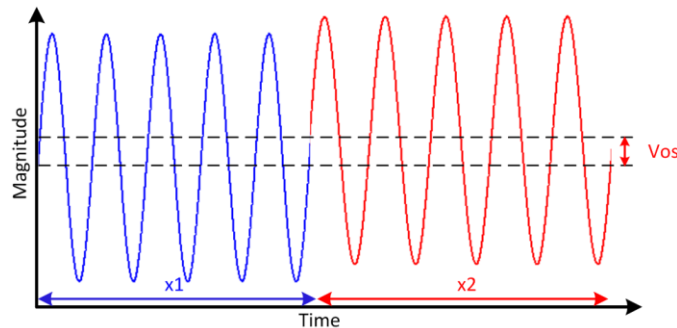


Figure 9.5. Two input signals using proposed method 2

The proposed method 2 can be described as follows: If a pure sinusoidal signal is used, The transition level of the ADC can be estimated by:

$$\hat{T}_j = -\cos(\pi \hat{t}_j), \quad (9.4)$$

where the estimated transition time is given by:

$$\hat{t}_j = \sum_{i=0}^j H_i / \sum_{i=0}^{N-1} H_i, \quad (9.5)$$

where $j = 0, 1, \dots, N-2$, $N = 2^n$. The real and estimated transition levels for the ADC are defined as T_j and \hat{T}_j , respectively. The transition time, t_j , is defined as the time at which the value of the sinusoidal input is equal to the j^{th} transition level of the ADC.

Two input sinusoidal signals with a constant offset, α , to test an n-bit ADC are given by:

$$x_1(t) = \cos(2\pi f_i t + \phi_0) + \sum_{k=2}^H A_k \cos(2\pi k f_i t + \phi_k) + W_1(t), \quad (9.6)$$

$$x_2(t) = \cos(2\pi f_i t + \phi_0) + \sum_{k=2}^H A_k \cos(2\pi k f_i t + \phi_k) + W_2(t) - \alpha, \quad (9.7)$$

where A_k is the k^{th} harmonics amplitude, f_i is input frequency, W_1 and W_2 are the noise from x_1 and x_2 , respectively.

From the two ADC outputs, two sets of histogram data can be obtained, given by: $H_{j,1}$ and $H_{j,2}$, respectively. Two sets of estimated transition time, $t_{j,1}$ and $t_{j,2}$, can also be obtained. Since the proposed method 2 uses two nonlinear sinusoidal inputs, for this case, Eq. (9.4) no longer holds, since the input signals have harmonic distortions. To consider harmonic distortions, the modified version of the ADC transition level, based on the two inputs can be obtained:

$$\hat{T}_{j,1} = -\cos(\pi \hat{t}_{j,1}) + \sum_{k=2}^H A_k \cos(k\pi \hat{t}_{j,1}), \quad (9.8)$$

$$\hat{T}_{j,2} = -\cos(\pi \hat{t}_{j,2}) + \sum_{k=2}^H A_k \cos(k\pi \hat{t}_{j,2}) - \alpha. \quad (9.9)$$

Since the ADC under test is the same and assuming its performance is the same during sampling the two inputs, the transition levels are the same, so $\hat{T}_{k,1} = \hat{T}_{k,2}$

$$\cos(\pi\hat{t}_{j,2}) - \cos(\pi\hat{t}_{j,1}) = \sum_{k=2}^H A_k [\cos(k\pi\hat{t}_{j,2}) - \cos(k\pi\hat{t}_{j,1})] - \alpha. \quad (9.10)$$

There are N-1 equations for j that have different values in Eq. (9.10). These equations are linear in H unknown variables: A_k and α . The least squares can be used to robustly estimate unknowns by minimizing the error energy:

$$\{\hat{A}_k, \hat{\alpha}\} = \arg \min \left\{ \sum_{j=0}^{N-2} \left[\cos(\pi\hat{t}_{j,1}) - \cos(\pi\hat{t}_{j,2}) - \alpha + \sum_{k=2}^H A_k [\cos(k\pi\hat{t}_{j,2}) - \cos(k\pi\hat{t}_{j,1})] \right]^2 \right\}. \quad (9.11)$$

Once the unknowns are estimated, the ADC transition level can be accurately estimated:

$$\hat{T}_j = -\cos(\pi\hat{t}_{j,1}) + \sum_{k=2}^H \hat{A}_k \cos(k\pi\hat{t}_{j,1}). \quad (9.12)$$

Therefore, INL_j and INL of the ADC can be accurately estimated:

$$INL_j = \frac{\hat{T}_j - \hat{T}_0}{\hat{T}_{N-2} - \hat{T}_0} (N-2) - j, \quad (9.13)$$

$$INL = |INL_j|_{\max}. \quad (9.14)$$

As shown in Figure 9.6, consider the samples falling into transition interval $[T_{j-1}, T_j]$:

$$T_{j-1} \leq x_1(n_l) = \cos(2\pi \frac{f_i}{f_s} n_l + \phi_0) + \sum_{k=2}^H A_k \cos(2\pi k \frac{f_i}{f_s} n_l + \phi_k) + W_1(n_l) < T_j, \quad (9.15)$$

$$T_{j-1} \leq x_2(n_m) = A_1 \cos(2\pi \frac{f_i}{f_s} n_m + \phi_0) + \sum_{k=2}^H A_k \cos(2\pi k \frac{f_i}{f_s} n_m + \phi_k) - \alpha + W_2(n_m) < T_j, \quad (9.16)$$

where f_s is the ADC sampling frequency, and n_l and n_m are the sampled indices whose input values fall into the interval $[T_{j-1}, T_j]$. $l = 1, 2, \dots, H_{j,1}$, $m = 1, 2, \dots, H_{j,2}$.

When the noise is taken into consideration, the effective offset $\alpha_{eff,j}$ is given by:

$$\alpha_{eff,j} = \alpha + \frac{\sum_{m=1}^{H_{j,2}} W_2(n_m)}{H_{j,2}} - \frac{\sum_{l=1}^{H_{j,1}} W_1(n_l)}{H_{j,1}}. \quad (9.17)$$

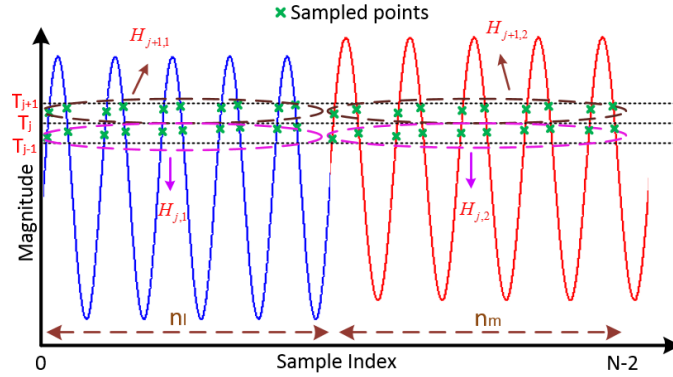


Figure 9.6. Illustration of noise averaging effect using the proposed method 2

Therefore, the non-constant part of the offset $\Delta\alpha_j$ is given by:

$$\Delta\alpha_j = \alpha_{eff,j} - \alpha = \frac{\sum_{m=1}^{H_{j,2}} W_2(n_m)}{H_{j,2}} - \frac{\sum_{l=1}^{H_{j,1}} W_1(n_l)}{H_{j,1}}. \quad (9.18)$$

Since the sample indices, n_l , consists of sampled indices from different periods, the sampled flicker noise will be different, as well as n_m . The histogram method helps average the noise. The flicker noise sampled from different time intervals can be averaged just like white noise. As a result, they will not accumulate over time and $\Delta\alpha_j$ is reduced.

In addition, when comparing $\Delta\alpha_j$ with nearby values, $\Delta\alpha_{j-1}$ and $\Delta\alpha_{j+1}$, the slope of the sine wave is almost the same, $H_{j,1} \approx H_{j-1,1}$, $H_{j,2} \approx H_{j-1,2}$.

$$\Delta\alpha_j - \Delta\alpha_{j-1} \approx \frac{\sum_{m=1}^{H_{j,2}} W_2(n_m) - \sum_{m=1}^{H_{j-1,2}} W_2(n_m)}{H_{j,2}} - \frac{\sum_{l=1}^{H_{j,1}} W_1(n_l) - \sum_{l=1}^{H_{j-1,1}} W_1(n_l)}{H_{j,1}}. \quad (9.19)$$

Since flicker noise is slowly changing over sample time. Thus, the sampled flicker noise in nearby consecutive points are very close to each other, $\sum_{m=1}^{H_{j,2}} W_2(n_m) \approx \sum_{m=1}^{H_{j-1,2}} W_2(n_m)$, and averaging makes their differences even smaller. Thus, the difference between $\Delta\alpha_j$ and its nearby values is very small.

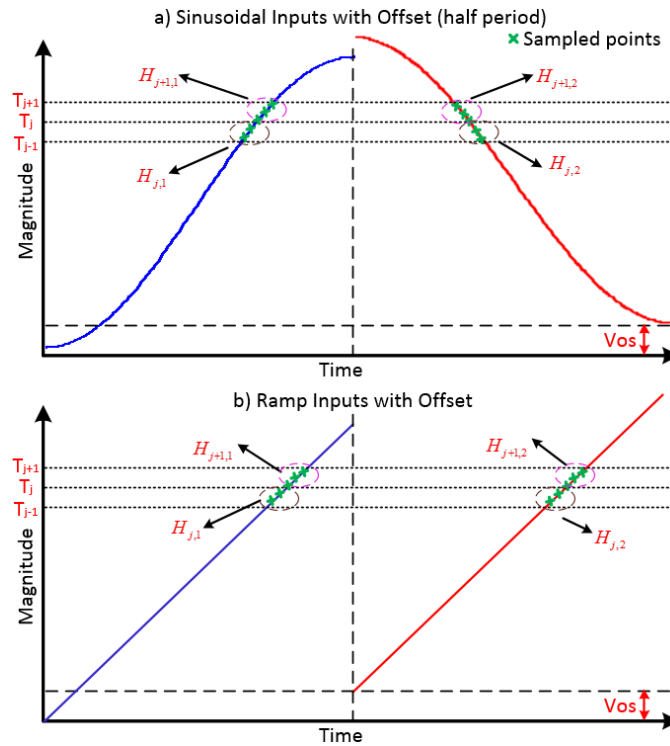


Figure 9.7. Comparison of a) sinusoidal inputs with half period and b) ramp inputs

Note, with more sine wave periods sampled, flicker noise will be further averaged and better estimates for ADC's INL_k can be obtained. This behavior is similar to the interleaved ramp inputs. In the extreme case, if only a half period sine wave is sampled, this

situation will be similar to a ramp input without interleaving. This is illustrated in Figure 9.7. Since n_l consists of sampled indices from consecutive time intervals, even with averaging,

the value $\sum_{l=1}^{H_{j,1}} W_1(n_l) / H_{j,1}$ is still larger than the previous case and the averaged result

$\sum_{m=1}^{H_{j,2}} W_2(n_m) / H_{j,2}$ from n_m will be a different value. As a result, $\Delta\alpha_j$ is much larger than the

previous case and the offset constancy will be corrupted by flicker noise.

C. Discussion

To further reduce the effects of flicker noise, the sine wave can be interleaved as well. Figure 9.8 shows the two sets of sine wave inputs with interleaving and offset. Similar to the previous methods, two inputs, red and blue are both sine waves with an offset in between, along with interleaving. At every other period, the sine wave shifts (red) and serves as another set of input to the ADC, while the blue sine wave serves as the original set of input to the ADC. In doing so, the flicker noise in the nearby samples will be further spread among different ADC transition levels. After the histogram, such errors introduced by flicker noise accumulation will be further reduced compared with method 1 and 2.

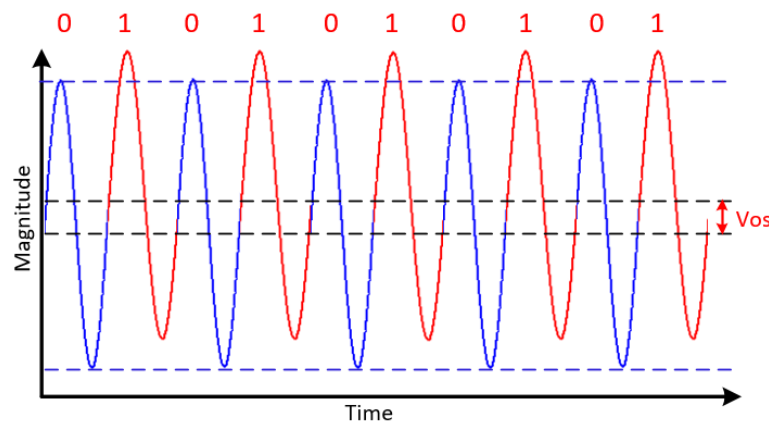


Figure 9.8. Two sine waves with offset and interleaving

The detailed steps to obtain ADC INL estimation is similar to method 2. However, the noise on the non-constant part of the offset $\Delta\alpha_j$ is different than previous methods.

From the previous analysis, we know the sample indices, n_l, n_m , consist of the sampled indices from different periods and the sampled flicker noise will be different. In this new method, the sample indices is further divided into samples from different periods, where the flicker noise is less likely to be similar. The histogram, $\Delta\alpha_j$ further reduces with averaging, which is smaller than methods 1 and 2. Similarly, the differences, $\Delta\alpha_j - \Delta\alpha_{j-1}$, will be smaller. These will help the flicker noise averaged further and the estimated INL will be more accurate. This is shown in Figure 9.9.

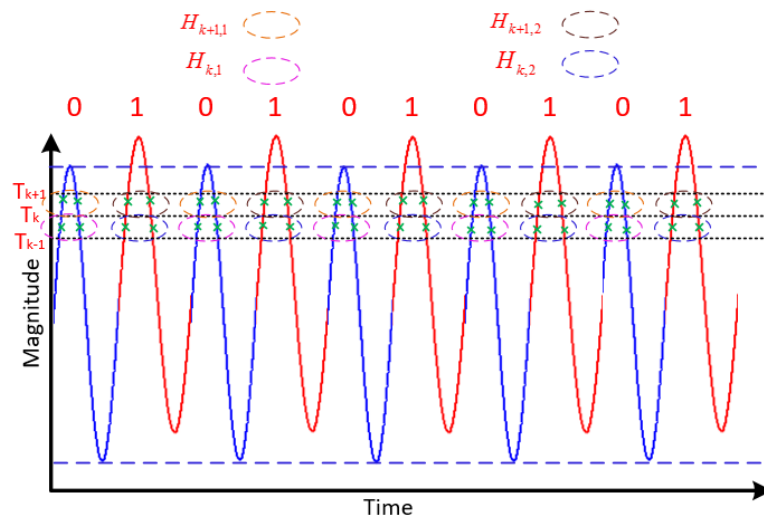


Figure 9.9. Illustration of noise averaging effect using two sine waves and interleaving

9.4 Simulation Results

In this section, the proposed methods are verified through extensive simulations to demonstrate their effectiveness in reducing flicker noise effects on the linearity test.

A. Comparison with CSI

These two methods are validated by simulations in MATLAB. A 16-bit nonlinear ADC with INL of 5 LSB was modeled. First, the original SEIR method was calculated using two nonlinear ramps with a constant offset between them. Ramp linearity is only 7-bits and the offset VOS is 1% of the total input range. For identifying the input nonlinearity, 20 sinusoidal basis functions are used. Since the original SEIR and CSI combined with SEIR are capable of handling normal/gaussian noise, and the goal of this chapter is to investigate the effects of flicker noise, only 0.5 LSB rms value for flicker noise is added.

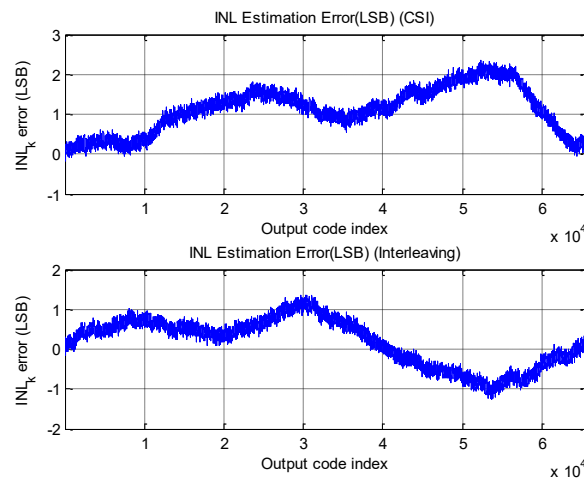


Figure 9.10. INL_k estimation results using CSI + SEIR (Top) and Interleaving + SEIR (Bottom)

The histogram method is used to test the INL of the ADC, with 32 hits per code for each ramp. Figure 9.10 shows the comparison of the true INL_k (blue) and estimated INL_k

using SEIR (red). Large red curve deviations from the blue curve can be observed. The difference between the true and estimated INL_k can be as large as 12 LSB. This shows the original SEIR method is sensitive to flicker noise.

Second, the CSI pattern was used to improve accuracy for the original SEIR method. A fourth order CSI pattern, which results in 32 triangle waves, was utilized to generate the input ramps. A small delay value is introduced for each triangle wave to guarantee no repetitive sampling occurs and the samples are evenly distributed. The same flicker noise data are used to compare the new estimation results with the original SEIR test results. Other test conditions are the same as the original SEIR test case. The effectiveness of the CSI pattern combined with the SEIR method is demonstrated in Figure 9.10 (Top). It can be seen that the INL_k estimation error is reduced to about 2 LSB, but the estimation error is still considered large and inaccurate.

Next, the interleaving pattern (proposed method 1) was used to compare its effectiveness versus CSI pattern. Similarly, 32 triangle waves generated other test conditions the same as the original SEIR test case. Figure 9.10 (Bottom) shows the estimation results using proposed method 1. The INL_k estimation error is smaller compared to the CSI case, but the observed estimation error is over 1 LSB.

When the input ramps are divided into more triangle waves, different results are obtained. The maximum INL_k estimation error is tabulated in Table 9.1 and show as two input ramps are divided into more triangle waves, smaller estimation errors are obtained. This is due to the fact that the flicker noise associated in the ramp is chopped into smaller segments as more triangle waves are used. Thus, the accumulation of noise becomes smaller. In addition, interleaving patterns have a better performance than CSI under different test

conditions. However, the error source is not eliminated, since the flicker noise continues accumulating over a shorter period of time. In addition, when dividing the input ramps into more triangle waves, the realization in practical testing will be more complicated.

Table 9.1. Maximum INL_k estimation error (LSB) vs number of interleaved triangle waves

Method Triangles used	CSI + SEIR	Interleaving + SEIR
32	2.2	1.4
64	1.5	1.2
128	1	0.8
256	0.9	0.7

Finally, statistical simulation is conducted to investigate the threshold rms value of the flicker noise. If the noise is within this threshold, then interleaving combined with SEIR is capable of estimating INL_k for the ADC accurately. Otherwise, both CSI and interleaving cannot resolve the issue of flicker noise in SEIR, and a new method will be needed in the future. The INL_k estimation error criteria is set within $\pm 0.5LSB$. Using this criteria, different rms values for flicker noise are simulated and the threshold rms values are obtained. A total of 2000 simulations are conducted with the same test setup as previous, using 128 triangle waves. Different ADCs are generated for each run and the flicker noise was different each time, but with the same rms value for every 500 runs. The rms value for flicker noise varies from 0.5 LSB to 0.15 LSB. Table 9.2 summarizes the averaged maximum INL_k estimation error with respect to different rms values of flicker noise. When 128 ramps are generated for implementing the interleaving pattern, Table 9.2 shows for 0.15 LSB rms value of flicker noise, the INL_k estimation results are within $\pm 0.5LSB$. Therefore, the threshold rms value for flicker noise is 0.15 LSB.

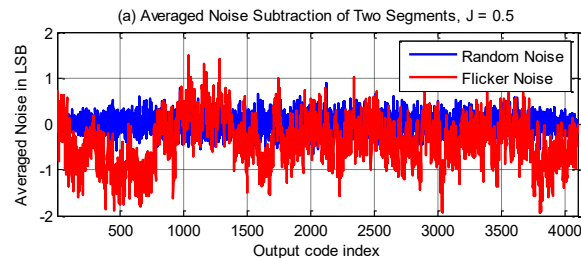
Table 9.2. Averaged maximum INL_k estimation error (LSB) vs rms value of flicker noise

RMS value of flicker noise (500 runs)	Maximum INL_k estimation error (averaged over 500 runs)
0.5	0.82
0.4	0.71
0.3	0.59
0.15	0.48

B. Simulation using sinusoidal

Extensive simulations are performed in MATLAB to validate functionality of the proposed method 2. Comparisons are made between sinusoidal inputs and ramp inputs. The effectiveness of the proposed method 2 is further verified when comparing the results with the presence of flicker and random noises, respectively. Furthermore, the proposed method 2 is compared with standard SHT with pure sinusoidal input and same rms value of random noise. All simulation results are in agreement with the analysis and prove its effectiveness.

Similar to the nonlinear ramp signal, harmonics are intentionally added to a pure sine wave, whose amplitudes and phases are randomly generated. The input signal purity (Total Harmonic Distortion) of the input sinusoidal signal is between -40 and -70dB. Offset is set to 1% of the ADC's full range.



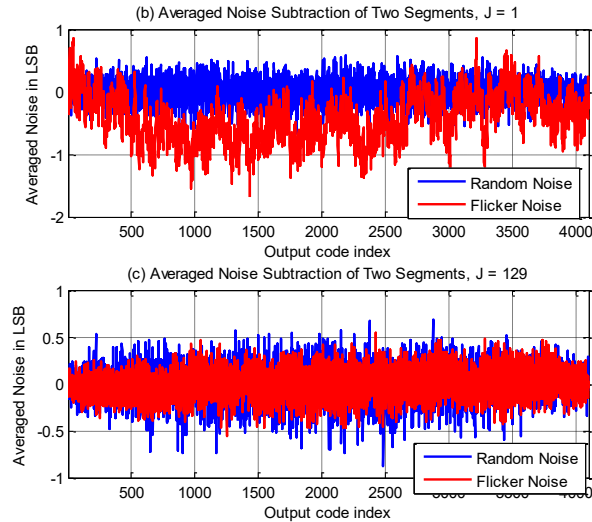


Figure 9.11. Averaged noise subtraction when a) $J=0.5$; b) $J=1$; c) $J=100$

Flicker noise is generated using the model in [13]. Both random and flicker noises have a mean value of 0 and standard deviation of 0.5LSB . SHT method is utilized to estimate the INL of the ADC, with 16 hits per code.

First, two input sinusoidals with 1% offset are generated to validate the effectiveness in averaging flicker noise. Flicker noise samples are grouped together when their input sinusoidals are in the same transition interval, which models the offset nonconstancy, $\Delta\alpha_j$. A total 4,095 transition intervals are generated and the number of periods tested is $J=0.5, 1$, and 100. The averaged noise between two signals were subtracted and the results are compared with random noise test cases shown in Figure 9.11.

Figure 9.11 shows when only a half period is sampled for each sinusoidal input, the averaged flicker noise from each interval shows large deviation from 0, which reflect the nonconstancy of the offset in the SEIR method. As the number of periods is increased, better averaged results are achieved. With $J=100$, the averaged results overlap with the random

noise test case well, demonstrating the flicker noise effect is reduced to the same level as random noise.

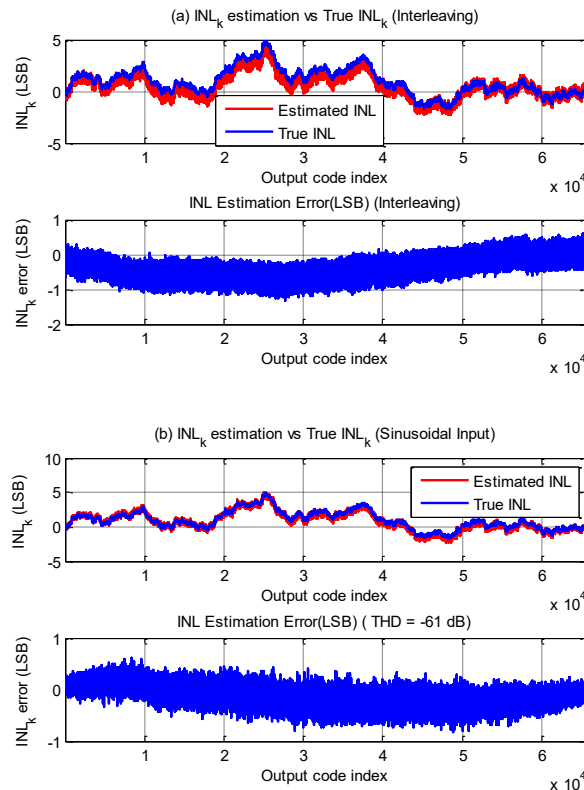


Figure 9.12. INL estimation using a) Ramp interleaving and b) Nonlinear sinusoidal

Second, the functionality of the proposed method 2 is validated to test a 16-bit ADC. The results are compared with interleaved ramp inputs divided into 128 triangle waves. Input sinusoidal nonlinearities are randomly generated with purity ranging from -40 to -70dB. All validated the proposed method 2, and one representative result is shown. J is chosen as 129 with 32 hits per code, while ramp inputs are sampled with 32 hits per code as well. However, in a real production test it could take 64 or even more hits per code for the high-resolution ADC linearity test. During analysis, there is no requirement on the structure of the ADC,

demonstrating the proposed method 2 is capable of testing different kinds of ADCs. The reason for choosing a flash ADC structure is the large number of independent error sources, which helps validate the robustness of the proposed method 3 against the most challenging situation.

As shown in Figure 9.12, when the two input signals are interleaved ramps, the INL estimation error shows a maximum of 1.1 LSB error. While using the sinusoidal inputs to test the same ADC, the maximum estimation error is reduced to 0.8LSB. This demonstrates the proposed method 2 estimates INL_k of the ADC accurately and is more effective to reduce the flicker noise effect than using interleaved ramps. In addition, the INL estimation results using the proposed method 2 are compared with the test case when random noise is present, instead of the flicker noise. Since the same ADC is tested, the INL curve is not shown again, only the INL estimation error is plotted in Figure 9.12.

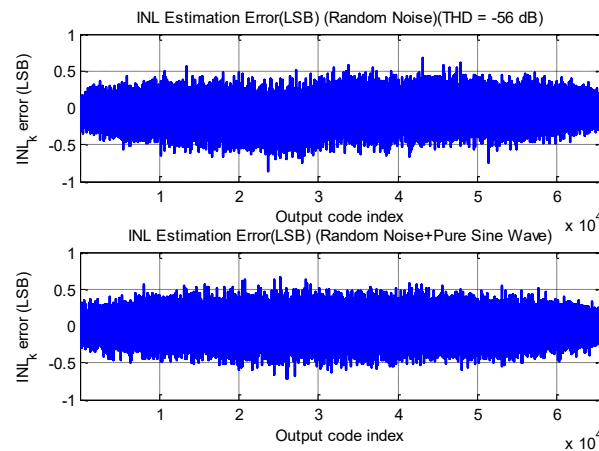


Figure 9.13. INL estimation using a) proposed method 2 and b) pure sinusoidal signal.

Compared with standard SHT, pure sinusoidal signal, and 0.5LSB random noise, the INL estimation error using the proposed method 2 showed the same level of accuracy with

only a low purity sinusoidal signal, as shown in Figure 9.13. This validates the proposed method 2, which can achieve accurate test results as the reference. In addition, when comparing the flicker and random noises test case, both results showed similar estimation error levels. The random noise case shows a flatter curve compared with the flicker noise case curve. This is due to the fact there are still small accumulations of flicker noise, but the estimation accuracy is in the same range. Again, this demonstrates the capability of the proposed method 3 to remove the flicker noise effect and accurately estimate the ADC's linearity performance against both random and flicker noises.

9.5 Conclusion

In this chapter, two new methods are introduced to accurately test linearity characteristics of high-resolution ADCs using low purity sinusoidal or ramp stimulus in the presence of flicker noise. The proposed methods overcome the original SEIR problem, which is vulnerable to flicker noise accumulation. With the same or less hits per code, the proposed methods are capable of estimating linearity performance of high-resolution ADC against flicker noise and random noise corruption. In addition, this strategy uses two low purity sinusoidal/ramp signals with a constant offset in between. These signals can be easily generated using readily available signal generators. Combined with its computational efficiency and low test cost, the new methods provide an alternative solution for high-resolution ADC linearity test and can be implemented into on-chip test environments.

References

- [1] Y. Zhuang, T. Chen, S. Chaganti and D. Chen, "Effect of Flicker Noise on SEIR for Accurate ADC Linearity Testing," *IEEE Int. Midwest. Symp.* pp. 1-4, Aug. 2015.
- [2] Y. Zhuang, T. Chen, S. Chaganti and D. Chen, "Accurate Linearity Testing with Impure Sinusoidal Stimulus Robust Against Flicker Noise," *IEEE VLSI Test Symp.* pp1-6, Apr.2016.
- [3] International Technology Roadmap for Semiconductors, <http://public.itrs.net>, 2013.
- [4] J. Doernberg, H.-S. Lee, and D.A. Hodges, "Full-Speed Testing of A/D Converters," *IEEE J. Solid State Circuits*, SC-19, pp. 820-827, Dec.1984.
- [5] A. van der Ziel, *Noise in Solid State Devices and Circuits*. New York: Wiley, 1986.
- [6] IEEE Standard for Terminology and Test Methods for Analog-to-Digital Converters, *IEEE Std.1241*, 2010.
- [7] IEEE Standard for Digitizing Waveform Recorders, *IEEE Std.1057*, 2007.
- [8] L. Jin, K. Parthasarathy, T. Kuyel, D. Chen and R. Geiger, 'Accurate testing of analog-to-digital converters using low linearity signals with stimulus error identification and removal', *IEEE Trans. Instrum. Meas.*, vol. 54, no. 3, pp. 1188-1199, Jun.2005.
- [9] L. Jin, D. Chen, and R. Geiger, "SEIR Linearity Testing of Precision A/D Converters in Nonstationary Environments With Center-Symmetric Interleaving," *IEEE Trans. Instrum. Meas.* vol.56, no 5, pp. 1776 – 1785, Sept.2007.
- [10] X. Dai, C. He, H. Xing, D. Chen, and R. Geiger, "An Nth-order central symmetrical layout pattern for nonlinear gradients cancellation," *IEEE Int. Symp. Circuits Syst.* 2005, pp. 4835–4838.

- [11] A. L. McWhorter, "*1/f noise and germanium surface properties*, " Semiconductor Surface Physics, Philadelphia: University of Pennsylvania Press, pp. 207, 1957.
- [12] F. N. Hooge and L. K. J. Vandamme, "Lattice scattering causes 1/f noise," *Phys. Lett.*, vol. 66A, pp. 315, 1978.
- [13] K.K. Hung, P. K. Ko, C. Hu, Y.C. Cheng, "A Unified Model for the Flicker Noise in Metal- Oxide-Semiconductor Field-Effect Transistors, " *IEEE Trans. on Electron Devices*. vol. 37, no. 3, pp. 654 – 665, Mar. 1990.

CHAPTER 10

SUMMARY

In this dissertation, several methods for accurate and robust spectral testing with relaxed instrumentation requirements for both single-tone and multi-tone test are presented. They focus on resolving one or several stringent test conditions simultaneously in the conventional spectral testing, regulated by IEEE standards. It is shown that these methods relaxed many stringent test conditions seen from conventional spectral testing. They can obtain accurate spectral performance of the device or signal under test, compared with a conventional test with much lower test costs and faster test time.

In this dissertation, three classes of methods for overcoming the above difficulties were presented. The first class of methods targeted the accurate single-tone spectral testing. The first method in this class successfully eliminated the need for coherent sampling, especially for signals with large distortions. The second method resolved the simultaneous non-coherent sampling, amplitude, and frequency drift in the spectral testing, the last two methods generated high-purity sine waves using cost-effective devices and test systems, which can serve the high-quality test stimulus in spectral testing. These proposed methods have been validated by both simulation and measurement results. They have demonstrated their high accuracy and robustness against various test conditions.

The second class of methods focused on the accurate multi-tone spectral testing. The first method in this class resolved non-coherent sampling in multi-tone spectral testing. The second method eliminated the need for pure source in multi-tone spectral testing. The third method generated the multi-tone sine wave with minimum peak-to-average power ratio for

various applications in testing and communications. Both simulation and measurement results validated the functionality and robustness of the proposed methods.

The third class introduced two proposed methods to reduce the flicker noise influence on accurate linearity test. Extensive simulation results verified their effectiveness to reduce flicker noise influence and achieve accurate linearity results.

Overall, these proposed methods have a huge impact on the accurate spectral testing in both industry and academia. All the proposed methods have achieved the low-cost test setup, and have proven to be effective on relaxing many of the stringent requirements on spectral testing. Their test results matched well with the reference results, which are obtained by conventional test methods from IEEE standards. Furthermore, the proposed methods have no prior knowledge on the DUTs performance, resolution or architecture. They can be implemented into board level or future on-chip BIST solutions, and have wide applications for various types of DUTs and test conditions.

In the future, more works can be done to further develop the proposed methods. One approach involves more detailed investigation for some of the proposed methods, and the validation using measurement results. Another approach is to develop new methods based on existing ones, and to resolve more non-ideal conditions simultaneously. This includes resolving non-coherent sampling, low purity test stimulus, clipped test signal, jittery clock, and unstable test environment. More importantly, although the proposed methods focus on signal and ADC spectral testing, their principles and approaches can be extended into other device and system testing such as amplifiers and DACs, making even bigger impact to the IC testing and measurement industry.